# Shape coexistence in atomic nuclei

Kris Heyde*

*Department of Physics and Astronomy, Ghent University,
Proeftuinstraat 86, B-9000 Gent, Belgium*

John L. Wood†

*School of Physics, Georgia Institute of Technology, Atlanta, Georgia 30332-0430, USA*

Shape coexistence in nuclei appears to be unique in the realm of finite many-body quantum systems. It differs from the various geometrical arrangements that sometimes occur in a molecule in that in a molecule the various arrangements are of the widely separated atomic nuclei. In nuclei the various "arrangements" of nucleons involve (sets of) energy eigenstates with different electric quadrupole properties such as moments and transition rates, and different distributions of proton pairs and neutron pairs with respect to their Fermi energies. Sometimes two such structures will "invert" as a function of the nucleon number, resulting in a sudden and dramatic change in ground-state properties in neighboring isotopes and isotones. In the first part of this review the theoretical status of coexistence in nuclei is summarized. Two approaches, namely, microscopic shell-model descriptions and mean-field descriptions, are emphasized. The second part of this review presents systematic data, for both even- and odd-mass nuclei, selected to illustrate the various ways in which coexistence is observed in nuclei. The last part of this review looks to future developments and the issue of the universality of coexistence in nuclei. Surprises continue to be discovered. With the major advances in reaching to extremes of proton-neutron number, and the anticipated new "rare isotope beam" facilities, guidelines for search and discovery are discussed.

DOI: 10.1103/RevModPhys.83.1467        PACS numbers: 21.60.−n, 23.20.−g

## CONTENTS

## I. INTRODUCTION

The observation that a particular atomic nucleus ($N$, $Z$ combination) can exhibit eigenstates with different shapes appears to be a unique type of behavior in finite many-body quantum systems. Such behavior is familiar in molecules: for example, the odors of oranges and lemons are due to two different "shapes" of a molecule called limonene. However, in molecules[1] these different shapes involve different

*kris.heyde@ugent.be
†john.wood@physics.gatech.edu

---

[1] In molecules this led to the term "isomerism." Thus, one can sensibly refer to "shape isomers" in nuclei. However, "nuclear isomers" have historically been used to describe long-lived excited states in nuclei with no implication that these states differ in shape from the ground state. The term shape isomer is occasionally used, and the terms "pairing isomer" (see Sec. III.A.7) and "fission isomer" (see Sec. III.A.8) are used in nuclear structure study.

geometrical arrangements of widely spaced atomic nuclei (constrained by identical chemical bonds). Atomic nuclei do not possess a substructure with widely spaced subunits.

In this review, we present an up-to-date view [we published two earlier reviews (Heyde *et al.*, 1983; Wood *et al.*, 1992) on the subject] of the experimental manifestation of shape coexistence in nuclei and theories that predict its occurrence. There appears to be a possibility that it occurs in all nuclei. It also appears to explain the apparent disappearance or ''collapse'' of the shell structure in nuclei. Understanding the occurrence of shape coexistence in atomic nuclei is arguably one of the greatest challenges faced by theories of nuclear structure.

Coexistence in nuclei has now been a feature of nuclear structure for over 50 years. It is our aim to explore, discuss, and review the conditions needed such that at a given number of protons $Z$ and neutrons $N$, shape coexistence becomes manifested. In our previous reviews we addressed its occurrence in odd-mass nuclei (Heyde *et al.*, 1983) and even-even nuclei (Wood *et al.*, 1992), and we gave a detailed perspective on the association of electric monopole $E0$ transitions with shape coexistence (Wood *et al.*, 1999). Since these earlier reviews, significant progress has been made toward a unified view of coexistence in nuclei, both theoretically and experimentally.

It would be fair to say that the status of coexistence in nuclei has evolved from an exotic rarity, via the perception that it is a phenomenon which exhibits ''islands of occurrence'' to the current position in which it occurs in all (but the lightest) nuclei. While coexistence has not yet been observed in all nuclei for which there are extensive spectroscopic data, in this review we illustrate the spectroscopic fingerprints by which it can be sought.

The first part of this review summarizes the theoretical status of coexistence in nuclei. Two approaches, namely, microscopic shell-model descriptions and mean-field descriptions, are emphasized. The status of these two approaches has advanced considerably since the earlier reviews and they now provide versatile tools with considerable predictive power. As in the earlier reviews, we address only the theoretical description of collective states built on coexisting (intrinsic) structures in an incidental manner. For a recent perspective on collective states in nuclei, see Rowe and Wood (2010).

The second part of this review presents systematic data, for both even- and odd-mass nuclei, selected to illustrate the various ways in which coexistence is observed in nuclei. We strongly emphasize the important interplay between experimental observation and theoretical description. The subject has advanced because of the interplay between the two.

The last part of this review looks to future developments and the issue of the universality of coexistence in nuclei. There are a number of key issues here. At present, no region of manifestation of coexistence has been thoroughly studied. Surprise occurrences continue to be discovered. With the advances in accessibility to extremes of proton-neutron number, and the anticipated new ''rare isotope beam'' facilities, strong guidelines for search and discovery are needed.

## II. THEORETICAL APPROACH

In this review, we explored the conditions such that at a given proton and neutron number $(Z, N)$, shape coexistence is manifested in the nuclear landscape. Shape coexistence is governed by the interplay between two opposing tendencies: On one side the stabilizing effect of closed shells and subshells which causes the nucleus to retain a spherical shape and, related to this, the cost in energy to redistribute protons and neutrons into an excited configuration. On the other side, the residual interactions between protons and neutrons, or, the correlation energy gain, in which the proton-neutron interaction energy is a major contribution and is mainly multiplicative in the number of interacting protons times the number of interacting neutrons, which drives the nucleus into a deformed shape.

Theoretically, there are mainly two complementary ways to progress to understand the appearance of shape-coexisting structures in nuclei.

In the first approach one starts from a spherical mean field (the well-known spherical shell model). The standard choice is to include only one major shell to describe the properties of nuclei situated between closed shells that are fixed by the magic numbers $Z, N = 2, 8, 20, 28, \ldots$. An important question is to find out how well the so-called double- (or single-) closed shells can be described by a set of fully occupied orbitals for the core nucleons and empty orbitals in the valence space. It turns out that multiple particle-hole ($m$p-$n$h) excitations across ''closed'' shells give rise to rather low-lying collective bands in, e.g., $^{16}$O, $^{40}$Ca, and $^{56}$Ni. This is a consequence of the large binding energy (proton-neutron and pairing energy, mainly) relative to the energy of the double- (or single-)closed shell. Even inversions in energy of the $m$p-$n$h configuration relative to energy of the 0p-0h closed shell can result (see, e.g., neutron-rich $N = 20$ and $N = 28$ nuclei, Sec. III.B.2). These $m$p-$n$h configurations give rise to collective excitations [$0^+$ states at low excitation energy, strong $B(E2)$ values in excited bands] that appear side by side with the low-lying states in which the starting core remains mainly a closed-shell system. As such, the ingredients to describe shape-coexisting phenomena can be met by including at least two major shells. Along the same lines, in particular, for nuclei far from the region of $\beta$ stability, one needs to know where the closed shells and subshells are situated. The latter, however, are clearly affected by the proton-neutron interaction and related monopole shifts (see Sec. II.A).

In the second approach, the two-body nucleon-nucleon force acts as a starting point and is used to obtain optimized single-particle states in a self-consistent way, according to Hartree-Fock (HF) theory constraining the nuclear density to exhibit different low-multipole (quadrupole, octupole, etc.) deformations. This approach results in an energy surface with a minimum energy that most often corresponds to a nonspherical density distribution. It is even possible to incorporate the strong pairing correlations that are active in the nucleus, which is formulated in Hartree-Fock-Bogoliubov (HFB) theory to simultaneously optimize both the mean single-particle field and the pairing (mean-pair field) properties in nuclei. As a result, coexisting shapes may appear for certain proton and neutron numbers. It is, however, important

that all symmetries that are broken in the HF or HFB approach be restored to construct states with fixed proton ($Z$) and neutron number ($N$), correct isospin $T$, and angular momentum $J$. These states then form a starting basis to determine the collective dynamics (collective wave functions, energy spectra, and other observables) going beyond the mean-field approach.

### A. Spherical shell-model approach

The shell model starts from a Hamiltonian

$$\hat{H} = \sum \varepsilon_a a_\alpha^\dagger a_\alpha + \frac{1}{4} \sum \langle \alpha\beta \mid V \mid \gamma\delta \rangle a_\alpha^\dagger a_\beta^\dagger a_\delta a_\gamma. \quad (1)$$

This Hamiltonian contains a set of single-particle energies $\varepsilon_a$ that can be determined from self-consistent HF calculations or from experimental proton and neutron separation energies near closed shells. The residual two-body nucleon-nucleon interaction, expressed by means of the two-body matrix elements $\langle \alpha\beta \mid V \mid \gamma\delta \rangle$, may result from an effective interaction derived from a fully microscopic approach using realistic forces (Kuo and Brown, 1966, 1968; Hjorth-Jensen, Kuo, and Osnes, 1995), but may also be of a more phenomenological origin, fixed from fitting energy eigenvalues to experimental energies (Brown and Wildenthal, 1988; Honma *et al.*, 2004, Honma *et al.*, 2009; Brown and Richter, 2006).

Knowledge of the variation of the single-particle energies moving away from the closed shells is a key issue for this discussion because it will to a large extent determine the energy gaps and, thus, the energy cost for creating particle-hole excitations across closed shells. Within the shell model, one can make use of effective single-particle energies (ESPE). They are defined (Otsuka *et al.*, 2001) as one-nucleon separation energies for an occupied orbital (or the extra binding gained by the addition of a nucleon to an unoccupied orbital). The concept of being able to relate one-nucleon energies as the difference in energy of an $A + 1(A - 1)$ and the $A$ particle system goes back to Koopman's theorem (Koopman, 1934) if the wave functions of these many-body systems are approximated by many-nucleon Slater determinants. These ESPE can be evaluated as the sum of bare single-particle energies $\varepsilon_a$ [with $a$ a shorthand notation for the set of quantum numbers $(n_a, l_a, j_a)$] with respect to a closed-shell core [see Eq. (1)] and the monopole part that can be extracted from the two-body residual interaction (Bansal and French, 1964; Poves and Zuker, 1981). This leads to the monopole part of the Hamiltonian $\hat{H}_{\mathrm{mon}}$, which can be written as

$$\hat{H}_{\mathrm{mon}} = \sum_i \epsilon_{\nu_i} \hat{n}_{\nu_i} + \sum_i \epsilon_{\pi_i} \hat{n}_{\pi_i} + \sum_{ij} V_{ij}^{\nu\pi} \hat{n}_{\nu_i} \hat{n}_{\pi_j}$$
$$+ \sum_{i \leq j} \frac{\hat{n}_{\nu_i}(\hat{n}_{\nu_j} - \delta_{ij})}{1 + \delta_{ij}} V_{ij}^{\nu\nu} + \sum_{i \leq j} \frac{\hat{n}_{\pi_i}(\hat{n}_{\pi_j} - \delta_{ij})}{1 + \delta_{ij}} V_{ij}^{\pi\pi},$$
$$(2)$$

where $\hat{n}_{\pi_i}$ and $\hat{n}_{\nu_i}$ are proton and neutron number operators. The $V_{ij}^{\rho\rho'}$ are centroids of the two-body interaction, or angular-momentum averaged matrix elements, defined as

(Bansal and French, 1964; Poves and Zuker, 1981; Dufour and Zuker, 1996)

$$V_{ij}^{\rho\rho'} = \frac{\sum_J \langle i_\rho j_{\rho'} | V | i_\rho j_{\rho'} \rangle_J (2J + 1)}{\sum_J (2J + 1)}, \quad (3)$$

where $\rho$ and $\rho'$ denote protons and neutrons, and the total angular momentum of a two-body state $J$ runs over all values allowed by the Pauli principle.

The spherical single-particle states, and the ESPE, corresponding to the monopole part of the Hamiltonian [see Eq. (2)], provide an important ingredient for the formation of shells and in the study of the variation of shell gaps as a function of proton (neutron) number. Large shell gaps obtained from the monopole Hamiltonian are a prerequisite to obtain reliable magic numbers. A reduction of the original spherical shell gaps may lead to formation of a deformed ground state, if the correlation energy of a given excited configuration and a decrease in the monopole part are large enough to make the corresponding intruder excitation energetically favorable.

Making use of the monopole Hamiltonian, defined before, the shell-model Hamiltonian of Eq. (1) can be partitioned as follows:

$$\hat{H} = \hat{H}_{\mathrm{mon}} + \hat{H}_M, \quad (4)$$

in which $\hat{H}_M$ contains all other multipole components (quadrupole, octupole, etc., and also pairing).

Even though the Hamiltonians of Eqs. (1) and (4) are equivalent, the latter representation is a good starting point in order to study the interplay between (i) the presence of energy gaps at the Fermi level, and, in particular, its variation with proton and neutron number moving away from the region of $\beta$ stability, described by $\hat{H}_{\mathrm{mon}}$; and (ii) the strong correlations among the valence nucleons that result from, in particular, pairing and the lower multipoles such as the quadrupole proton-neutron interactions, described by $\hat{H}_M$.

In most large-scale shell-model calculations, single-particle energies and two-body effective interactions are fixed for a given mass region and model space (one or more major shells relative to the well-known closed shells). Then solving the eigenvalue problem for the Hamiltonian of Eq. (1) needs a basis that follows from a repartition of the valence nucleons over the available single-particle orbitals in the model space. Powerful shell-model codes have been constructed over the years and work either in the $m$ scheme of Slater determinants (ANTOINE) or in an angular-momentum $J$-coupled basis (NuShell and NuShellX, NATHAN) (Caurier, Nowacki, and Poves, 2005; Brown and Rae, 2007).

### 1. Doubly closed shell nuclei

The first question that arises in the study of shape coexistence has to do with the stability of the well-known doubly closed shell nuclei, such as $^{16}$O and $^{40}$Ca, in which a $0^+$ state appears as the first-excited state at 6.05 and 3.35 MeV, respectively, against many-particle many-hole excitations ($m$p-$n$h). The issue of a stable shell closure against these excitations is critical in order to make the nuclear shell-model tractable (Caurier *et al.*, 2005).

In order to provide an answer to the question whether a given shell closure is well preserved in a given nucleus, one has to extend the shell-model basis considerably with many more configurations relative to an inert core. We illustrate this point by studying, e.g., $^{40}$Ca and ask how well this appears to be a doubly closed shell nucleus with fully occupied $1s_{1/2}$, $1p_{1/2,3/2}$ and $2s_{1/2}$, $1d_{3/2,5/2}$ orbitals for both protons and neutrons.

Calculations by Caurier *et al.* (2007), allowing for up to 10p-10h excitation from the upper part of the $sd$ shell ($2s_{1/2}$, $1d_{3/2}$ orbitals) into the full $fp$ shell have put a useful benchmark on the appearance of deformed coexisting configurations. Figure 1 shows the energy of the lowest $0^+$ unperturbed $n$p-$n$h configurations (dashed lines). Here the diagonal energies $n\hbar\omega$ have been corrected for the $fp$ monopole interaction energy, expressed by $V_1$, and the $(2s_{1/2}, 1d_{3/2}) - fp$ monopole interaction energy, expressed by $V_2$ [see Eqs. (2) and (3)], resulting in the energy

$$E_{\text{unpert},n} = n\hbar\omega + \tfrac{1}{2}n(n-1)V_1 + n(12-n)V_2, \qquad (5)$$

where $n$ denotes the number of particles in the $fp$ shell. The lowest $0^+$ eigenvalues, resulting from diagonalizing the Hamiltonian in each $n$p-$n$h subspace separately, are given by the full lines.

Here one notices that the lowest 4p-4h and even 8p-8h $0^+$ states, which lie at a high unperturbed energy because of the energy "cost" to construct such configurations, can be lowered and even occur at almost the same excitation energy. It is only after including the interaction and coupling the different $n$p-$n$h subspaces that the experimental spectrum of $0^+$ states is reproduced with spherical, deformed, and even superdeformed bands [the higher-spin states have been shown to agree well with the data as can be seen in Caurier *et al.*
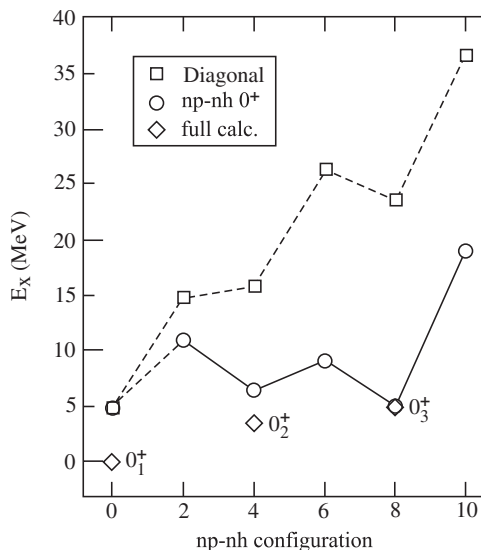


FIG. 1.   Energies for the different $n$p-$n$h configurations in the Ca isotopes. Open squares (dashed lines) correspond to the lowest $0^+$ unperturbed $n$p-$n$h configuration corrected for the monopole interaction energy (see text), the open circles (full lines) correspond to the lowest $0^+$ state from diagonalizing in the $n$p-$n$h subspaces separately, and the diamonds show the three lowest-lying $0^+$ states from the fully mixed calculation. From Caurier *et al.*, 2007.

(2007)]. The experimental levels of $^{40}$Ca, highlighting, in particular, the deformed bands, are shown in Fig. 41. We mention that these calculations result in a shell closure at $Z = 20$ and $N = 20$ varying between 65% and 75% . The values of $V_1$ and $V_2$ influence the closed-shell component, and in order to reproduce the experimental $0^+_{2,3}$ a different set of $V_1$ and $V_2$ can bring this percentage up to 75% without invoking important changes to all calculated properties.

Similar shell-model calculations have been performed for $^{16}$O, $^{36}$Ar, and $^{56}$Ni (Caurier, Nowacki, and Poves, 2005; Horoi *et al.*, 2006) with much the same conclusions. In the latter case, full $fp$ calculations have been performed allowing for the excitation of all 16 particles from the completely filled $1f_{7/2}$ orbital, which serves as the reference in the naive shell-model approach to describe $^{56}$Ni, into the upper orbitals of the $fp$ shell (Horoi *et al.*, 2006). Similar to the situation in $^{40}$Ca, 4p-4h excitations show up forming a low-lying coexisting band extending up to high spin.

We note here that near degeneracies of intrinsic state energies for many-particle many-hole deformed states were shown to result from deformed Hartree-Fock calculations using Skyrme effective interactions in $^{40}$Ca about 20 years ago by Zheng, Berdichevsky, and Zamick (1988a, 1988b). The possibility of associating a 12p-12h intrinsic band in $^{40}$Ca with a molecular resonance in the reaction $^{20}$Ne + $^{20}$Ne was raised by Zheng, Zamick, and Berdichevsky (1990). In these papers the question was raised whether or not these surprising degeneracies might lead to some underlying symmetry.

Besides carrying out these large-scale shell-model calculations, as discussed before, Rowe, Thiamova, and Wood (2006) and Thiamova, Rowe, and Wood (2006) showed that, starting from a spherical harmonic oscillator basis and using a quadrupole-quadrupole residual interaction, the unperturbed excitation energy for a given $n$p-$n$h excitation, which is $n\hbar\omega$, can gain a large amount of correlation energy for SU(3) configurations of maximum weight, given by

$$E_{LM}^{N(\lambda,\mu)} = \left\{ [N(n\text{p-}n\text{h}) - N_0] \right.$$
$$\left. - \frac{\langle N(\lambda, \mu); LM \mid \hat{C}_{\text{SU}(3)} \mid N(\lambda, \mu); LM \rangle}{4N_0} \right\} \hbar\omega.$$
$$(6)$$

Here $N(n\text{p} - n\text{h})$ and $N_0$ denote the number of oscillator quanta in the $n$p-$n$h configuration and the closed-shell reference state, respectively, $\hat{C}_{\text{SU}(3)}$ is the SU(3) Casimir operator, and $\lambda$ and $\mu$ are the SU(3) quantum numbers. Even though the model is schematic, the resulting energy gain over the unperturbed $n$p-$n$h energy is essentially identical to the energy gain obtained in the shell-model calculation, discussed above. This emphasizes the large energy gain for U(3) lowest-grade states (Rowe, Thiamova, and Wood, 2006), i.e., producing low-lying shape-coexisting states.

### 2. Single-closed shell nuclei: $N = 20$ and $N = 28$

Experimental evidence has shown that for a number of nuclei situated in the $sd$ shell, with neutron number at the supposedly closed-neutron shell $N = 20$ (e.g., Na, Mg, Al), the $S_{2n}$ values point toward a zone of increased binding energy. Calculations (mainly by the Strasbourg-Madrid

group), incorporating 2p-2h neutron excitations across the $N = 20$ shell, have been carried out and show that the energy of these configurations could indeed drop and even cross the regular $0\hbar\omega$, $N = 20$ closed-shell configuration, resulting in a different structure appearing at low excitation energy (Caurier *et al.*, 1998). This is illustrated in Fig. 2 for the Mg nuclei in which the monopole gap, which is related to the gap in the single-particle spectrum appearing between the filled *sd* shell and the unfilled *fp* shell, is shown.

Figure 2 shows that a minimum in energy is reached at $N = 20$, increasing when adding neutrons to the *fp* shell-model orbitals. Next, the correlation energy $\Delta(E)_{\text{corr}}$, defined as

$$\Delta(E)_{\text{corr}} = \langle (2\text{p-}2\text{h}); 0^+ \mid \hat{H} \mid (2\text{p-}2\text{h}); 0^+ \rangle$$
$$- \langle (0\text{p-}0\text{h}); 0^+ \mid \hat{H} \mid (0\text{p-}0\text{h}); 0^+ \rangle, \quad (7)$$

is shown and gives the extra binding energy within the truncated spaces, as a result of creating a 2p-2h neutron excitation relative to a closed $N = 20$ core. It is immediately clear that the intruder configuration, in particular, at and near to $N = 20$, corresponds to a more correlated state compared to the $0\hbar\omega$ states. Thus, low-lying 2p-2h intruder configurations are favored only at and near to the $N = 20$ neutron shell closure.

Similar shell-model calculations have been performed at the $N = 28$ shell closure, incorporating 2p-2h neutron

excitations from the $1f_{7/2}$ into the higher-lying *pf* orbitals. Results are obtained from the $Z = 28$ doubly closed shell $^{56}$Ni nucleus, down to the $Z = 12$, 14, neutron-rich, Mg and Si nuclei (Caurier, Nowacki, and Poves, 2004).

The results of the $N = 20$ and $N = 28$ regions can be combined and are shown in Fig. 3, in which the energy of the lowest $0^+$ 2p-2h intruder configuration is given relative to the $0\hbar\omega$ reference energy. It is clear that at $N = 20$ a zone of "inversion" appears in which the intruder configuration becomes the lowest-lying state. Here we point out that the large drop and "flat" behavior in energy of the $0_2^+$ intruder states fits well with the schematic analysis of intruder $0^+$ states described in Sec. II.A.3.a, and more, in particular, in Fig. 4. In Fig. 4, one observes a rather flat variation of the intruder excitation energy as a function of $N$ (or $Z$).

For the $N = 28$ isotones, on the other hand, the stability of $^{48}$Ca inhibits the formation of such an inversion but allows for low-lying intruder $0^+$ states in $^{52}$Cr. However, moving to the neutron-rich $N = 28$ nuclei, it shows that for $^{40}$Mg and $^{42}$Si, an inversion appears, mainly because of the large correlation energy and the almost constant monopole energy for $Z \leq 20$. Mixing is needed to obtain a more realistic description in the $N = 28$ region, which requires large-scale shell-model calculations with, for $Z \leq 20$, a valence space that consists of the full *sd* shell for the protons and the *pf* shell for neutrons. For $Z > 20$, the full *fp* shell for both protons and neutrons has been used (Caurier, Nowacki, and Poves, 2004).

The first set of conclusions following from the above shell-model studies is the fact that, if one enters a region of nuclei with a number of valence protons and a closed-neutron shell or subshell, one has to consider the balance between, on one side, the tendency to stabilize nuclei in a spherical shape for $0\hbar\omega$ configurations, and, on the other side, the deformation-driving tendency when allowing the closed shells to be broken with the subsequent formation of 2p-2h, etc. configurations.

One can deduce an approximate expression for the correlation energy which varies as $n_{\text{val}} \Delta n_{\text{p-h}}$ with $n_{\text{val}}$ the number of valence nucleons outside of the closed shells and $n_{\text{p-h}}$, the number of particle-hole pairs excited across the closed shell. Such a dependence results when the residual proton-neutron
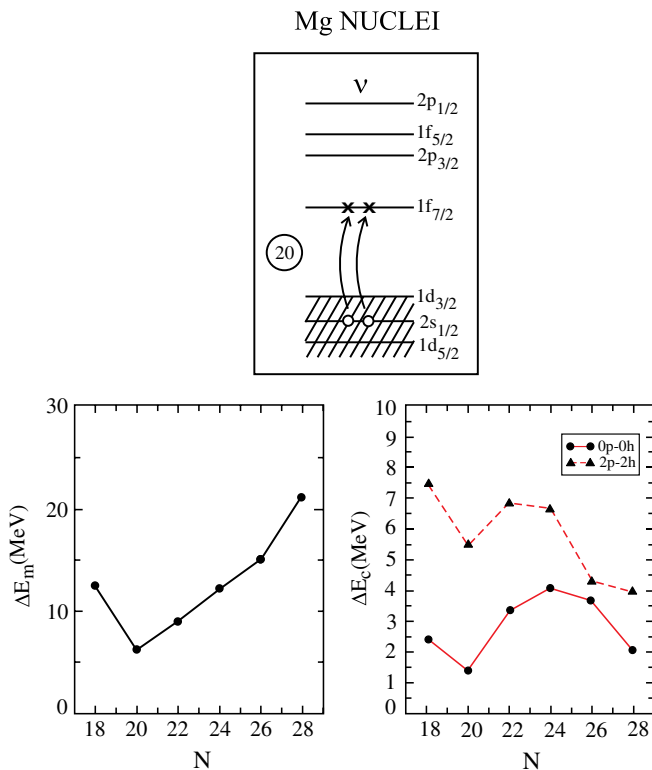


FIG. 2 (color online). Schematic view of the 2p-2h neutron excitations from the *sd* shell into the *fp* shell (upper panel). In the lower part, the energy gap which equals the difference of the monopole energy for the normal and 2p-2h intruder $0^+$ configuration (left panel) and the correlation energy in the normal and 2p-2h intruder $0^+$ configuration [as derived from Eq. (7)] (right panel) are given for the Mg ($Z = 12$) nuclei. From Caurier *et al.*, 1998.
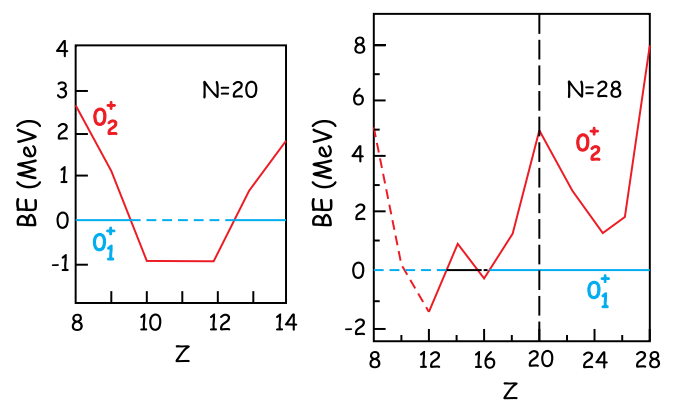


FIG. 3 (color online). Relative position of the lowest normal and lowest neutron 2p-2h intruder $0^+$ states, resulting from diagonalizing in the separate subspaces. From Caurier *et al.*, 1998, and Caurier, Nowacki, and Poves, 2004.
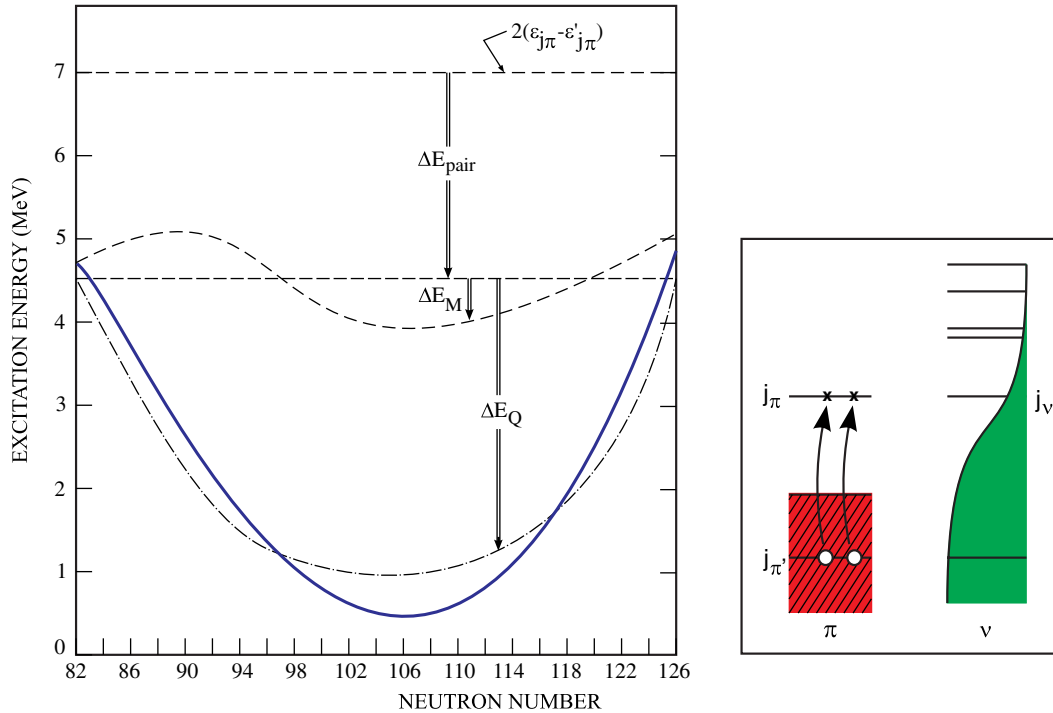
FIG. 4 (color online).   The different energy terms, contributing to the energy of the lowest proton 2p-2h $0^+$ intruder state for heavy nuclei. On the right-hand side, a schematic view of the excitation is given. On the left-hand side, the unperturbed energy, the pairing energy, the monopole energy shift, and the quadrupole energy gain are presented, albeit in a schematic way.

interaction is approximated by a separable quadrupole-quadrupole force and using the technique described by Heyde *et al.* (1987).

To quote Brown (2002) "These correlated ground states might be misinterpreted in terms of shell quenching where the actual spherical gap vanishes. The gap may become smaller in these situations, but the essential physics is in the pairing and deformed correlations."

### 3. Heavy nuclei: The Sn ($Z = 50$) and Pb ($Z = 82$) regions

It is clear that, even though the nuclear shell model contains the correct ingredients to describe the balance between closed shells, low-lying intruder states, and even inversions of $n$p-$n$h configurations relative to the $0\hbar\omega$ closed-shell configuration, such calculations cannot be carried out for nuclei heavier than mass $A = 80$ in the framework of the nuclear shell model because the model spaces are too large. Inevitably, one has to restrict the model spaces, however, keeping the essential physics content, if one intends to progress and reach the Sn and Pb nuclei in which, in particular, for the latter region and during the last decade, a major step forward has been made in studying the neutron-deficient isotopes (see Sec. III).

In this section, we discussed a truncation of the full shell-model space to the use of nucleon pairs, built from realistic collective $J = 0$ ($S$ pair) and $J = 2$ ($D$ pair) pairs, only. This truncation allows one to concentrate on low-lying quadrupole excitations. We also discuss the fact that one needs to include pair excitations across (sub)shells in order to describe shape coexistence in heavy nuclei. Along this line, we present a schematic model that accounts for the generic nucleon number $N$ (or $Z$) dependence of intruder $0^+$ excitations. The

interacting boson model (IBM) serves as a phenomenological approach to describe both regular and intruder states on equal footing. Applications to Cd and Pb nuclei, using the IBM approach, are also presented.

*a. Shell-model truncation: S and D pair shell model and the sd interacting boson model*

One of the major problems in keeping with the standard shell-model approach is the fact that all possible partitions of the number of active protons and neutrons over the chosen model space have to be considered. A crucial step is to truncate the shell-model basis into a subspace that allows us to treat low-lying quadrupole excitations and intruder excitations moving across closed shells (or subshells). An approach that starts from a nucleon-pair approximation to the full shell-model space, i.e., the nucleon-pair shell model (NPSM), was proposed by Chen (1997). Here the building blocks of the model are realistic collective pairs with $J = 0, 2, \ldots$.

What remains difficult, even in the NPSM, is the way to introduce $n$p-$n$h nucleon-pair excitations across the known closed shells. In Secs. II.A.1 and II.A.2, it was shown that these across-shell excitations are essential to describe intruder states and shape coexistence. Extending the model space brings the NPSM to its limits. It is, in particular, the fact that the Pauli principle has to be treated exactly, since we are using fermions, which causes the calculation time to grow quickly with the number of valence particles and $n$p-$n$h excitations.

The interacting boson model, on the other hand, approximates the quadrupole collective subspace of the full shell-model space by using $s$ and $d$ bosons only. This has been

amply discussed by Iachello and Arima (1987), Iachello and Van Isacker (1991), and Frank and Van Isacker (1994).

In order to include the effect of intruder excitations and related shape coexistence (described via $n$p-$n$h nucleon-pair excitations) or the presence of inversion of less and more strongly deformed states, within the $sd$-boson model approach, we have to extend the standard way of counting bosons as nucleon pairs outside of a closed shell by also explicitly taking into account the pair excitations across the closed shell. This was first introduced by Duval and Barrett (1981, 1982), making no explicit distinction between the particlelike or holelike character of the bosons. The drawback is the fact that experimental information on intruder states is needed in order to constrain some of the parameters in the model, thereby restricting predictions in unexplored mass regions. This approach was later applied to various mass regions for heavy nuclei (see Sec. II.A.3.b for more details). The idea of particlelike and holelike bosons has been introduced and it was demonstrated that they can be handled using a formalism much like isospin, called intruder ($I$) spin (Heyde et al., 1992; De Coster et al., 1996b, 1997, 1999; Lehmann et al., 1997, and see Fig. 25).

As shown before (Heyde et al., 1987; Wood et al., 1992), if one allows the formation of proton 2p-2h excitations across the closed core, e.g., $Z = 50$ for the Sn nuclei, $Z = 82$ for the Pb nuclei, it is possible to derive a simple expression for the energy of the lowest-lying intruding (or shape coexisting) $0^+$ states. The idea is illustrated in Fig. 4.

In the specific case of 2p-2h proton excitations, the energy expression of the lowest $0^+$ intruder configuration can be derived as

$$E_{\text{intr}}(0^+) = 2(\varepsilon_{j_\pi} - \varepsilon_{j'_\pi}) - \Delta E_{\text{pair}} + \Delta E_M + \Delta E_Q, \qquad (8)$$

where the first term describes the unperturbed energy needed to create a 2p-2h configuration (defined by the energy of the proton single-particle orbitals), the second term describes the pairing energy gain ($0^+$ pair states are formed as the lowest-lying ones), the third term describes the monople correction to the proton single-particle energy (which is changing with changing neutron number), and the fourth term describes the proton-neutron quadrupole binding energy. Using the fermion S and D pair truncation (see Sec. II.A.3.a), and perturbation theory, an expression for $\Delta E_Q$ can be derived (Heyde et al., 1987). Using the SU(3) approximation to describe the partition of S and D pairs in the intruder configuration and using the interacting boson model approximation (IBM-2), mapping the S and D pairs into $s$ and $d$ bosons, a simple expression for the quadrupole energy gain can be derived as

$$\Delta E_Q \simeq 4\kappa_0 \sqrt{\Omega_\pi - N_\pi} \sqrt{\Omega_\nu - N_\nu} N_\nu, \qquad (9)$$

where $N_\rho$ ($\rho = \pi, \nu$) is the number of valence proton and neutron pairs outside of the closed shells and $\Omega_\rho$ ($\rho = \pi, \nu$) are the degeneracies corresponding to the proton and neutron orbitals for the relevant mass region.

*b. Applications of shell-model "truncations"*

The approach, including explicitly 2p-2h, 4p-4h, etc., pair excitations across the $Z = 50$ and $Z = 82$ closed shells, using a truncation to a boson model space containing $N$ and also $N + 2$, $N + 4, \ldots$ bosons, has been used to study shape-coexisting states in both the Sn and Pb regions.

In the Sn region, most applications have been aimed at understanding the extra low-spin $0^+, 2^+, \ldots$ states at low excitation energy in the even-even Cd nuclei (Jolie and Heyde, 1990; Heyde et al., 1995; Jolie and Lehmann, 1995; Lehmann and Jolie, 1995; De Coster, Decroix, and Heyde, 1996; Lehmann et al., 1997). There has been an attempt to also study the even-even Te nuclei, but the results reached were not conclusive with regard to the presence of intruder bands (Rikovska et al., 1989). The manifestation of shape coexistence in the Sn region is discussed in Sec. III.

We emphasize here the Pb isotopes which form a unique "laboratory" in which almost all degrees of freedom show up, from typical shell-model nuclei with a few neutron holes being active inside the $N = 126$ closed shell, to the midshell region with the unexpected appearance of collective bands. The presence of a variety of nuclear shapes in the Pb region was proposed by Nazarewicz (1993). The whole Pb region is a beautiful example of shape coexistence as discussed in Sec. III.A.1.

The method to incorporate 2p-2h and 4p-4h excitations has been applied to the Pt, Hg, Pb, and Po nuclei. Early calculations (Duval and Barrett, 1981, 1982; Barfield et al., 1983; Barfield and Barrett, 1984) concentrated on Hg nuclei, where the first evidence for shape-coexisting bands was experimentally shown to exist. The concept of $I$-spin symmetry (De Coster et al., 1997) was instrumental in allowing calculations to be carried out in the Pb region (Fossion et al., 2003; Hellemans et al., 2005; Hellemans, Baerdemacker, and Heyde, 2008). The results give rise to shape-coexisting bands of 2p-2h and 4p-4h character mainly near the neutron $N = 104$ midshell region (see Sec. III for a discussion of the experimental data). The issue of shape coexistence in the Pt nuclei has also been addressed, in particular, by Harder, Tang, and Isacker (1997) and, recently, by Frank, Van Isacker, and Vargas (2004), McCutchan, Casten, and Zamfir (2005), Morales et al. (2008), McCutchan et al. (2008), and Garcia-Ramos and Heyde (2009) (see also remarks in Sec. III.C.6). Likewise, calculations for the Po nuclei have been carried out, also based on the use of $I$-spin symmetry (De Coster et al., 1999; Oros et al., 1999).

### B. Mean-field approach

In the mean-field approach, the motion of nucleons as independent (quasi)particles is derived starting from effective forces and using self-consistent Hartree-Fock(-Bogoliubov) [HF(B)] theory. The effective forces used have been tuned to describe global nuclear properties such as charge radii and ground-state binding energies throughout the nuclear mass surface, encompassing spherical nuclei, near closed shells (Vautherin and Brink, 1972), and deformed nuclei (Vautherin, 1973). Minimizing the Hartree-Fock energy, under the constraint of keeping a number of nuclear multipole moments fixed, can be performed over a range of collective parameters (quadrupole, octupole, etc.). Most often, this results in a deformed nuclear shape (see Fig. 5). Bender, Flocard, and Heenen (2003) recently reviewed self-consistent mean-field models.

The main ingredients in the self-consistent mean-field approach encompass the following:

(i) A nucleon-nucleon effective interaction has to be chosen so that the behavior of the nuclear binding energy is well described throughout the whole nuclear mass region, covering spherical nuclei near closed shells as well as deformed nuclei. In recent studies, the interactions used go back to the seminal work of Skyrme (Skyrme, 1956, 1959a, 1959b) and Gogny (Gogny, 1973, 1975; Dechargé and Gogny, 1980).

(ii) The single-particle wave functions and the corresponding occupation probabilities are derived self-consistently through a variational method applied to the energy, with the addition of constraints on multipole moments and pairing properties describing the nucleus.

(iii) The nuclear many-body wave function is built from independent (quasi)particle states.

(iv) Restoration of the symmetries that are broken in the intrinsic frame. This can be performed by projecting the mean-field states onto fixed particle number $(N, Z)$, isospin $(T)$, and angular momentum $(J)$.

The equations describing the mean-field properties are the well-known HFB equations, or an approximate set of HF+BCS equations when a two-step procedure is used in which the particle-hole correlations are considered in the first step (solving the HF equations), and the particle-particle pairing correlations are put in afterward (solving the BCS equations). From the solutions, one can construct a set of HFB (or HF+BCS) wave functions $| \Phi(q) \rangle$ generated in a self-consistent way in which the collective constraining coordinate $q$ acts as a semiclassical parameter (most often quadrupole deformation). As a consequence, the intrinsic state breaks a number of basic symmetries of the exact many-body states as defined in the laboratory frame. Therefore, one has to restore these broken symmetries by projecting the mean-field states onto a fixed $N$, $Z$, $T$, and $J$ to produce physical states $| J, M; q \rangle$ [see Bender, Flocard, and Heenen (2003) for technical details].

Figure 6 shows the decomposition of the energy of $^{186}$Pb, starting from the $(Z = 82, N = 104)$ number-projected energy (the small dotted line, also marked "Mean-field"), into its various $J$ components $(J = 0, 2, \ldots, 10)$ (various types of dashed lines). The energies are normalized to the particle-number-projected energy where the minimum appears for the spherical state. Both the prolate (positive $q \equiv \beta_2$ values) and oblate (negative $q \equiv \beta_2$ values) $J$-projected energy curves are shown. The energy difference for these $J$ curves corresponds to the rotational energy of the mean-field states. This is a particularly interesting example, discussed in Sec. III, for the Pb mass region.

Inspecting Fig. 6, one notices that for a given energy one cannot uniquely specify a given mean-field projected state. In order to obtain a genuine energy spectrum that can be compared with experimental data, one should go beyond the mean-field approach and diagonalize the Hamiltonian $\hat{H}$ in the space $\{| JM; q \rangle\}$ of projected states. It is the parameter $q$ that acts as a general collective coordinate that will generate the optimal superposition of projected mean-field states denoted as

$$| JM; k \rangle = \sum_q f_{J,k}(q) | JM; q \rangle, \tag{10}$$

where $f_{J,k}(q)$ are weight functions to be determined from the stationarity condition for the generator coordinate ground state [also called the GCM method, see Chap. 10 in Ring and Schuck (1980)]

$$\frac{\delta}{\delta f_{J,k}^*} \frac{\langle JM; k | \hat{H} | JM; k \rangle}{\langle JM; k | JM; k \rangle} = 0. \tag{11}$$

This variational method leads to the Hill-Wheeler-Griffin equations (Hill and Wheeler, 1953; Griffin and Wheeler, 1957) that determine the eigenstates $| JM; k \rangle$ and corresponding energy eigenvalues $E_{J,k}$:

$$\sum_{q'} [\langle JM; q | \hat{H} | JM; q' \rangle - E_{J,k} \langle JM; q | JM; q' \rangle] f_{J,k}(q') = 0. \tag{12}$$

For each value of $J$, the angular-momentum projected GCM method results in a correlated "ground state" and, in addition, a set of excited states from orthogonalization to the ground state [the weight functions $f_{J,k}(q)$ do not form an
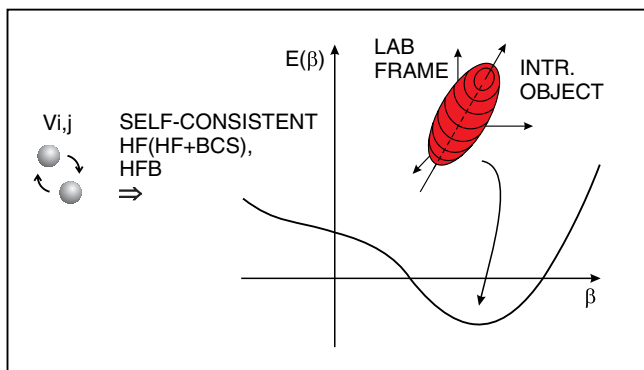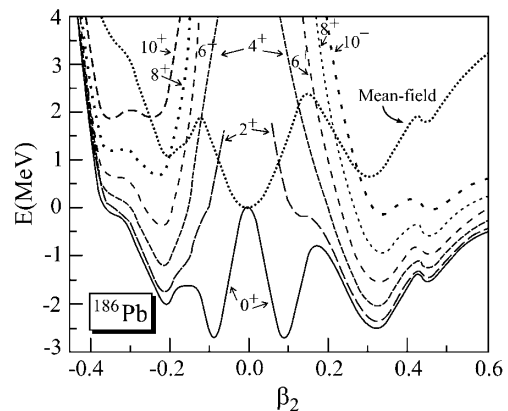


FIG. 5 (color online). Illustration of the energy surface $E(\beta)$ for a single collective parameter (quadrupole deformation $\beta$) which follows from self-consistent Hartree-Fock-(Bogoliubov) calculations.



FIG. 6. Particle-number projected mean-field (small dotted curve and marked as "Mean-field") as well as the particle- and angular-momentum projected energy curves (full, long-dashed, etc. lines), up to spin $J = 10$ for $^{186}$Pb, as a function of the quadrupole deformation variable $\beta_2$. From Duguet et al., 2003.

orthogonal set and are coherent states]. The correct collective wave function can be expressed in the basis of the intrinsic states by the transformation $g_{J,k}(q) = \langle JM; k \mid JM; q \rangle$.

For the nucleus $^{186}$Pb, discussed in Fig. 6, the GCM method results in the energy spectrum shown in Fig. 7. In this figure, the projected energy curves are drawn again as a reference. This allows us to make a presentation of the resulting energy spectrum, because the collective wave functions $g_{J,k}(q)$ exhibit a given spread around the maximum probability. The bars represent the energies $E_{J,k}$ for each of the states that are plotted at the mean deformation $\bar{q}_{J,k}$ in the intrinsic frame and are defined as

$$\bar{q}_{J,k} = \int g_{J,k}^2(q) q dq. \qquad (13)$$

Thus, not only can the energy spectrum (now normalized to the lowest $J^\pi = 0^+$ state) be seen, but at the same time information about the value of the collective quadrupole parameter $q$ is apparent.

Many calculations have been carried out during the last decades either starting from Skyrme forces [the recent studies make use of the SLy4 or SLy6 (Chabanat *et al.*, 1998) for the particle-hole channel to which a density-dependent delta pairing for the particle-particle channel (Rigollet *et al.*, 1999) has been added] or starting from the Gogny force. Recent studies using the Gogny force make use of the D1S parametrization (Berger, Girod, and Gogny, 1984, 1991). In view of the manifestation of shape coexistence, discussed in depth in Sec. III, throughout the nuclear mass surface, we present here the relevant references. The references in the next two paragraphs use either Skyrme forces or the Gogny D1S interaction to calculate configuration mixing of angular-momentum and particle-number-projected mean-field states by means of the GCM.

Skyrme forces have been applied to the study of light nuclei starting from a HF+BCS approach for $^{24}$Mg (Valor, Heenen, and Bonche, 2000; Bender and Heenen, 2008), $^{32}$S, $^{36}$Ar, $^{38}$Ar, and $^{40}$Ca (Bender, Flocard, and Heenen, 2003), the neutron-deficient Kr nuclei (Bender, Bonche, and Heenen,



FIG. 7. Energy spectrum for the lowest-lying positive-parity bands in $^{186}$Pb with even angular momentum $J$ and $K = 0$ as a function of the quadrupole deformation parameter $\beta_2$. The particle- and angular-momentum projected energy curves are given as a reference. The excitation energy is derived from measuring the energy relative to the energy of the $0_1^+$ ground state. From Duguet *et al.*, 2003.

2006), and the neutron-deficient Pb nuclei (Heenen *et al.*, 2001; Bender *et al.*, 2002; Duguet *et al.*, 2003; Smirnova, Heenen, and Neyens, 2003; Bender *et al.*, 2004; Bender and Heenen, 2005).

The finite-range Gogny force has been used, in particular, by the Madrid group, using the HFB approach, studying light nuclei such as $^{30,32,34}$Mg and $^{32,34,36,38}$Si nuclei (Rodríguez-Guzmán, Egido, and Robledo, 2000a), the $N \approx 20$ nuclei (Rodríguez-Guzmán, Egido, and Robledo, 2000b), the $N \approx 28$ nuclei (Rodríguez-Guzmán, Egido, and Robledo, 2002a), the Mg isotopes (Rodríguez-Guzmán, Egido, and Robledo, 2002b), a possible shell closure at $N = 32$ or $34$ (Rodríguez and Egido, 2007), nuclei in the Sn region (Anguiano, Egido, and Robledo, 2002; Rodríguez, Egido, and Jungclaus, 2008), a study of the rare-earth Nd nuclei (Rodríguez and Egido, 2008), and also the neutron-deficient Pb nuclei (Chasman, Egido, and Robledo, 2001; Egido, Robledo, and Rodríguez-Guzmán, 2004; Rodríguez-Guzmán, Egido, and Robledo, 2004).

More restricted self-consistent Skyrme Hartree-Fock plus BCS calculations have been carried out for the neutron-deficient Kr and Sr isotopes by Sarriguren (2009) and for the neutron-rich Yb, Hf, W, Os, and Pt nuclei (Sarriguren, Rodríguez-Guzmán, and Robledo, 2008). Calculations have been carried out for the Pd, Xe, Ba, Nd, Sm, Gd, and Dy rare-earth nuclei, aiming to study the evolution of the minima characterizing the energy surfaces (Robledo, Rodríguez-Guzmán, and Sarriguren, 2008). A recent study of the energy surfaces covering the full triaxial landscape was carried out by Rodríguez-Guzmán *et al.* (2010) for the even-even Pt nuclei.

A different approach in studying the dynamics of the full five-dimensional collective model (5DCH) results in the construction of a collective Bohr Hamiltonian in which the deformation dependence of the parameters (moments of inertia, mass parameters, and energy of the zero-point motion) is determined from microscopic self-consistent mean-field studies. It was shown that if the overlap of the mean fields at different values of the collective coordinate $q$ and $q'$, i.e., $\mathcal{I}(q, q') \equiv \langle \Phi(q) \mid \Phi(q') \rangle$, is *approximated* by a Gaussian overlap (GOA), a Taylor expansion up to second order in the nonlocality $q - q'$ of the Hill-Wheeler equation gives rise to a collective Schrödinger equation (Ring and Schuck, 1980; Bender, Heenen, and Reinhard, 2003). There has been quite some debate about which masses are to be used: the GCM +GOA masses (Peierls and Yoccoz, 1957) or the adiabatic time-dependent Hartree-Fock (ATDHF) masses (Thouless and Valatin, 1962). In most applications, the Inglis-Belyaev formula for the moments of inertia (Inglis, 1956; Belyaev, 1961) and the cranking approximation to calculate both the mass parameters associated with the $\beta$, $\gamma$ coordinates and the zero-point energy correction associated with the rotational and vibrational kinetic energy (Girod and Grammaticos, 1979) are used. As a consequence, these studies to solve the 5DCH can be regarded as a modern version of the model of Baranger and Kumar (Baranger and Kumar, 1968; Kumar, 1974).

Within this spirit, the Gogny force has been widely used solving the approximated 5DCH Schrödinger equation. Early calculations concentrated mainly on the collective potential
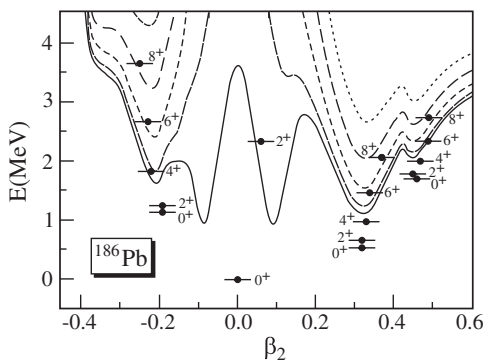
for some rare-earth nuclei and nuclei in the Pb region (Girod and Reinhard, 1982; Girod *et al.*, 1989). A more detailed study was carried out for the $^{190,192,194}$Hg nuclei by Delaroche *et al.* (1989). Recently, the full solution of the collective 5DCH has been studied within constrained HFB theory based on the Gogny D1S force. Studies in the Pb mass region have been carried out (Libert, Girod, and Delaroche, 1999), and also studying shell closure for light nuclei at $N = 16$ (Obertelli *et al.*, 2005) and for the $N = 20$ and $N = 28$ neutron-rich nuclei (Peru, Girod, and Berger, 2000) and the role of triaxiality in the light Kr nuclei (Girod *et al.*, 2009). An overview of low-lying collective properties over the whole mass region has been given, using the same methods, by Delaroche *et al.* (2010).

A different approach was proposed by Walecka who developed a relativistic mean-field formulation (RMF) (Walecka, 1974). A detailed discussion on the Lagrangians used is given in several review papers (Serot and Walecka, 1986; Reinhard, 1989; Serot, 1992; Ring, 1996). A study within the relativistic Hartree-Bogoliubov (RHB) framework was performed specifically concentrating on shape coexistence in the Pt-Hg-Pb nuclei (Nikšić *et al.*, 2002). Within the RMF approach, beyond-relativistic-mean-field studies were performed recently, also incorporating configuration mixing of mean-field wave functions projected onto angular momentum $J$ and particle number ($N, Z$), using the GCM approach, restricting to axially symmetric systems (encompassing vibrational and rotational degrees of freedom) with applications for $^{32}$Mg and $^{194}$Hg (Nikšić, Vretenar, and Ring, 2006a) (only $J$ projected) and for $^{24}$Mg, $^{32}$S, and $^{36}$Ar ($J$ and particle number projected) (Nikšić, Vretenar, and Ring, 2006b). Even more general studies have been performed using projected states starting from triaxial quadrupole constraints on the mean-field level with applications to the neutron-rich Mg nuclei (Yao *et al.*, 2009) as well as using the resulting three-dimensional relativistic mean-field wave functions in a GCM configuration mixing calculation (Yao *et al.*, 2010) with application for $^{24}$Mg. We mention that more restricted studies of potential energy surfaces, aiming at the study of triaxial ground-state shapes for the Sm and Pt nuclei, making use of the three-dimensional RHB model have been performed (Nikšić *et al.*, 2010) also.

Relativistic mean-field theory was also used to extensively study the 5DCH, starting from the relativistic energy density functional, and applied to the even-even Gd nuclei (Nikšić *et al.*, 2009) and recently to the study of even-even Ba and Xe nuclei (Li *et al.*, 2010).

## C. Similarities between shell-model and mean-field approaches

We come to the point that shell-model and mean-field approaches, if technically possible, lead to much the same physics. It seems clear that starting from a spherical mean field only, and getting both the advantages and disadvantages from the ensuing spherical closed-shell configurations near stability, one inevitably runs out of computer capabilities. Moreover, the model wave functions do not give genuine physics insight (billions of components). Still, this approach is a consistent and robust approach with strong predictive power, such that systematic deviations between experiment

and theory have to be taken seriously and cannot be hidden by parameter changes. On the other hand, making use of self-consistent mean-field methods, one starts from an effective nucleon-nucleon interaction in order to derive an optimized deformed (quadrupole deformation, pairing, etc.) basis $|\Phi(q)\rangle$. Whereas the shell-model space itself is a Hilbert space, the set of Slater determinants constitutes a geometrical surface within the Hilbert space [see Rowe and Wood (2010) for a more detailed exposition]. The mean-field method produces an energy surface which is semiclassical. As a consequence and in order to reach results to be compared with the data in nuclei, one needs to go beyond the mean-field approximation. Here the technicalities of projecting from the intrinsic frame to the lab frame, with good $J, N, Z, \ldots$ are demanding when exploring the full space of the $\beta$, $\gamma$ quadrupole variables. Moreover, one has to take into account mixing of the various intrinsic projected states in order to arrive at the exact eigenstates. Calculations starting from a spherical shell-model basis, or, using mean-field methods (applied to the Mg, S, and Zr istopes) resulted in a strong resemblance [see Reinhard *et al.* (1999) for a detailed discussion]. A particular example is $^{40}$Ca for which both the shell-model results (see Sec. II.A.1 and Fig. 1) and beyond-mean-field calculations (Bender, Flocard, and Heenen, 2003) are available.

## III. MANIFESTATION OF COEXISTENCE IN NUCLEI

The occurrence of energy gaps, due to spherical shells or subshells, and the mixing of the resulting proton and neutron configurations are the essential ingredients to a unified view of coexistence in nuclei. Figure 8 shows the regions of shape coexistence that are discussed in this review and their location with respect to magic numbers.

We present the experimental data that motivate this unified view in a particular order. We first review mass regions for which extensive data support the widespread and unequivocal manifestation of shape coexistence, i.e., the regions centered
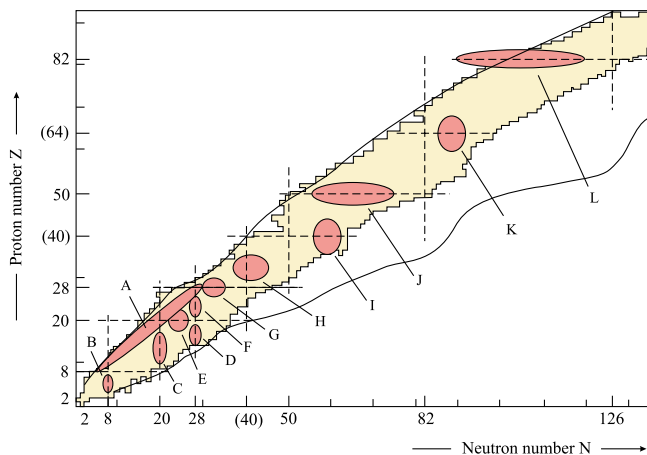


FIG. 8 (color online).   The main regions of nuclear shape coexistence discussed in Sec. III are shown in relationship to closed shells. Regions A, F: see Sec. III.B.1; regions B, C, D, and E: see Sec. III.B.2; region G: see Sec. III.A.8; region H: see Sec. III.A.5; region I: see Sec. III.A.3; region J: see Sec. III.A.2; region K: see Sec. III.A.4; and region L: see Sec. III.A.1.

on $(Z, N) \sim (50, 66)$ and, especially, $(82, 104)$, where the major shell gaps at 50 and 82 dictate the structures. This is followed by the $(Z, N) \sim (40, 60)$ region where subshell gaps are the cause of shape coexistence. We then present the $(Z, N) \sim (64, 90)$ region in terms of coexisting structures that strongly mix.

The presentation of phenomenology continues with key observations which support coexistence in some other mass regions in heavy nuclei, specifically, the $(Z, N) \sim (36, 40)$ region and another mass region $(Z, N) \sim (54, 70)$, where transfer reaction spectroscopic fingerprints suggest that future exploration is warranted.

We then turn to the issue of shape coexistence in light nuclei. It is in light nuclei that the phenomenon was first postulated, by Morinaga (1956), in $^{16}$O. We provide an updated view of nuclei around $^{40}$Ca and cover the newly established cases around $^{56}$Ni. It is also in light nuclei that some major surprises have emerged: specifically, for $(Z, N) \sim (4, 8)$, $(12, 20)$, and $(14, 28)$. We present some details of these active regions of investigation, with the caution that these are difficult regions to study and consequently the details are still incomplete and sometimes contradictory.

It appears that, without exception, low-lying excited $0^+$ states are associated with shape coexistence. The occurrence of $0^+$ states in nuclei has been the subject of many interpretations. There is no debate regarding their universal appearance as the ground states of doubly even nuclei: This is the result of residual pairing correlations which cause protons and neutrons to separately form $J = 0$ Cooper pairs (Bohr, Mottelson, and Pines, 1958; Brink and Broglia, 2005). The issue of excited $0^+$ states in doubly even nuclei is still a matter of open discussion (see Sec. III.C.3).

## A. Heavy and medium-heavy nuclei

### 1. $Z \sim 82$ nuclei

The neutron-deficient isotopes at and near $Z = 82$ exhibit the most extensive manifestation of shape coexistence known anywhere on the nuclear mass surface. However, the study of this region has been challenging because it is centered on isotopes that lie far from $\beta$ stability. Consequently, experimental investigations demanded the use of some of the most extreme methods ever developed for far-from-stability nuclear structure study.

The first indication of shape coexistence in this region was totally unexpected and came from optical hyperfine structure studies of the Hg isotopes and the observation of an enormous isotope shift between $A = 187$ and 185 (Bonn *et al.*, 1972). An up-to-date summary of isotope shift data is shown for the region in Fig. 9. The extreme staggering of the even-odd Hg isotope shifts was soon explained by in-beam spectroscopy (Rud *et al.*, 1973; Proetel, Diamond, and Stephens, 1974), and decay scheme spectroscopy (Hamilton *et al.*, 1975; Cole *et al.*, 1976) that revealed excited $0^+$ states upon which rotational bands are built. A summary of coexisting bands in the even-mass Hg isotopes is shown in Fig. 10. The observation of a set of collective bands, built on top of the intruder $0^+$ state with a minimum in the excitation energy near the neutron $N = 104$ midshell point, is in line with the general neutron number dependence as illustrated in Fig. 4.
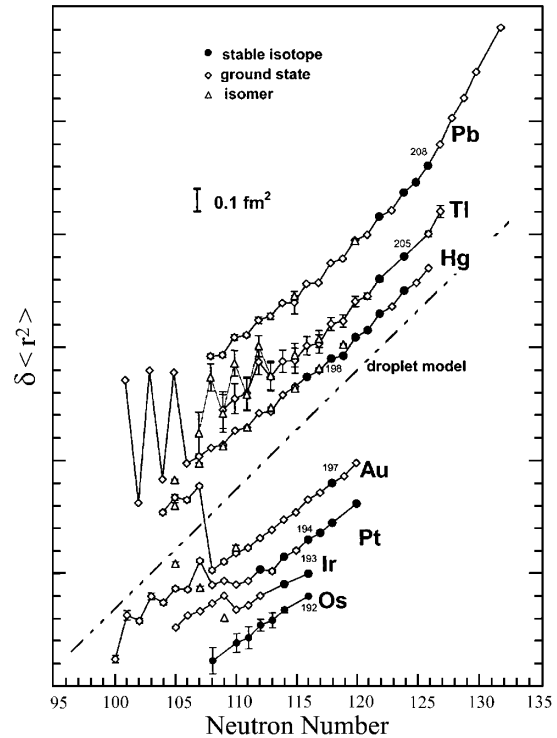


FIG. 9. Isotope shift systematics for the Os-Pb isotopes. The large increases and "staggering" in the $N \sim 104$ region are the result of states in these nuclei with different quadrupole deformations. Note particularly $^{185}$Hg, which possesses the largest known isomer shift. The trend in $\delta\langle r^2\rangle$ with $N$ (and therefore $A$) for a droplet model is shown. From Klüge and Nötershäuser, 2003.

Figure 9 illustrates a spectroscopic fingerprint that plays a leading role in the exploration of shape coexistence in nuclei. Isotope shift data are a model-independent view of nuclear structure (Otten, 1989). The increase in the mean-square charge radius between the ground states of $^{186}$Hg and $^{185}$Hg
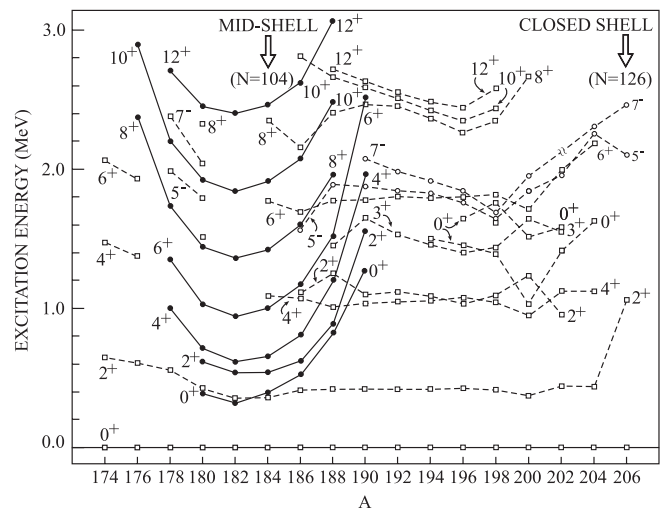


FIG. 10. Systematics of excited states in the even-Hg isotopes. Note the "parabolic intrusion" of the closely spaced bands of states (marked with solid lines) with $J = 0, 2, 4, \ldots$ centered on $^{182}$Hg ($N = 102$). The data are taken from Nuclear Data Sheets. Some recent lifetime data can be found in Grahn *et al.* (2009).

K=11⁻

high-K or high-M states

K=8⁻

J=12⁺

0⁺

0⁺

0⁺

0⁺ states
- ambiguous
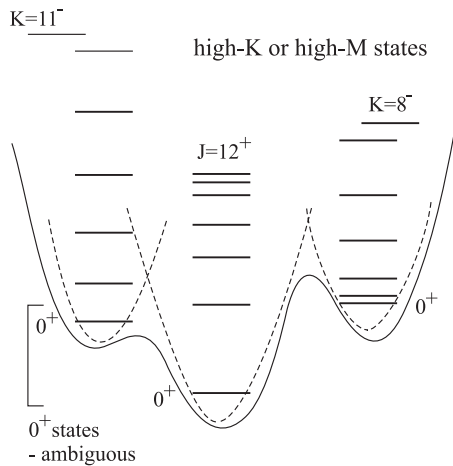
FIG. 11. Schematic view of characteristic states, in particular, emphasizing high-spin isomeric states, as indicators of shape coexistence ("high-*M*" should read "high-*J*"). From Dracoulis, 2000.

(isotope shift) and between the ground state and isomeric state of $^{185}$Hg (isomer shift) is directly related to large differences in nuclear deformation. The key prerequisite for a measurable mean-square charge radius is that the nuclear species, ground state or isomeric state, live long enough to be isolated for optical hyperfine spectroscopic measurements.

Further discussion of the structure of $^{185}$Hg and the fact that its neighbors do not have reported isomer shifts is taken up shortly. Other occurrences of large isotope and isomer shifts are described later.

The emerging picture in the Hg isotopes ($Z = 80$) (see Fig. 10) raised the question of the survival of the $Z = 82$ closed shell in this region. This led to intensive study of the even- and odd-Pb isotopes. A landmark paper was the observation of multiple low-lying excited $0^+$ states in $^{186}$Pb using $\alpha$-decay spectroscopy of $^{190}$Po (Andreyev *et al.*, 2000). The discovery of a spherical high-spin isomeric state and two deformed, high-*K* isomeric states in $^{188}$Pb was instrumental in characterizing the presence of coexisting nuclear shapes (Dracoulis, 2000) as shown in Fig. 11.

$\alpha$-decay spectroscopy, combined with in-beam $\gamma$-ray spectroscopy, particularly using recoil-decay tagging (Paul *et al.*, 1995), has led to a clear picture of coexisting states in the even- and odd-mass Pb isotopes (Julin, Helariutta, and Muikku, 2001) and is shown in Figs. 12 and 13, respectively.

Figure 12 reveals that three coexisting structures (cf. Fig. 11) occur systematically in the even-Pb isotopes. This can be discerned from the dashed lines connecting the various states in these isotopes. In $^{188}$Pb the two deformed structures are connected by $E0$ transitions (Dracoulis *et al.*, 2003) and in $^{194,196}$Pb one of the deformed structures and the spherical structure are connected by $E0$ transitions

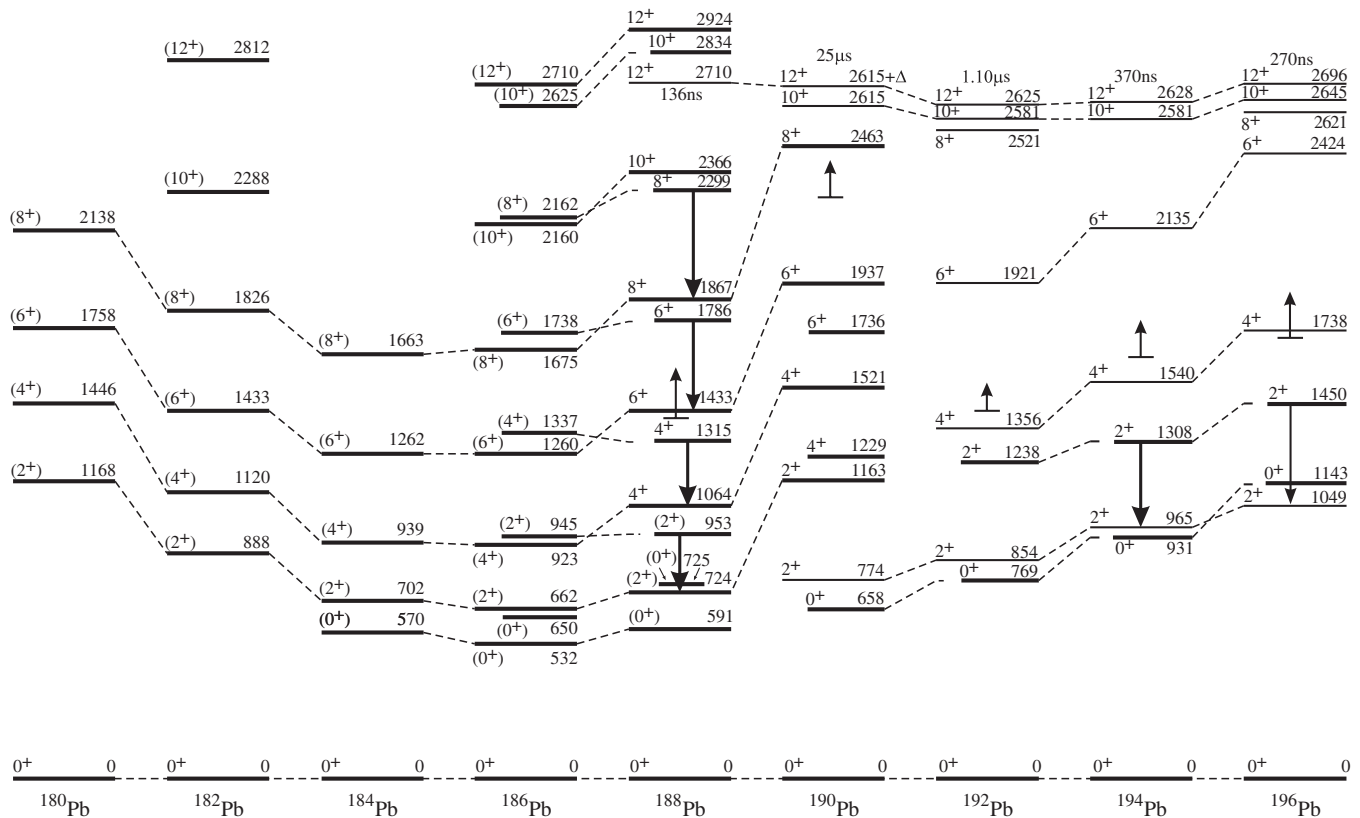FIG. 12. Systematics of excited states in the even-Pb isotopes. Note the parabolic intrusion of states centered on $^{186}$Pb ($N = 104$). Heavy downward arrows indicate states connected by $E0$ transitions. Upward pointing arrows indicate excitations above which states have been omitted. Lifetimes of the $J = 12$ seniority isomers are given: Note that this state coexists with intruder states in $^{188}$Pb, particularly with a *K* isomer shown in Fig. 23 (discussed further in the text). The data are from Julin, Helariutta, and Muikku (2001), Dracoulis *et al.* (2003, 2004), Pakarinen *et al.* (2007), Rahkila *et al.* (2010), and Nuclear Data Sheets. There are recent lifetime data for $^{188}$Pb (Dewald *et al.*, 2003; Grahn *et al.*, 2006, 2008) and $^{186}$Pb (Grahn *et al.*, 2006, 2008).

(Van Duppen *et al.*, 1985). There are currently few spectroscopic clues (see below) as to the nature of these coexisting structures.

Transitions with *E*0 components are a model-independent signature of the mixing of configurations with different mean-square charge radii (Heyde and Meyer, 1988; Wood *et al.*, 1999). Assuming two configurations, with mixing amplitudes *a* and $\sqrt{1-a^2}$, the expression for the strength of the *E*0 transition is given as (Wood *et al.*, 1999)

$$\rho^2(E0) = \frac{Z^2}{R_0^4}a^2(1-a^2)[\Delta\langle r^2\rangle]^2, \qquad (14)$$

with the nuclear radius $R_0 = r_0 A^{1/3}$ and $\Delta\langle r^2\rangle \equiv \langle r^2\rangle_1 - \langle r^2\rangle_2$. Knowing the experimental excitation energies and the experimental value of $\rho^2(E0)$, an estimate of the mixing matrix element and the energies of the unmixed configurations can be deduced. Currently, a lack of lifetime data for the requisite states in $^{188}$Pb precludes this.

The $K^\pi = 11^-$ isomer (cf. Fig. 11, not shown in Fig. 12), interpreted as an oblate intruder structure, has been systematically characterized by the measurement of its quadrupole moment in $^{196}$Pb (Vyvey *et al.*, 2002b) and $^{194}$Pb (Vyvey *et al.*, 2002a) using level-mixing spectroscopy and in $^{192,194}$Pb (Ionescu-Bujor *et al.*, 2007) using $\gamma$-ray time-differential perturbed angular distributions, and by *g* factor measurements in $^{194,196}$Pb (Vyvey *et al.*, 2004) and $^{188}$Pb (Ionescu-Bujor *et al.*, 2010). A review by Neyens (2003) discusses experimental methods and results for moments in this region in detail. Dracoulis *et al.* (2005) discussed the oblate

deformation of the $11^-$ isomers in $^{194,196}$Pb from the perspective of their *E*3 decay strengths.

Figure 13 shows coexisting structures in the odd-Pb isotopes, inferred from *E*0 transitions and $\alpha$-decay hindrance factors. Hindrance factors for an $\alpha$-decay branch to an excited state are defined in Van Duppen and Huyse (2000). The spin sequences in $^{195,197}$Pb indicate a decoupled $1i_{13/2}$ band; this supports an oblate deformation (Griffin *et al.*, 1991; Vanhorenbeeck *et al.*, 1991). The $\alpha$-decay hindrances reflect similarities between the $1i_{13/2}$ states in the Pb isotopes and the $1i_{13/2}$ parent states in the Po isotopes. The *E*0 transitions between the pairs of $1i_{13/2}$ states in the Pb isotopes indicate that these are mixed configurations, hence the similar $\alpha$-decay hindrance factors. A notable change has occurred for $^{187}$Pb: this is commented on shortly.

Because this mass region exhibits many $\alpha$-decaying isotopes, this has been used indirectly in recoil-decay tagging and as a spectroscopic fingerprint (Van Duppen and Huyse, 2000) for identifying "intruder" states. Following the first such use of $\alpha$-decay widths in the identification of odd-proton intruder states in the odd-Tl and odd-Bi isotopes (Coenen *et al.*, 1985), the method was extended to even-even nuclei (Van Duppen *et al.*, 1985). A concise summary of this "fingerprinting" of intruder states and shape coexistence is portrayed in Figs. 14 and 15. We also note a formalism (Wauters, Bijnens, Folger *et al.*, 1994; Van Duppen and Huyse, 2000; Xu and Ren, 2007) for extracting mixing of coexisting configurations from $\alpha$-decay widths.

Figure 14 illustrates the manner in which excited $0^+$ states can be observed far from stability if $\alpha$ decay occurs.
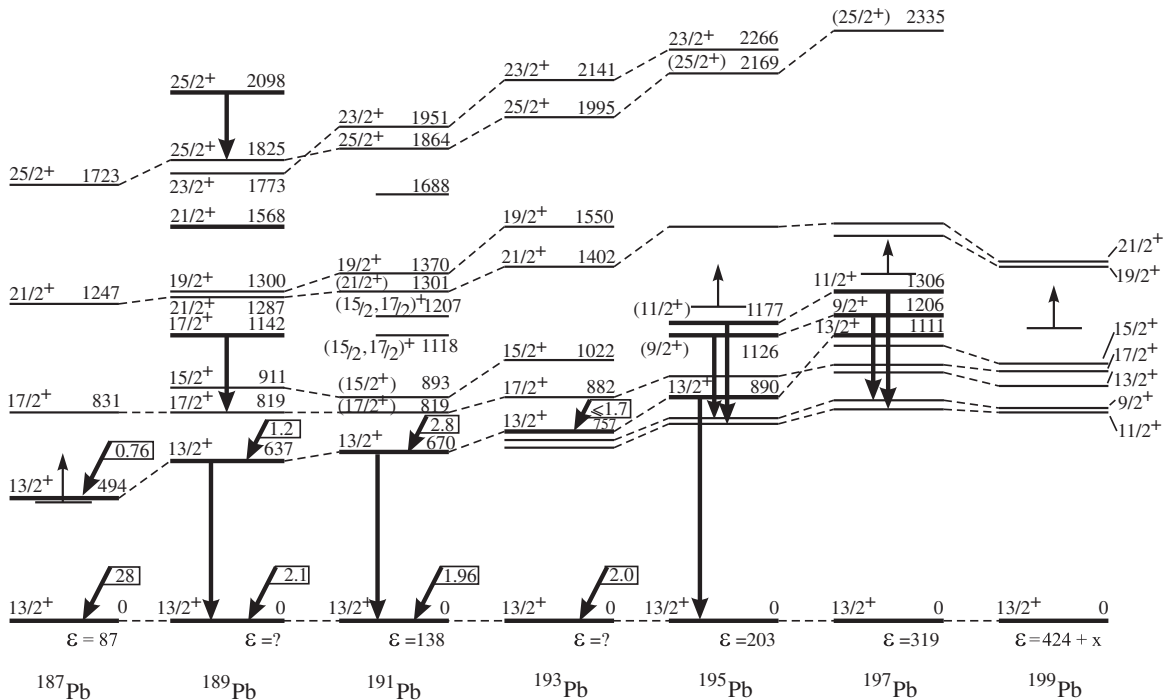


FIG. 13. Systematics of excited states in the odd-Pb isotopes. Heavy vertical downward arrows indicate states connected by *E*0 transitions. Diagonal arrows indicate states populated in $\alpha$ decay, with hindrance factors shown in the boxes. Vertical upward arrows indicate energies above which states with positive parity have been omitted. Dashed lines connect states with probable similar structures. The data are from Coenen (1985), Andreyev *et al.* (2002) ($^{187}$Pb $\alpha$-decay hindrance factors), Baxter *et al.* (2005), Dracoulis *et al.* (2009), Van de Vel *et al.* (2002) ($^{191,193}$Pb $\alpha$-decay hindrance factors), and Nuclear Data Sheets.

Generally, the population of excited $0^+$ states far from stability is extremely difficult because experimental probes are limited to in-beam reaction spectroscopy which only populates states near the yrast line (states with highest spin at lowest energy), and $\beta$ decay which predominantly populates states within $1\hbar$ of the spin of the parent nucleus. Although $\alpha$-decay branches decrease rapidly with increasing excitation in the daughter nucleus, by achieving high statistics in $\alpha$ spectroscopy, it is possible to elucidate vital excited $0^+$ state information.

Figure 14 shows how $\alpha$-decay hindrance factors may provide detailed spectroscopic information. The hindrance factors in the decay of $^{188}$Po to $^{184}$Pb reveal that the ground state of $^{188}$Po must be strongly deformed because of the large favoring of its decay to the strongly deformed excited $0^+$ state in $^{184}$Pb at 570 keV (cf. Fig. 12). In turn, the hindrance factor in the decay of $^{200}$Rn to the excited state in $^{196}$Po at 558 keV, of Fig. 16, suggests that $^{200}$Rn does not have a deformed ground state. Further, the hindrance factors in the decays of $^{180,182,184}$Hg to $^{176,178,180}$Pt reveal a rapid change in the $0^+$ state structures of the Pt isotopes.

Figure 15 demonstrates how odd-mass nuclei, which have far more complicated excitation spectra than their doubly even neighbors, have been explored using $\alpha$ decay. In some instances, it has only been possible to determine excitation

energies by $\alpha$-decay energy differences because the "internal" nuclear decays ($\gamma$ decay or internal conversion) are too hindered, e.g., $^{189,191}$Tl (Coenen et al., 1985), or too low in energy to be observed. Often, $\alpha$-decay spectroscopy avoids extraordinary complexity encountered when using in-beam reaction spectroscopy or $\beta$-decay spectroscopy because the $\alpha$-decay energy differences impose stringent constraints on the assignment of internal transitions via coincidence spectroscopy.

Figure 15 also shows the power of $\alpha$-decay hindrance factors as "spectroscopic factors" for the identification of specific shell-model (often intruder) configurations. Indeed, the observation of the unhindered pattern of Bi ground-state decays to Tl intruder states and Bi intruder-state decays to Tl ground states, evident in the figure, was a notable advance in the study of detailed nuclear structure far from stability (Coenen et al., 1985).

The use of $\alpha$ decay in recoil-decay tagging for in-beam $\gamma$-ray spectroscopy and as a spectroscopic fingerprint provided the necessary access to the Po isotopes ($Z = 84$) where shape coexistence is now well established following some of the most demanding detailed nuclear spectroscopic studies ever carried out far from stability. The occurrence of shape coexistence in the even-mass Po isotopes is summarized in Fig. 16.
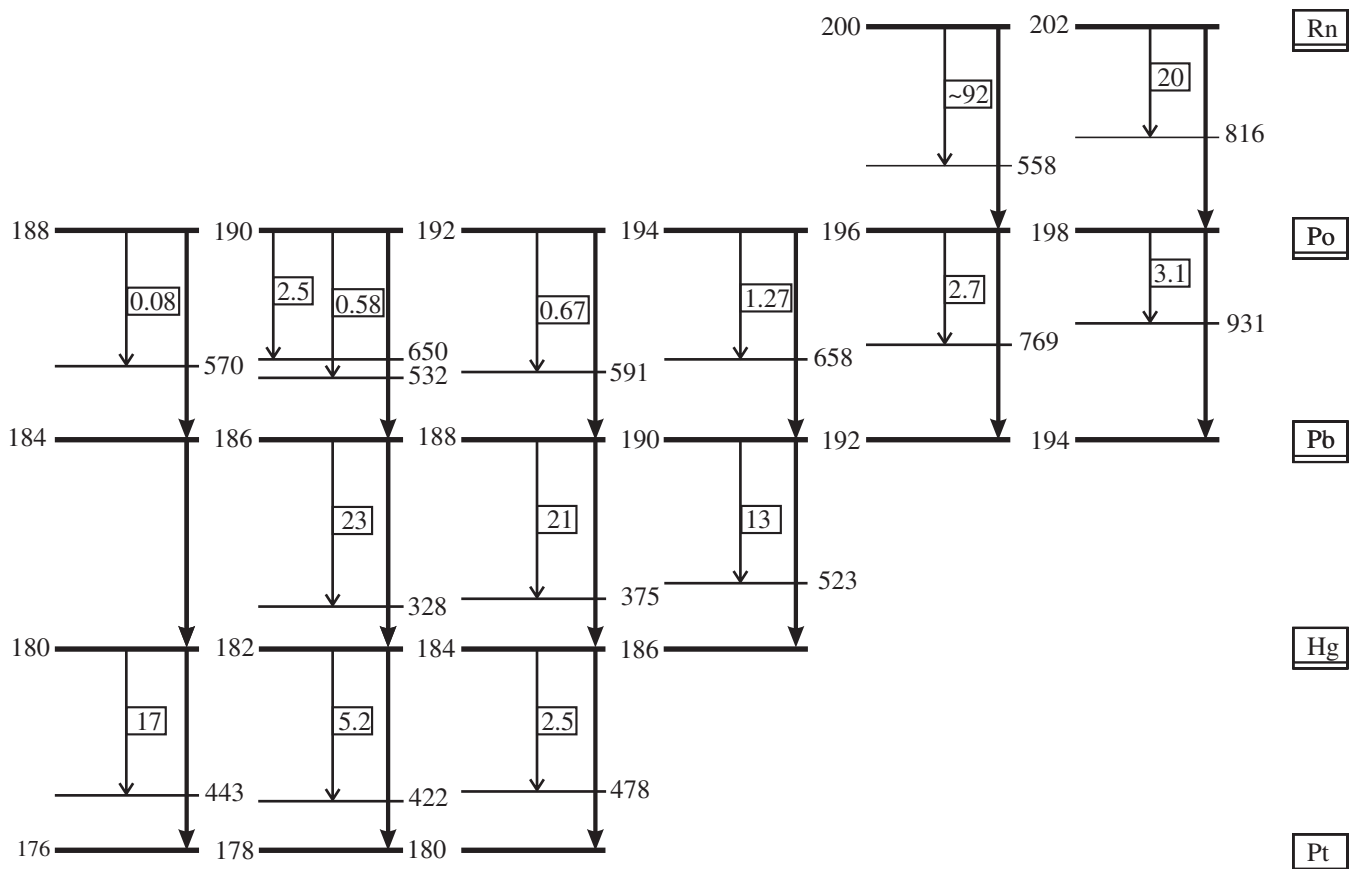


FIG. 14.   Systematics of $\alpha$-decay hindrances to excited $0^+$ states in the even-Rn, even-Po, even-Pb, even-Hg, and even-Pt isotopes: The ground-state-to-ground-state hindrance factors (numbers given in the boxes) are all normalized to unity. The $^{200}$Rn$(0_1^+) \rightarrow {}^{196}$Po$(0_2^+)$ $\alpha$-hindrance factor of $\sim$92 is the highest $0^+ \rightarrow 0^+$ value known. Note the $^{188}$Po$(0_1^+) \rightarrow {}^{184}$Pb$(0_2^+)$ $\alpha$-hindrance factor of 0.08: This implies that the normalization is to a strongly hindered (ground-state-to-ground-state) transition. The data are from Nuclear Data Sheets [except for $^{188}$Pb$(\alpha)^{184}$Hg, the hindrance factor is from Wauters, Bijnens, Dendooven et al. (1994), but see comment in Nuclear Data Sheets].
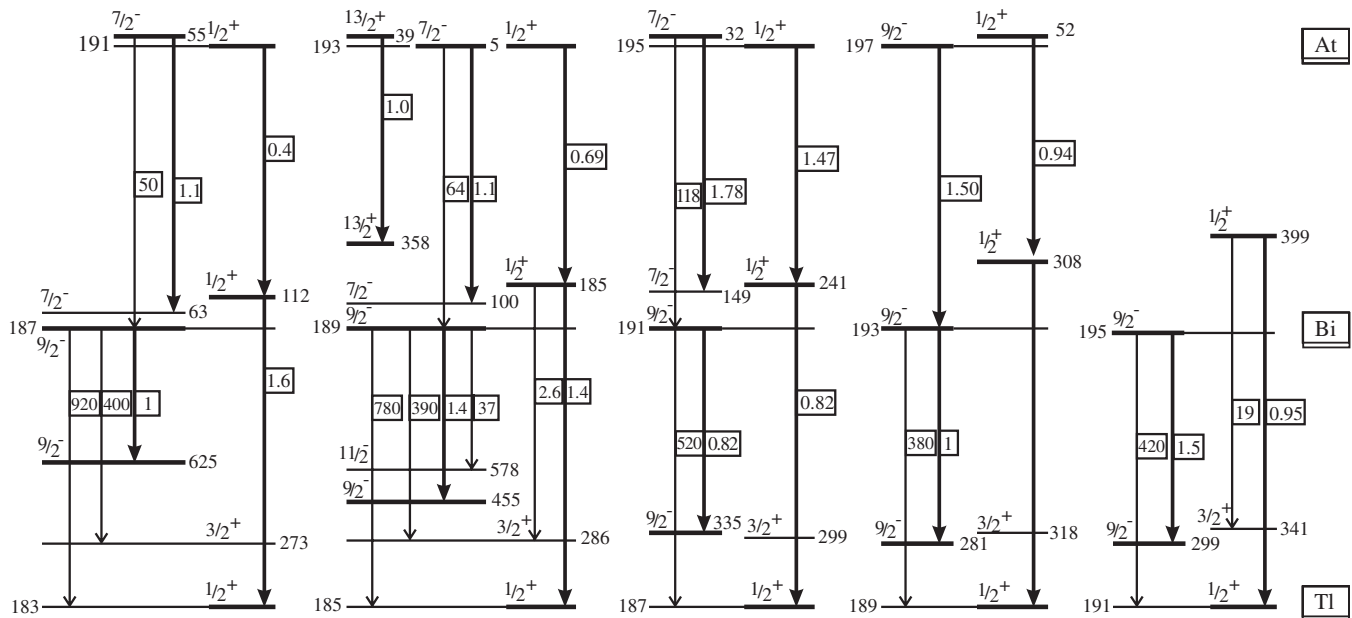
FIG. 15. Systematics of $\alpha$-decay hindrances between the odd-At, odd-Bi, and odd-Tl isotopes: The hindrance factors (numbers given in the boxes) are normalized to the neighboring even-even ground-state-to-ground-state $\alpha$-decay strengths. Note the manner in which the low hindrance factors pick out the intruder states on either side of the $Z = 82$ shell closure ($3s_{1/2}$ intruder states in the Bi and At isotopes and $1h_{9/2}$ intruder states in the Tl isotopes). The data are from Kettunen *et al.* (2003) and Nuclear Data Sheets [except for $^{183,189}$Tl, the energies of the $9/2^{-}$ states are from Andreyev *et al.*, 2006 and from Coenen *et al.*, 1985, respectively].

Figure 16 supports the interpretation that in the even-Po isotopes a deformed structure intrudes below the spherical $j = 9/2$ seniority structure, i.e., a "broken" $j = 9/2$ pair with $J = 2, 4, 6,$ and 8, to become the ground state between $^{196}$Po ($N = 112$) and $^{194}$Po ($N = 110$). The excited $0^{+}$ states in $^{196,198}$Po are shown to be populated by $^{200,202}$Rn $\alpha$ decay in Fig. 14. The irregularities in the energies of the $2^{+}$ states indicate that strong mixing must be occurring around $^{196}$Po. The isotopes $^{191,193}$Po can be inferred to likely possess deformed ground states: This would explain the $\alpha$-decay hindrance factors for the population of the two $J^{\pi} = 13/2^{+}$ states in $^{187}$Pb, shown in Fig. 13. This intrusion at $N = 112/110$ is an unexpected result: In the Hg isotopes ($Z = 80$), which "mirror" the Po isotopes ($Z = 84$) with respect to the $Z = 82$ closed shell, the intruding $0^{+}$ deformed states (cf. Fig. 10) never become the ground-state structure. Recently, laser hyperfine spectroscopy (Cocolios *et al.*, 2011) confirmed this picture.

In our earlier reviews we separately presented rudiments of the details summarized above. It is now evident that a unified view is suggested which involves a "parabolic" intrusion of configurations across the $Z = 82$ closed shell. This is dramatized by the energy systematics for the lowest intruding coexisting structures in the odd-Tl and odd-Bi isotopes and the even-Pb isotopes, shown in Fig. 17. Evidently there is a simple pattern that is nearly quantitative, i.e., the Tl and Bi intruder-state energies are close to one-half of the Pb $0^{+}$ excited-state energies. This is consistent with the energies scaling as the number of correlated proton pairs, i.e., the Tl $\pi$(1p-2h) and Bi $\pi$(2p-1h) excitation energies are almost exactly one-half the Pb $\pi$(2p-2h) excitation energies, which implies that the odd-mass intruder-state energies are not, to first order, dependent on the configurations of the unpaired

protons. It appears that this independence is complemented, for the $1h_{9/2}$ ground state of the odd-Bi isotopes and intruder states of the odd-Tl isotopes, in their similar magnetic moments (Neyens, 2003).

The parabolic pattern exhibited in Fig. 17 for $N > 108$ breaks down for $N < 108$. A more detailed view of the odd-Tl isotopes is provided by the collective band structures built on the intruder states, shown in Fig. 18. Bands built on both the $1h_{9/2}$ and $1i_{13/2}$ intruder configurations are evident. But there are two bands associated with each of these configurations, a strongly coupled spin sequence and a decoupled spin sequence [cf. Stephens (1975)], with small and large $B(E2)$ values, respectively. These can be interpreted as weakly deformed oblate and strongly deformed prolate structures. The point to note is that the parabolic minima are at different locations for the different bands. In particular, the more deformed bands have minima at $N = 102$, cf. the less deformed $1h_{9/2}$ minimum at $N = 108$ and, with reference to Figs. 12 and 17, the even-Pb isotopes at $N = 104$.

The well-established occurrence of intruder states and shape coexistence in the even-Hg, even-Pb, and even-Po isotopes, and the odd-Tl, odd-Pb, and odd-Bi isotopes raises the question of where such states appear in, e.g., the even-Pt and odd-Pt, odd-Au, odd-Hg, and odd-Po isotopes. The spectroscopic elucidation of such structures has proven to be highly demanding. The decay schemes are extremely complex, and low-energy, highly converted transitions [see, e.g., Roussière *et al.* (1998)] must be reliably identified and located in the odd-mass decay schemes. This has necessitated using coincidence spectroscopy between $\gamma$ rays and conversion electrons. An example of the complexity that can be handled is provided by studies of $^{187}$Au (Rupnik *et al.*, 1998) and $^{185}$Pt (von Schwarzenberg, 1991; Schwarzenberg, Wood,
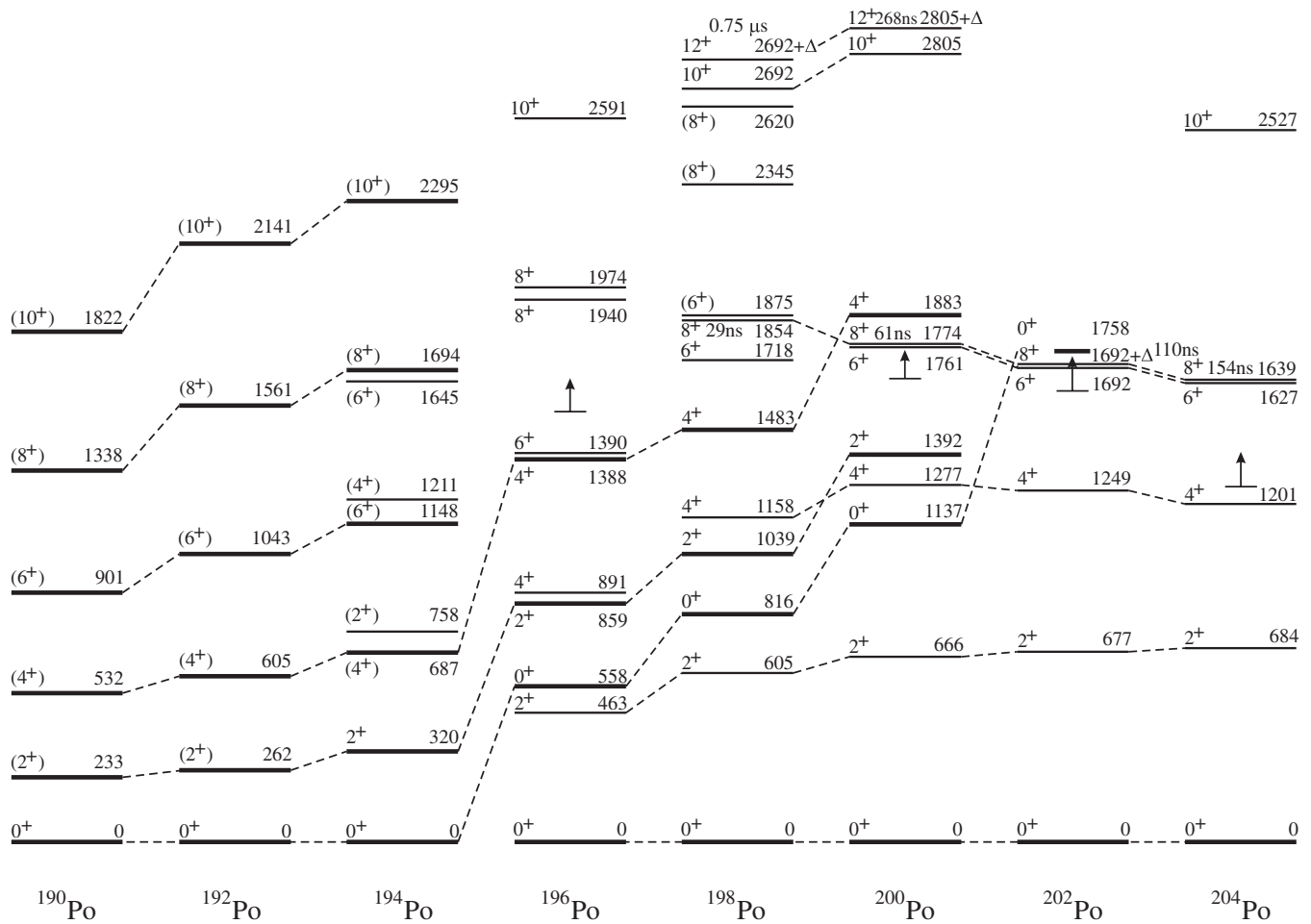
FIG. 16. Systematics of excited states in the even-Po isotopes. Seniority isomers with $J = 8$ are indicated by their half-lives. Evidently, the intruding deformed states become the ground states for $^{190,192,194}$Po. The data are from Helariutta *et al.* (1999) and Nuclear Data Sheets. There are recent lifetime data for $^{194}$Po (Grahn *et al.*, 2006, 2008).

and Zganjar, 1992; von Schwarzenberg, Wood, and Zganjar, 1998). The lowest-energy coexisting structures in $^{185}$Pt are identified by von Schwarzenberg, Wood, and Zganjar (1998). Multiple-coexisting structures in $^{187}$Au are shown in Fig. 19.

Intruder states in the odd-Au isotopes have been systematically explored by $\gamma$-ray and conversion electron spectroscopy following $\beta$ decay of high- and low-spin Hg isomers (Kortelahti *et al.*, 1988; Papanicolopoulos *et al.*, 1988; Rupnik *et al.*, 1995, 1998), and by in-beam $\gamma$-ray spectroscopy. Figure 20 summarizes the results from the in-beam $\gamma$-ray spectroscopy studies. Similar to the odd-Tl isotopes, decoupled spin sequences built on the $1h_{9/2}$ and $1i_{13/2}$ intruder configurations are evident, again with large $B(E2)$ values.

The emergence of a simple unified pattern of behavior for intruder states and shape coexistence in this region points to the possibility of systematically occurring multiparticle–multihole configurations. For example, $^{187}$Au has $\pi(3h)$, $\pi(1p\text{-}4h)$, $\pi(2p\text{-}5h)$, and $\pi(3p\text{-}6h)$ states with associated collective bands [cf. Fig. 19 and Rupnik *et al.* (1995, 1998)] and these should persist throughout the odd-Au isotopes in this region. Such states have been seen in $^{185}$Au (Kortelahti *et al.*, 1988; Papanicolopoulos *et al.*, 1988). The
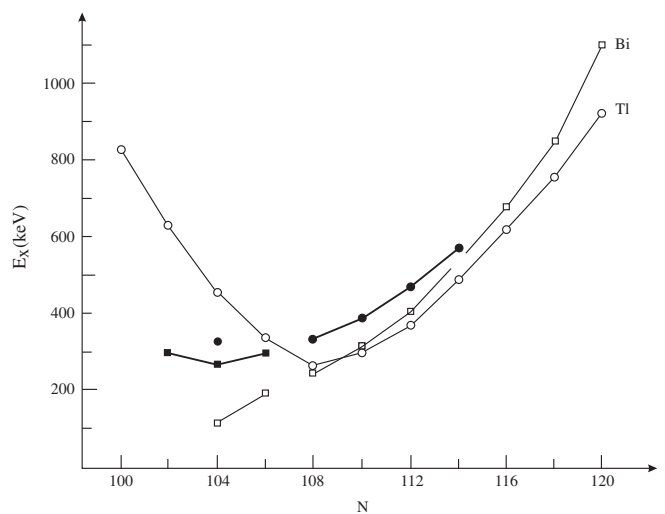


FIG. 17. Systematics of the odd-Tl $\pi(1p\text{-}2h)$, odd-Bi $\pi(2p\text{-}1h)$, and even-Pb $\pi(2p\text{-}2h)$ intruder-state energies (the even-Pb energies are divided by 2). Note the strong correlation of the three quantities: This is discussed further in the text. For the even-Pb isotopes, the candidate $\pi(4p\text{-}4h)$ states are shown as solid squares. The data are from Nuclear Data Sheets.
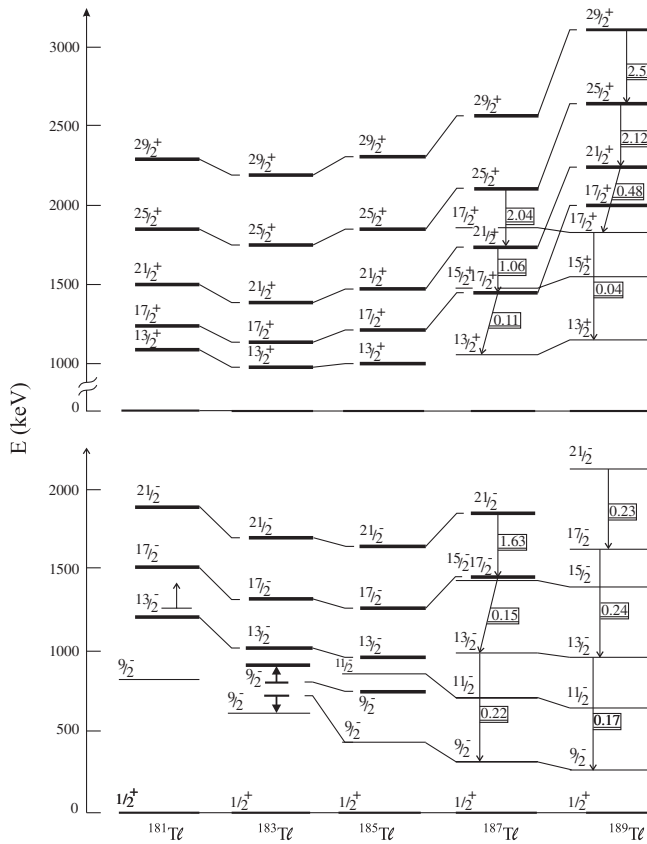
FIG. 18. Systematics of bands observed built on the lowest $9/2^-$ and $13/2^+$ states in the odd-Tl isotopes. Strongly coupled bands with small $B(E2)$ values and decoupled bands with large $B(E2)$ values are observed (the values are given in $[e\,b]^2$ in the boxes, these can be converted to W.u. for $A \approx 188$ by $\approx \times 160$). Mixing and repulsion of two $9/2^-$ configurations in $^{183}$Tl are indicated. The parabolic energy trends are discussed in the text. The data are from Raddon *et al.* (2004), Chamoli *et al.* (2005), Carpenter *et al.* (2009), and Nuclear Data Sheets.

Tl isotopes should exhibit $\pi(1h)$, $\pi(1p\text{-}2h)$, $\pi(2p\text{-}3h)$, and $\pi(3p\text{-}4h)$ states with associated collective bands. Figures 18 and 20 indicate the possibilities for systematic occurrence of such structures in the odd-Tl and odd-Au isotopes, respectively.

The observation of coexisting structures in odd-Hg isotopes has proven extremely challenging because of the low-energy excitations of key states. The current view is presented in Fig. 21. The occurrence of $\alpha$-decaying spherical and deformed states in the odd-Pb isotopes has facilitated the elucidation of these structures. Hindrance factors provide a valuable spectroscopic fingerprint. Evidently, whether or not the high-spin isomers live long enough for optical hyperfine spectroscopy is a delicate ordering of the spins and parities of the low-lying excited states.

The fairly complete systematics of deformed states, from the well-deformed ground states of the rare-earth isotopes to the lead isotopes, reveals a smooth trend with a remarkable feature in both even and odd isotones: The deformation is consistent with being the greatest as the $Z = 82$ closed shell is approached. This is shown for the $N = 105$ isotones in Fig. 22 and for the $N = 106$ isotones in Fig. 23.
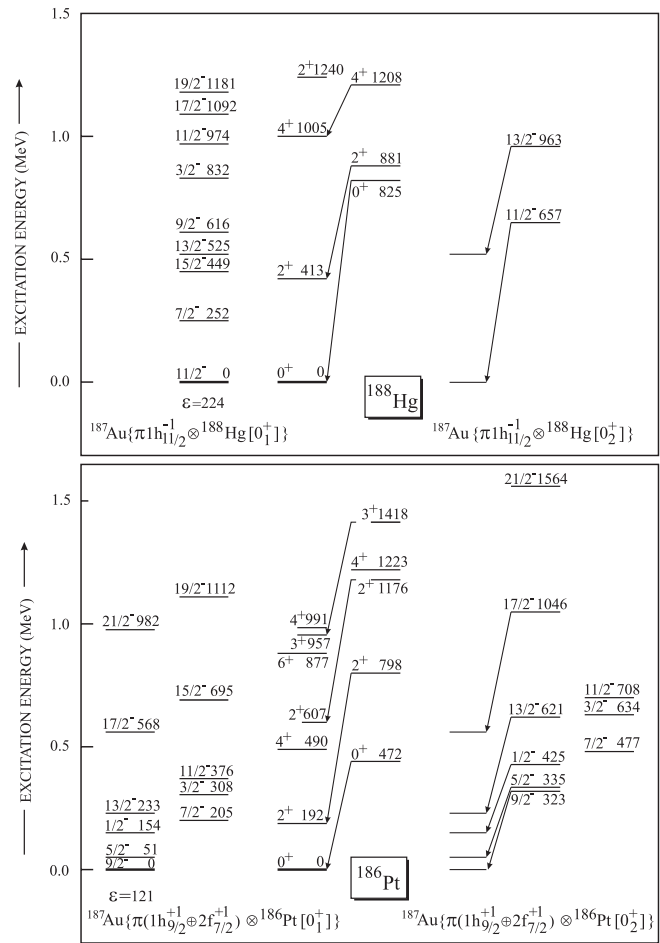


FIG. 19. Multiple-coexisting structures in $^{187}$Au. The upper part of the figure shows the states assigned as the coupling of the $1h_{11/2}$ proton hole to a $^{188}$Hg core for which there are $\pi(2h)$ and $\pi(2p\text{-}4h)$, $0_1^+$ and $0_2^+$ states, respectively, i.e., $\pi(3h)$ and $\pi(2p\text{-}5h)$ states. The lower part of the figure shows states assigned as the coupling of the $1h_{9/2}$ proton particle to a $^{186}$Pt core for which there are $\pi(4h)$ and $\pi(2p\text{-}6h)$, $0_2^+$ and $0_1^+$ states, respectively, i.e., $\pi(1p\text{-}4h)$ and $\pi(3p\text{-}6h)$ states. Details of the coupling of particles and holes to the Pt and Hg cores are given by Rupnik *et al.* (1995, 1998); a simple perspective is provided by Meyer-Ter-Vehn (1975a, 1975b), and Stephens (1975). Transitions with observed $E0$ components are marked by arrows. The data are from Nuclear Data Sheets.

The systematics depicted in Fig. 22 can be presented from a different perspective if they are looked at as if the lowest states shown in $^{183}$Pt and $^{185}$Hg are the ground states. One would deduce that the well-deformed rare-earth region persists at least to $Z = 80$. Figure 23 conveys this perspective and extends the view of comparative deformations all the way to $Z = 82$. The suggestion of a slightly less-deformed region centered on $Z = 72$ is misleading as the $K^\pi = 8^-$ band in $^{178}$Hf mixes with a second $K^\pi = 8^-$ band. See also Dracoulis *et al.* (2006) for a discussion of mixing in these $K^\pi = 8^-$ bands. (Note that the $K^\pi = 8^-$ configuration in the $N = 106$ isotones is the neutron two-quasiparticle state formed from $7/2^-[514]$ and $9/2^+[624]$, which are two of the Nilsson states shown in Fig. 22.) Later we discuss this perspective of intruder states and shape coexistence in a global framework.
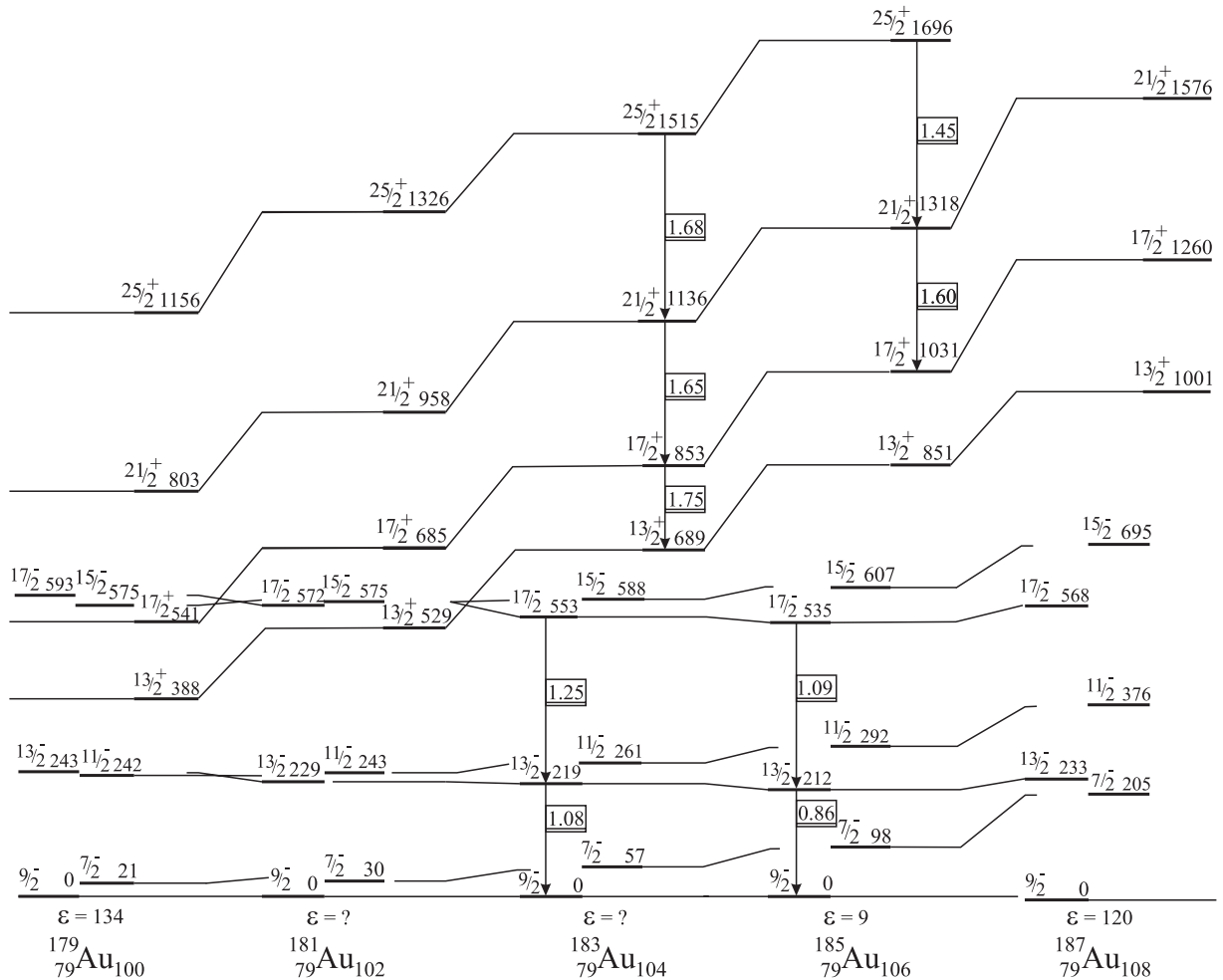
FIG. 20. Systematics of bands built on the lowest $9/2^-$ and $13/2^+$ states in the odd-Au isotopes. Decoupled bands with large $B(E2)$ values (given in $[e\,b]^2$ in the boxes) are observed. The $7/2^-$ states result from the $2f_{7/2}$ intruder configuration. Details are discussed in the text. The data are from Joshi *et al.* (2002, 2004), Venhart *et al.* (2011), and Nuclear Data Sheets.

There are suggestions for the occurrence of shape coexistence in lighter odd-Au isotopes (Kondev *et al.*, 2001; Mueller *et al.*, 2004), at low spin in $^{179}$Au (Venhart *et al.*, 2011), in lighter odd-Hg nuclei (Jenkins *et al.*, 2002; Kondev *et al.*, 2002), and in neutron-deficient even-Os (Davidson *et al.*, 1994; Kibédi *et al.*, 1994) and even-W (Kibédi *et al.*, 2001) isotopes.

**2. $Z \sim 50$ nuclei**

Shape coexistence at and near $Z = 50$ is centered on the stability line and is therefore easily accessible to detailed study. However, all but the lowest-energy shape-coexisting states lie above the pairing gap and thus demand a variety of spectroscopic techniques for their characterization.

The first indication of shape coexistence in this region was, as with the $Z = 82$ region, totally unexpected and came from in-beam $\gamma$-ray spectroscopy of the even-Sn isotopes (Bron *et al.*, 1979). Much of what is known about this region is already covered in our earlier reviews (Heyde *et al.*, 1983; Wood *et al.*, 1992), and so we only touch on a few new insights in this section.

Figure 24 shows the simple relationships that exist between odd-In, odd-Sb, and even-Sn isotopes that are similar to those

shown in Fig. 17 for the $Z = 82$ region. Figure 25 shows the simple relationships that exist between multiparticle–multihole intruder states in even-even nuclei in the $Z = 50$ region. This figure illustrates the concept of "intruder spin" (Heyde *et al.*, 1992; De Coster *et al.*, 1996). Note that for $I = 1$ bands, $^{116}$Sn is the most collective. The occurrence of $2_2^+$, $3_1^+$, $4_2^+$, ... states in, e.g., $^{110}$Ru and $^{112}$Pd (see Nuclear Data Sheets) suggests that such states should occur as intruder states; see, e.g., Fig. 25 in Wood *et al.* (1999).

Since our last review (Wood *et al.*, 1992) experimental work has extended the collective bands in $^{112-118}$Sn (Schimmer *et al.*, 1992; Wirowski *et al.*, 1995; Savelius *et al.*, 1998; Gableske *et al.*, 2001; Ganguly *et al.*, 2007; S. Y. Wang *et al.*, 2010), and identified candidate bands in $^{110}$Sn (Wolinska-Cichocka *et al.*, 2005) and $^{108}$Sn (Wadsworth *et al.*, 1993, 1996; Juutinen *et al.*, 1997). Lifetime data are now available for collective band members in $^{112}$Sn (Ganguly *et al.*, 2007) and $^{114}$Sn (Gableske *et al.*, 2001). Negative parity bands have been proposed in $^{114}$Sn (Schimmer *et al.*, 1992; Wirowski *et al.*, 1995; Gableske *et al.*, 2001); and collective bands have been proposed in $^{111}$Sn (Gangopadhyay *et al.*, 1995; LaFosse *et al.*, 1995; Wolinska-Cichocka *et al.*, 2005) and with lifetimes (Ganguly *et al.*, 2008), $^{113}$Sn
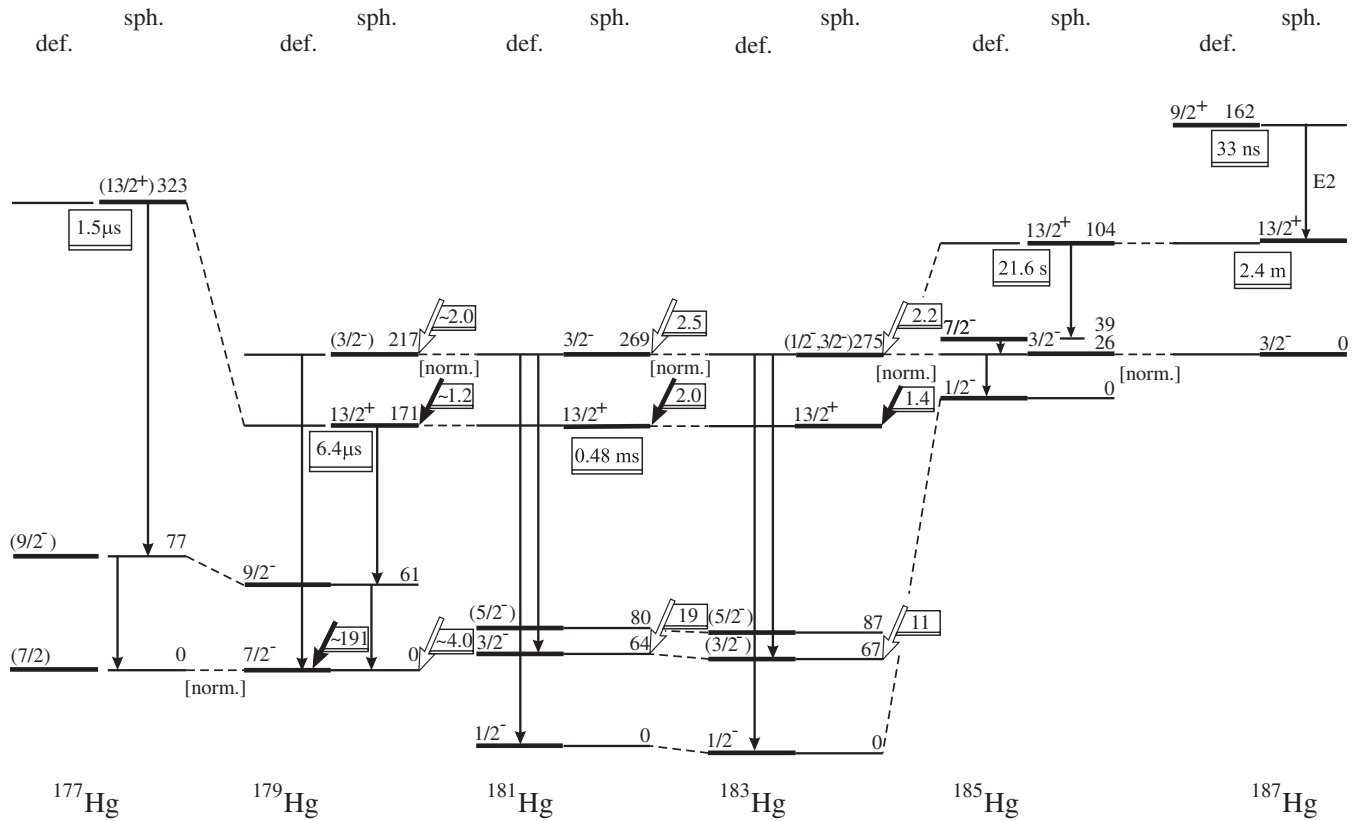
FIG. 21.   Systematics of the low-lying states in the odd-Hg isotopes near $N \sim 104$. Selected $\gamma$-ray transitions are shown as vertical arrows: in $^{177-183}$Hg, observed following $\alpha$ decay; in $^{185,187}$Hg observed associated with decay of isomers. $\alpha$-decay feedings (from Pb parent nuclei) are shown as diagonal arrows: solid for decays of the odd-Pb $1i_{13/2}$ isomers, open for the odd-Pb $3p_{3/2}$ ground states. $\alpha$-decay hindrance factors, normalized to the neighboring doubly even ground-state-to-ground-state transitions, are shown in boxes attached to the arrows. States are grouped as spherical and deformed: The large isomer shift observed in $^{185}$Hg, cf. Fig. 9, is between the ground state and 104 keV isomer. The data are from Andreyev *et al.* (2009a, 2009b) and Nuclear Data Sheets.

(Chakrawarthy *et al.*, 1998; Sears *et al.*, 1998), and $^{115}$Sn (Sears *et al.*, 1997; Savelius *et al.*, 1998).

### 3. $Z \sim 40$, $N \sim 60$ nuclei

The structure of nuclei in the $Z \sim 40$, $N \sim 60$ region has long been recognized to be dominated by a sudden onset of

deformation in going from $N = 58$ to $N = 60$ (Cheifetz *et al.*, 1970; Federman and Pittel, 1977, 1979). Figure 26 shows the dramatic change in the isotope shifts $\delta \langle r^2 \rangle$ and two-neutron separation energies $S_{2n}$ that occur at $N = 60$, which directly signify a major change in ground-state structure. The data presented here show that this results from the crossing of coexisting structures.



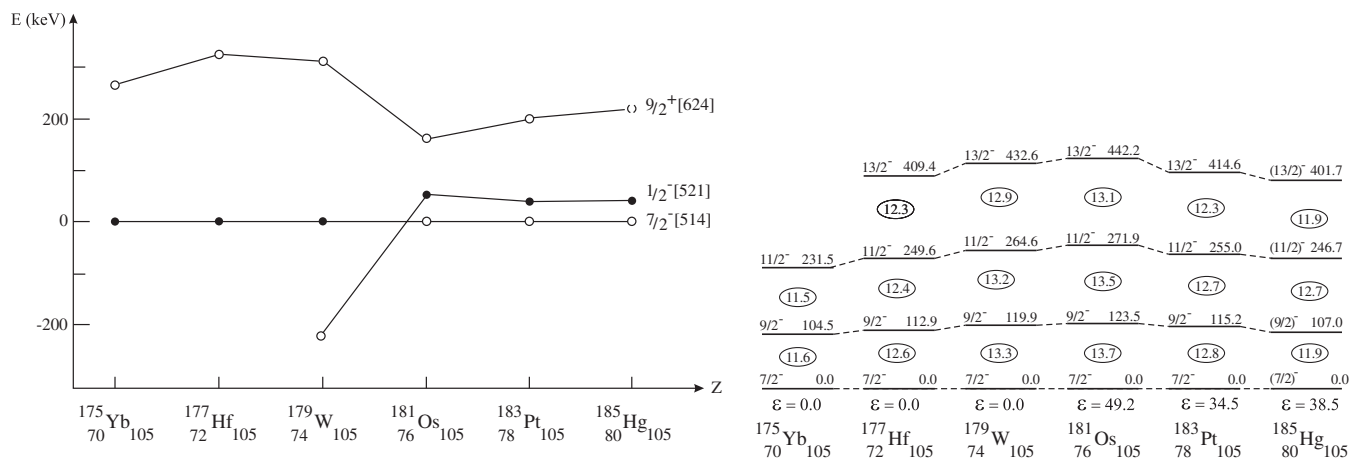FIG. 22.   Systematics of Nilsson states (left-hand side) and rotational energy parameters (right-hand side) in the $N = 105$ isotones. Note the smooth trend of Nilsson single-particle energies from nuclei with well-deformed ground states into the spherical region. The rotational parameters indicate equal or greater deformation at $Z = 80$ than at $Z = 72$. The data are from Kilcher *et al.* (1988) and Nuclear Data Sheets.

15⁻  3574
14⁻  2749        14⁻  3042                    (10.3)      15⁻  3476      15⁻  3874      15⁻  4212
        (11.3)              (10.9)      14⁻  3265    (9.3)        (9.7)        (9.4)
13⁻  2256  13⁻  2433  13⁻  2736    (10.4)      14⁻  3197  14⁻  3583  14⁻  3930
  (10.8)      (11.4)            13⁻  2973    (9.6)        (9.9)        (10.0)
12⁻  1974  12⁻  2137  12⁻  2451    (10.5)      13⁻  2928  13⁻  3305  13⁻  3650
  (10.9)      (11.6)      (11.0)    12⁻  2701    (9.8)        (9.8)        (9.6)
11⁻  1711  11⁻  1859  11⁻  2187    (10.5)      12⁻  2674  12⁻  3049  12⁻  3399
  (11.0)      (11.7)      (11.0)    11⁻  2450    (9.9)        (10.0)      (10.5)
10⁻  1470  10⁻  1601  10⁻  1945    (10.5)      11⁻  2436  11⁻  2810  11⁻  3147
  (11.0)      (11.9)      (11.0)    10⁻  2220    (9.9)        (9.9)        (9.2)
9⁻  1249   9⁻  1364   9⁻  1726    (10.4)      10⁻  2217  10⁻  2592  10⁻  2945
  (11.0)      (12.1)      (11.0)    9⁻  2014    (9.9)        (9.9)        (9.7)
8⁻  1050   8⁻  1147   8⁻  1529    (10.1)      9⁻  2018   9⁻  2394   9⁻  2752
                          10⁻  1832   (9.9)        (9.8)        (9.7)
                          8⁻       8⁻  1840   8⁻  2217   8⁻  2577

11.4s        4.0s        5.5ms        0.78ms       1.0ms        82µs        830ns

$^{176}_{70}$Yb$_{106}$   $^{178}_{72}$Hf$_{106}$   $^{180}_{74}$W$_{106}$   $^{182}_{76}$Os$_{106}$   $^{184}_{78}$Pt$_{106}$   $^{186}_{80}$Hg$_{106}$   $^{188}_{82}$Pb$_{106}$
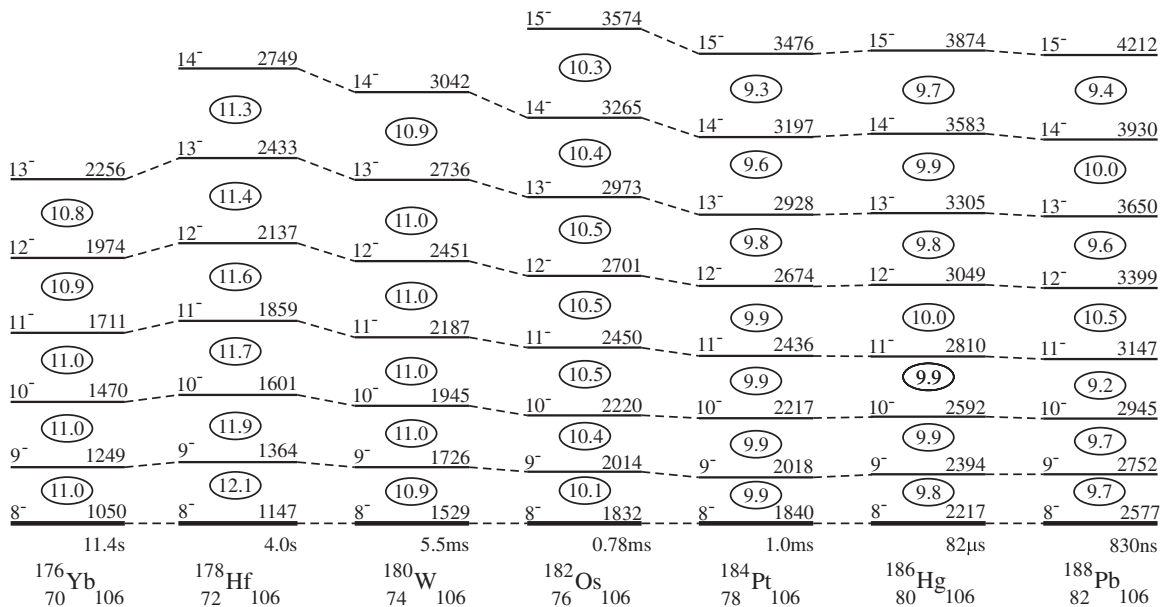
FIG. 23. Systematics of $K^\pi = 8^-$ isomers in the $N = 106$ isotones. Rotational parameters deduced from a rigid rotor energy relationship are shown circled and reveal that this deformed structure persists to the closed-shell nucleus $^{188}$Pb. Note also that $^{188}$Pb supports this deformed $K$ isomer, an oblate $K^\pi = 11^-$ isomer, and a seniority isomer, the $J = 12$ isomer (cf. Figs. 11 and 12): This occurrence of three completely different kinds of isomerism dramatizes the role of coexistence at $Z = 82$ which cannot be described as a "collapse of the shell structure." Half-lives of the band heads are shown. The data are from Dracoulis *et al.* (2004), Ncapayi *et al.* (2005), and Nuclear Data Sheets.

The neutron-rich $N = 58$ isotones $^{96}$Sr and $^{98}$Zr exhibit well-defined shape coexistence, shown in Fig. 27. The neighboring $N = 59$ odd-mass isotones, $^{97}$Sr and $^{99}$Zr, also exhibit shape coexistence, shown in Fig. 28.

Two-nucleon and $\alpha$-cluster transfer data for this region, shown for the Zr and Mo isotopes in Figs. 29 and 30, reveal that pairing collectivity for the $0^+$ ground states and first-excited states for some of these isotopes exhibits a "coexisting" character, i.e., transfer strength goes strongly to more than one "condensate." This raises a whole new perspective for the interpretation of $0^+$ states in collective nuclei. We discuss these features further in Sec. III.C.3.
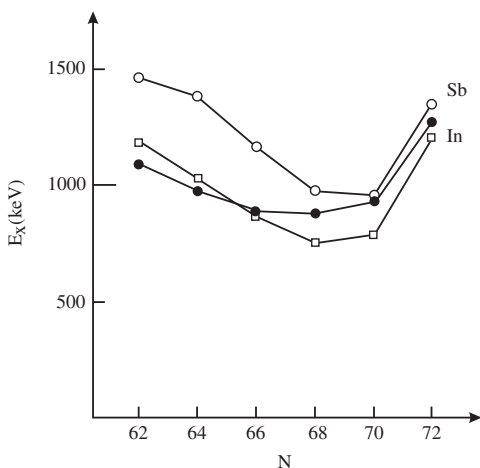
FIG. 24. Systematics of the odd-In $1/2^+$ $\pi$(1p-2h), odd-Sb $9/2^-$ $\pi$(2p-1h), and even-Sn $\pi$(2p-2h) intruder-state energies (the even-Sn energies are divided by 2). This systematic is similar to that shown in Fig. 17. The data are from Nuclear Data Sheets.

The $E0$ transitions, shown in Fig. 27, are among the strongest known anywhere on the mass surface (Wood *et al.*, 1999). They indicate that, e.g., the 853 and 1859 keV $0^+$ states in $^{98}$Zr are primarily configurations of spherical origin and are strongly mixed with the $0^+$ deformed configuration underlying the deformed band. The appearance of strong $E0$ transitions in the $N = 60$ isotones, shown in Fig. 31, reveals the persistence of coexisting structures in this region. Evidently, the effect is still manifested in $^{102}$Mo, but is far less extreme, and it appears to have gone away in $^{104}$Ru. However, Fig. 32 shows static and dynamic quadrupole moment data for $^{104}$Ru which reveals that the shape coexistence persists. Figure 32 presents static and dynamic quadrupole moment data for $^{108}$Pd which shows that shape coexistence is present in this nucleus also.

The isotopes presented above all lie in open-shell regions and so the standard interpretation of shape coexistence as resulting from intruder configurations across closed shells cannot be the explanation. A unified interpretation of these coexisting structures can be given if subshell gaps are invoked as also giving rise to intruder configurations. The conventional view of subshell structure with respect to its influence on nuclear collectivity is that it does not play a role because pairing "smears out" subshell occupancies into a uniform distribution. This view needs reassessment.

The presence of shape-coexisting structures in this region provides a simple explanation of the remarkable systematic of $S_{2n}$ and $\delta\langle r^2\rangle$ values for isotope chains, shown in Fig. 26. They can be understood as *suppressed* collectivity of a ground-state structure centered on $Z = 40$ for $N < 60$ and normal collectivity for $N \geq 60$. This dramatizes the role of subshells in controlling collective behavior in an important way.
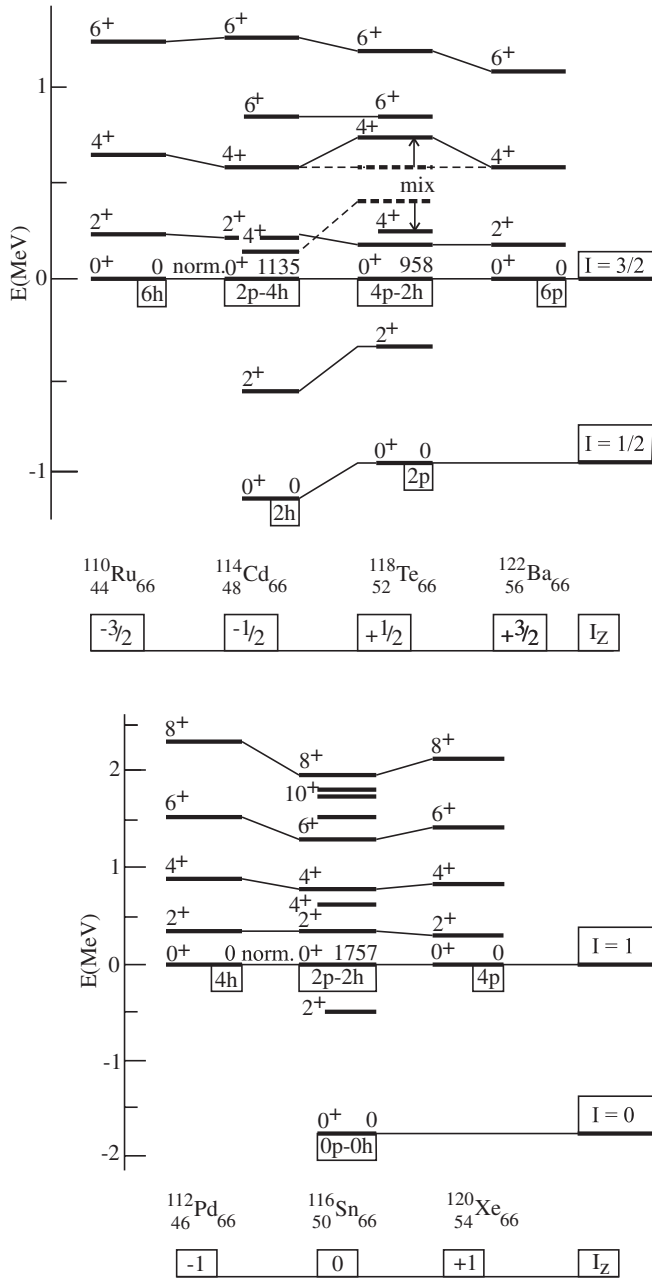
FIG. 25. Intruder states in $^{114}$Cd and $^{118}$Te (upper part) and $^{116}$Sn (lower part) classified by "intruder spin," $I$: The multiplet of states labeled, e.g., as $I = 3/2$ are formed from the sequence of six active protons configurations—$\pi(6h)$, $\pi(2p\text{-}4h)$, $\pi(4p\text{-}2h)$, and $\pi(6p)$, respectively; with standard SU(2) labels and interpretation given for the various multiplets. The figure is similar to one shown in De Coster, Decroix, and Heyde (1996).

## 4. $Z \sim 64$, $N \sim 90$ nuclei

The nuclei in the $Z \sim 64$, $N \sim 90$ region are centered on the stability line and have been the subject of some of the most intensive and varied spectroscopic and theoretical studies of collectivity anywhere on the mass surface. The primary interest in this region is the rapid onset of deformation in going from $N = 86$ to $N = 92$. Figure 33 shows the systematics of the isotope shifts and two-neutron separation energies for this region: These quantities exhibit a near identical
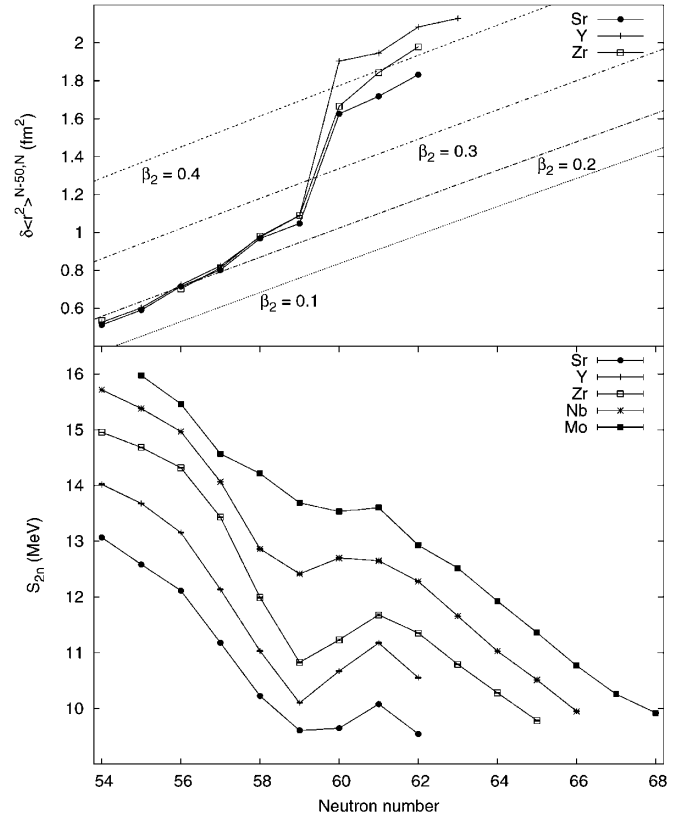


FIG. 26. Isotope shifts $\delta\langle r^2\rangle$ in fm$^2$ and two-neutron separation energies $S_{2n}$ in MeV for selected isotopic chains across the $N = 60$ region. From Hager *et al.*, 2007.

pattern to that observed in the $Z \sim 40$, $N \sim 60$ region; cf. Fig. 26. The clear manifestation of shape coexistence at $N = 58$, 60, cf. Figs. 27 and 31, strongly suggests that the $Z \sim 64$, $N \sim 90$ region be considered from the perspective of coexisting shapes. Indeed, this is a key issue in the interest of achieving a unified view of shape coexistence in nuclei.

The issue of shape coexistence in this region is subtle because, except for $^{150}$Sm where there is a clear candidate for a strongly deformed excited band in the presence of predominantly weakly deformed bands (Wood *et al.*, 1992), there are no obvious differences in band energy spacing or $B(E2)$ values. Figure 34 shows the $E0$ transition strengths in the even-mass $N = 90$ isotones. [A similar pattern occurs for $N = 88$ (Wood *et al.*, 1999).] These suggest that strong mixing may occur between the lowest two $K = 0$ bands. Traditionally, the low-lying first-excited $0^+$ state in the $N = 90$ isotones has been regarded as the textbook example of a $\beta$ vibration (Garrett, 2001). However, if this interpretation is correct, then a two-phonon $0^+$ excited state should be observed with significant $E2$ decay strength to the one-phonon band.

A search for intrinsic $E2$ strength in $^{152}$Sm using multistep Coulomb excitation reveals that intrinsic strength exists only between the purported $\beta$ band and a $K = 2$ band (Kulp *et al.*, 2008). The emerging picture in $^{152}$Sm indicates coexisting pairs of bands with $K^\pi = 0^+$, $2^+$, and $0^-$ (Kulp *et al.*, 2008; Garrett *et al.*, 2009). The similarity in the energy spacing of these bands is consistent with strong mixing of coexisting
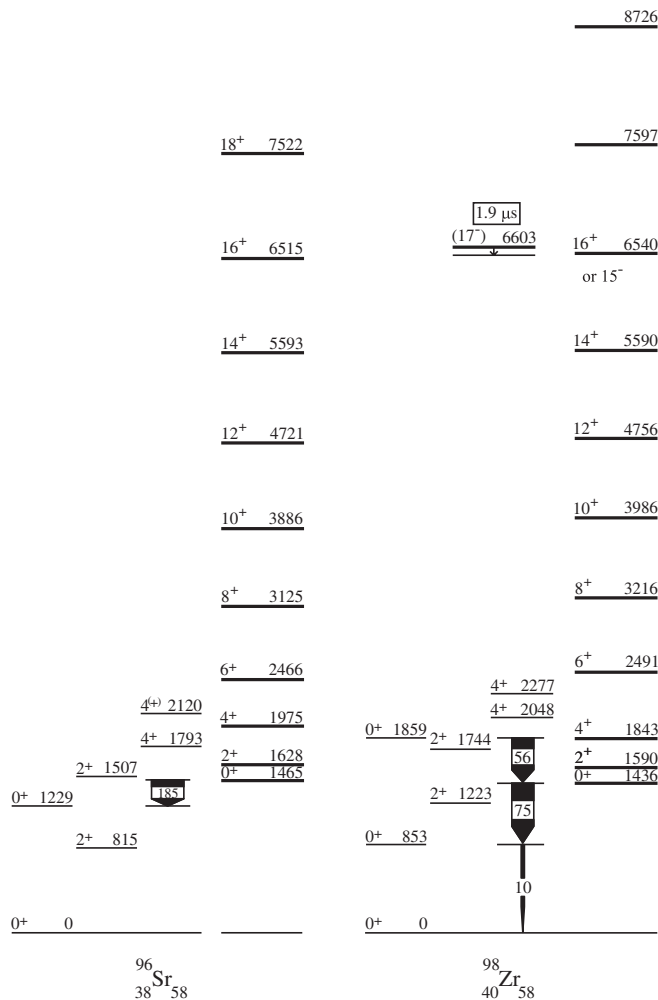
FIG. 27. Shape coexistence in the $N = 58$ isotones, $^{96}$Sr and $^{98}$Zr. The vertical arrows indicate $E0$ transitions with their observed values for $\rho^2(E0) \times 10^3$; the value for $^{96}$Sr is the largest known for $A > 56$. The cascade of two strong $E0$ transitions in $^{98}$Zr is discussed in the text. The data are from Wu *et al.* (2004), Simpson *et al.* (2006), and Nuclear Data Sheets.

FIG. 28. Shape coexistence in the $N = 59$ isotones, $^{97}$Sr and $^{99}$Zr. The three deformed bands with $K^\pi = 3/2^+, 3/2^-$, and $9/2^+$ correspond to the Nilsson configurations [411 ↑], [541 ↑], and [404 ↑] (with the notation $[N, n_z, \Lambda, \Sigma]$), respectively. The data are from Urban *et al.* (2001, 2003, 2004), Wu *et al.* (2004), and Nuclear Data Sheets.

bands with different deformations. The pattern of $E0$ transition strength between the two $K = 0$ bands necessitates such strong mixing (Kulp, 2009).

### 5. $Z \sim 34$, $N \sim 40$ nuclei

Shape coexistence in the $Z \sim 34$, $N \sim 40$ region extends from the stability line to the proton-drip line. The study of this region has been difficult because the features are not as distinctive as in nuclei, e.g., in the $Z = 50$, 82 regions, and this is probably because it is obscured by strong mixing (cf. the situation at $Z \sim 64$, $N \sim 90$).

Shape coexistence in this region was first proposed in $^{72}$Se (Hamilton *et al.*, 1974). A limited view of shape coexistence in this region was presented in our earlier review (Wood *et al.*, 1992). However, it is now becoming evident that the role of subshells is important for understanding coexistence and collectivity, in general, in this region.

A key contribution to the identification of coexistence in this region has come from multistep Coulomb excitation.
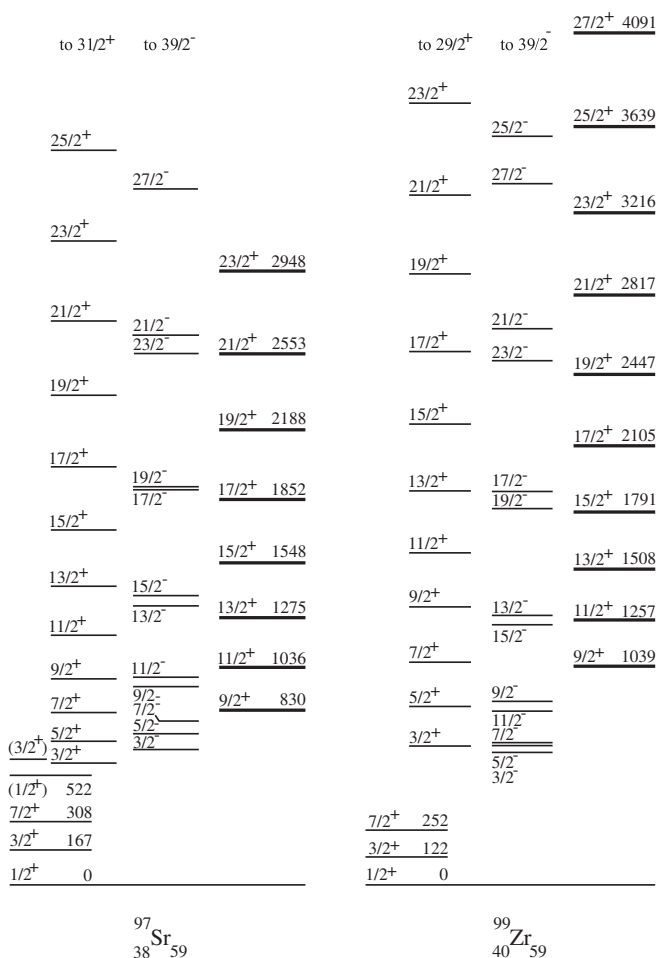
Figure 35 shows $\langle Q^2 \rangle$ for the even-Ge isotopes that are strongly supportive of different shapes for the ground and first-excited $0^+$ states in these nuclei. A broader view of data such as those shown in Fig. 35 (lower part) is discussed in Sec. III.C (see Tables IV and V).

Pairing is evidently playing an important role in the low-energy structure of these isotopes, as revealed by the two- and four-nucleon transfer strengths shown in Fig. 36. Indeed, it is possible to elucidate the pair configurations of these isotopes from detailed transfer reaction spectroscopy data shown in Fig. 37. We note that the pairing structure in this region, and for $^{76}$Ge and $^{76}$Se, in particular, is of considerable interest currently with respect to double-$\beta$ decay (Schiffer *et al.*, 2008; Kay *et al.*, 2009; Menéndez *et al.*, 2009; Simkovic, Faessler, and Vogel, 2009; Moreno *et al.*, 2010).

The role of subshells and their occupancy with respect to the low-energy structure of the even-mass germanium isotopes received considerable attention in the period 1975–1985. This was motivated by the low excitation energy of the first-excited $0^+$ state in $^{76}$Ge (cf. Fig. 35):
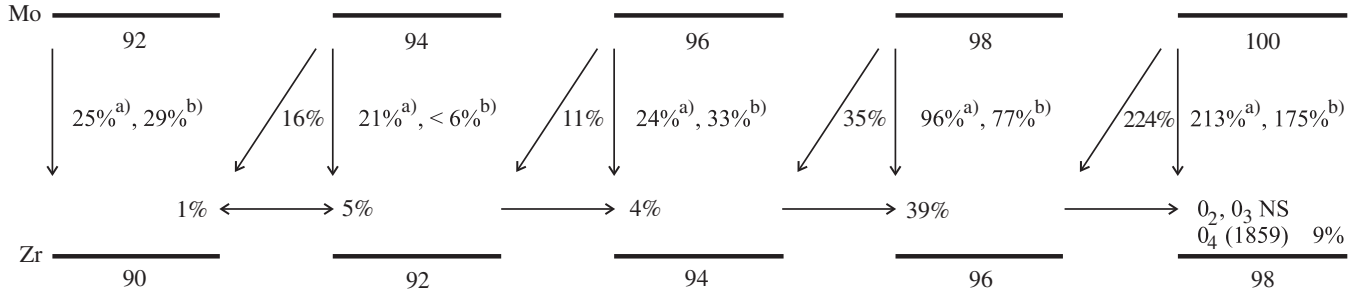
FIG. 29. Two-nucleon and multinucleon transfer strengths to $0_2^+$ states in the Zr isotopes, given relative to 100% for $0_1^+$ states. The strengths marked a) are from ($^6$Li, $^8$B) reactions, and b) are from ($^{14}$C, $^{16}$O) reactions. The data are from references given in Nuclear Data Sheets.

The fact that it is the first-excited state in this nucleus means that it is unlikely to be a "quadrupole collective" excitation. This resulted in a program of single-nucleon and multinucleon transfer reaction spectroscopy, particu- larly by Vergnes and co-workers and Fortune and co- workers, which, in its details, is unequalled anywhere else on the nuclear mass surface. Figures 35–37 summa- rize this.
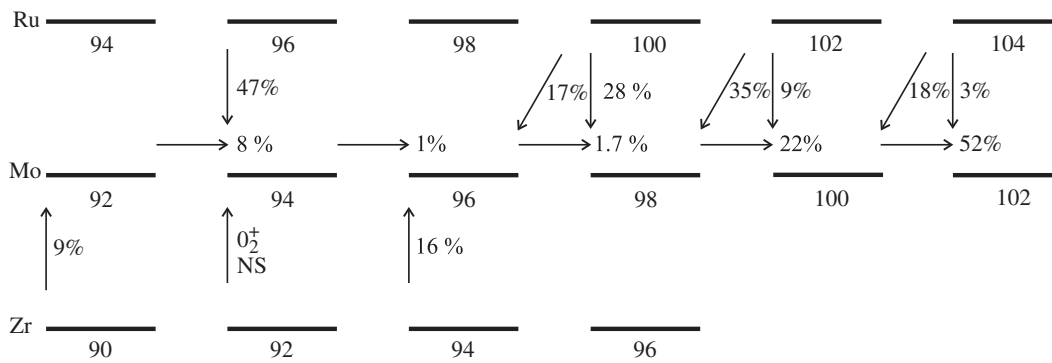


FIG. 30. Two-nucleon and multinucleon transfer strengths to $0_2^+$ states in the Mo isotopes, given relative to 100% for $0_1^+$ states (NS = not seen). The data are from Nuclear Data Sheets.
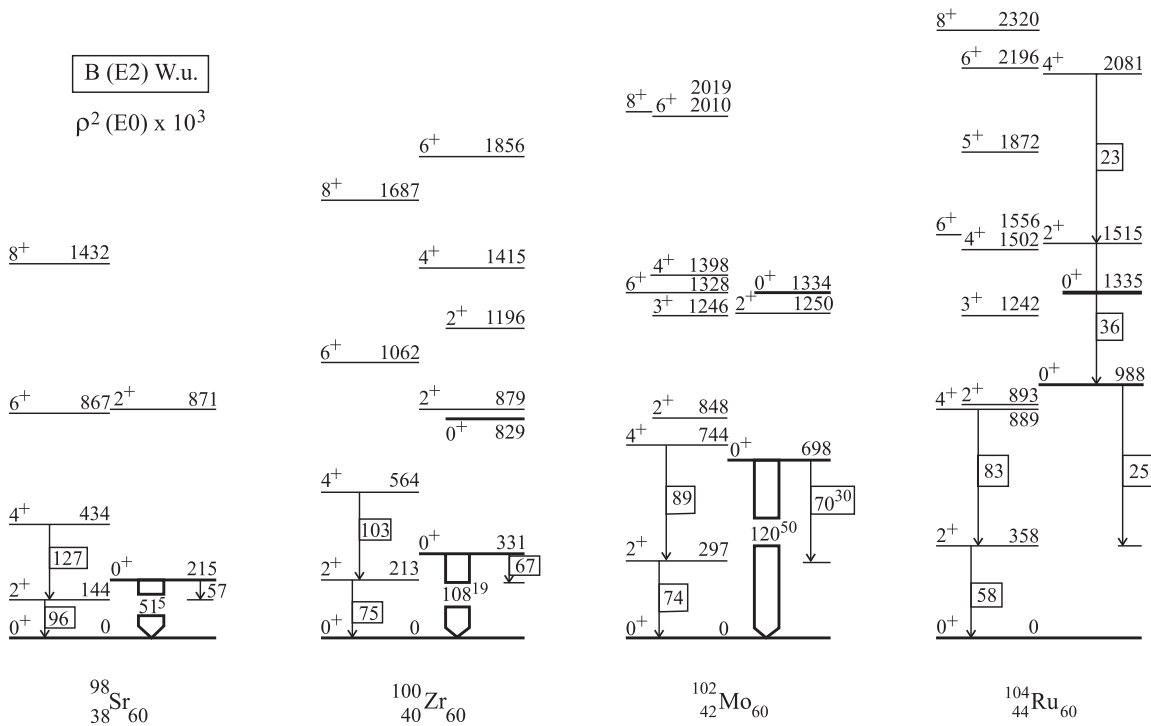


FIG. 31. Systematics of low-lying collective states in the $N = 60$ isotones. Light vertical arrows show selected transitions with their $B(E2)$ values, and heavy vertical arrows show selected transitions with their $\rho^2(E0) \times 10^3$ values. The data are from Kibédi and Spear (2005), Srebrny *et al.* (2006), and Nuclear Data Sheets.
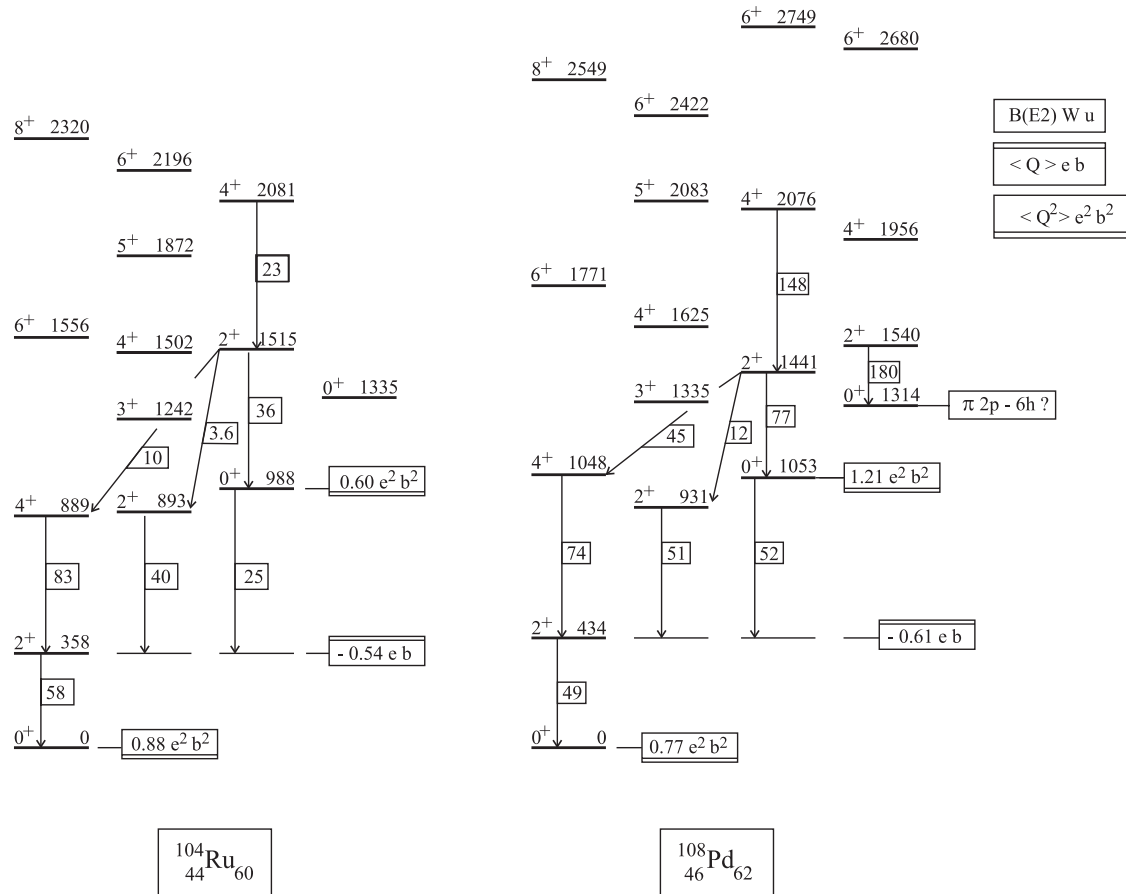
FIG. 32.   Electric quadrupole collectivity in $^{104}$Ru and $^{108}$Pd. Arrows indicate selected transitions with their $B(E2)$ values. Boxes with a double underline give $\langle Q^2 \rangle$ values in units $e^2\,b^2$ obtained by summing over squares of $E2$ matrix elements. Boxes with a double overline give the quadrupole moments $\langle Q \rangle$ in $e\,b$. (We refer the interested reader to the cited multi-Coulex papers for details of sign convention and determination.) A candidate $\pi$(2p-6h) band is indicated in $^{108}$Pd. The data are from Srebrny *et al.* (2006), Svensson *et al.* (1995), and Nuclear Data Sheets.

The work of the Vergnes and Fortune groups demonstrates what is needed to understand the emerging picture of collectivity in nuclei that we present here, namely, that coexisting structures (quadrupole and pairing) are probably present in all nuclei. The first work to bring focus to the issue of the nature of the low excitation of the $0^+$ first-excited state in $^{76}$Ge was by Ardouin, Tamisier, Berrier *et al.* (1975) and Ardouin, Tamisier, Vergnes (1975b) which showed that this state is strongly populated in *one-proton* stripping reactions. This was followed by two-neutron pickup reaction (Vergnes *et al.*, 1976a, 1976b; Guilbault *et al.*, 1977; Ardouin, Remaud *et al.*, 1978b), one-proton pickup reaction (Rotbard *et al.*, 1977, 1978), two-neutron stripping reaction (Ardouin, Lebrun *et al.*, 1978a; Vergnes *et al.*, 1978; Lebrun *et al.*, 1979; Vergnes *et al.*, 1979), $(\alpha, p)$ reaction (Rotbard *et al.*, 1980), $\alpha$-particle stripping reaction (Ardouin, Hanson, and Stein, 1980), and $\alpha$-particle pickup reaction (Van den Berg *et al.*, 1982) studies. This systematic study led to a series of two-neutron stripping reaction studies (Lafrance *et al.*, 1978; Mateja *et al.*, 1978; Mordechai *et al.*, 1978, 1979; Becker *et al.*, 1982). The emerging picture was presented by Ardouin, Lebrun *et al.* (1978a), and an extensive survey was given by Vergnes at the 1979 Rhodos Conference (Vergnes, 1980).

The wave functions for the ground and first-excited $0^+_{1,2}$ states used in analyzing the transfer data have been described as a product of a proton and neutron configuration, using $^{70}$Ge ($Z = 32$, $N = 38$) as the reference nucleus, with the particular choice

$$| \Phi^\pi(^A\text{Ge}; 0^+_1) \rangle = \alpha_A\,|\,(2p_{3/2})^4_0 \rangle + \beta_A\,|\,(2p_{3/2})^2_0(1f_{5/2})^2_0 \rangle,$$
(15)

with the orthogonal combination for the $0^+_2$ excited state, for the proton part, and a neutron wave function which is the same for the $0^+_{1,2}$ states, i.e., $|\,\Phi^\nu(^A\text{Ge}; 0^+_1) \rangle = |\,\Phi^\nu(^A\text{Ge}; 0^+_2) \rangle$. The data allow one to extract the proton part (Van den Berg *et al.*, 1982) of the wave function. On the other hand, Becker *et al.* (1982) assumed that the proton structure remained the same at low excitation energies when analyzing the transfer data, making the particular choice

$$| \Phi^\nu(^{70+n}\text{Ge}; 0^+_1) \rangle = \alpha_n\,|\,(2p_{1/2})^2_0(1g_{9/2})^{n-2}_0 \rangle$$
$$+ \beta_n\,|\,(1g_{9/2})^n_0 \rangle,$$
(16)

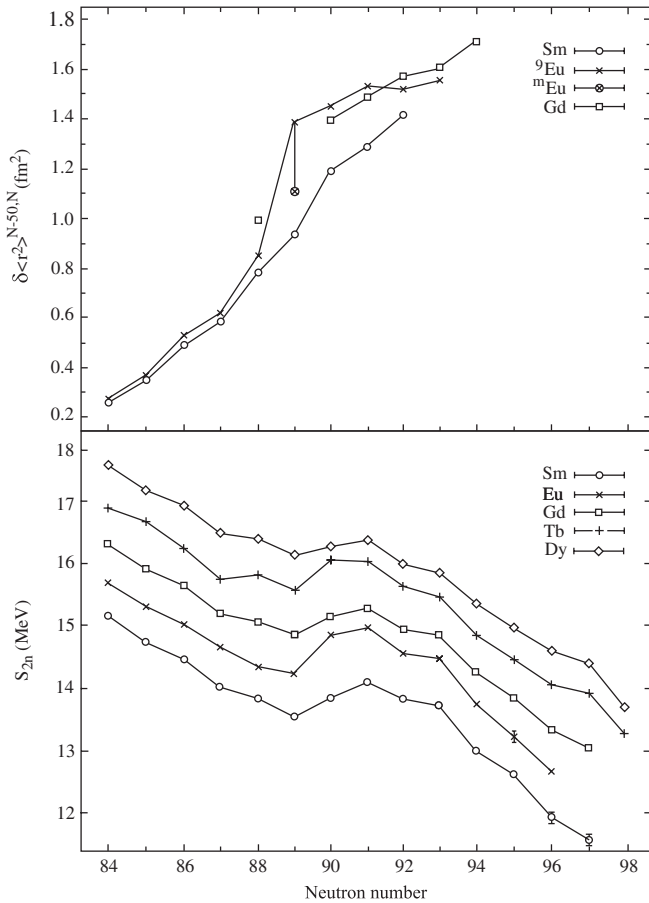with the orthogonal combinations for the $0^+_2$ excited state, for the neutron part, and a proton wave function which

FIG. 33.   Isotope shifts $\delta\langle r^2\rangle$ in fm$^2$ and two-neutron separation energies $S_{2n}$ in MeV for selected isotopic chains across the $N = 90$ region. The data are from Nadjakov, Marinova, and Gangrsky (1994) and Audi, Wapstra, and Thibault (2003).
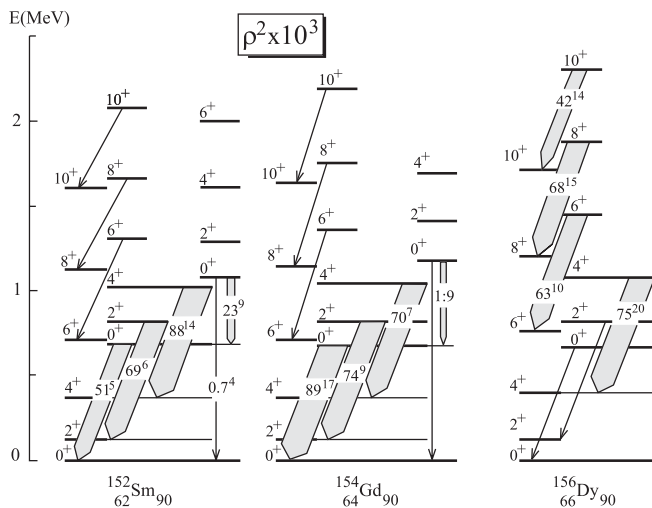


FIG. 34.   Systematics of $\rho^2(E0) \times 10^3$ values in the $N = 90$ iso-tones. The large values indicate underlying coexistence of bands with different deformations that mix strongly. The level data are taken from Nuclear Data Sheets. The $\rho^2(E0) \times 10^3$ values are taken from Kibédi and Spear (2005) for $0_2^+ \rightarrow 0_1^+$, from Wood *et al.* (1999) for $2_2^+ \rightarrow 2_1^+$, and are calculated using lifetime data (Klug *et al.*, 2000; Tonev *et al.*, 2004; Möller *et al.*, 2006) and electron data in Nuclear Data Sheets for other transitions.
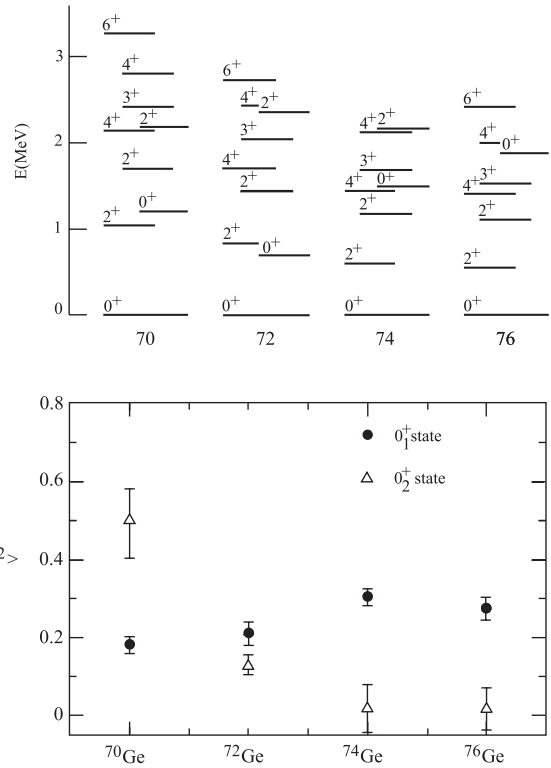


FIG. 35.   Low-lying states in $^{70-76}$Ge (upper part) and $\langle Q^2\rangle$ values in $e^2$ b$^2$ for the $0_1^+$ and $0_2^+$ states in these Ge isotopes (lower part). The lower part is taken from Sugawara *et al.* (2003) and the data in the upper part are from Podolyák *et al.* (2004) and Nuclear Data Sheets. (Note that in the lower part, the value of $\langle Q^2\rangle$ for the $0_2^+$ state in $^{70}$Ge, cf. Table IV, should be 0.64 and not 0.50.)

is the same for the $0_{1,2}^+$ states, i.e., $|\Phi^\pi(^{70+n}\mathrm{Ge}; 0_1^+)\rangle = |\Phi^\pi(^{70+n}\mathrm{Ge}; 0_2^+)\rangle$. The results extracted from these analyses are illustrated in Fig. 37. A more general analysis should have both a changing proton and neutron part in the wave function but lack of data did not allow us to extract a more consistent description.

The details of proton and neutron orbital occupancies that resulted from the above-cited literature led to a series of phenomenological analyses by Fortune and co-workers (Carchidi *et al.*, 1984; Fortune, Carchidi, and Mordechai, 1984; Carchidi and Fortune, 1985; Fortune and Carchidi, 1985; Carchidi and Fortune, 1986; Carchidi, Fortune, and Burlein, 1989) and others (Johnstone and Castel, 1986) and resulted in debate (Fortune *et al.*, 1987; Vergnes and Rotbard, 1988) and further insights connecting to $E2$ properties of nuclei (Fortune and Carchidi, 1987; Carchidi and Fortune, 1988a, 1988b). Indeed, the work of Carchidi and Fortune (1988b), extended the insight provided by the Ge isotopes to an analysis of the Zr and Mo isotopes (cf. Figs. 29 and 30).

Theoretical work that addressed the low excitation energy of the first-excited $0^+$ state in $^{72}$Ge investigated collective excitations and their coupling to $2qp$ excitations, covering various techniques such as Didong *et al.* (1976), Kumar (1978), Gangopadhyay (1999), and Guo, Maruhn, and Reinhard (2007), and, stemming from the above-cited work of Vergnes and co-workers, by Ahalpara and Bhatt (1982). The early work of Iwasaki *et al.* (1976), Weeks *et al.* (1981),
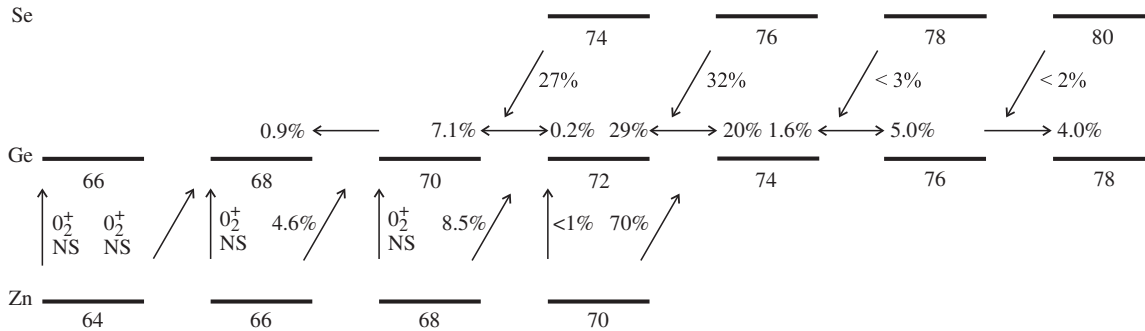
FIG. 36. Two-nucleon and multinucleon transfer strengths to $0_2^+$ states in the Ge isotopes, given relative to 100% for $0_1^+$ states (NS = not seen). The data are from Ardouin, Hanson, and Stein (1980), Boucenna *et al.* (1990), and references given in Nuclear Data Sheets.

Takada and Tazaki (1986), and Joubert *et al.* (1994), using boson mapping techniques, emphasized the importance of coupling quadrupole and pairing vibrations. The particular situation of an almost degenerate $j = 1/2$ orbital ($2p_{1/2}$) with a higher-lying high-$j$ orbital ($1g_{9/2}$) results in a strong interaction coupling the two excitation modes at $N = 40$ and was suggested to be at the origin of the specific energy dependence of the $0_2^+$ excited state. We revisit the role of $j = 1/2$ orbitals, in close proximity to high-$j$ orbitals, in Sec. III.C.3. Recently, Hasegawa, Mizusaki *et al.* (2007), Honma *et al.* (2009), and Robinson, Zamick, and Sharon (2011) (large-scale shell-model studies) also concentrated on the Ge isotopes near $N = 40$. From these calculations, it turns out

that the single-particle gap between the $1g_{9/2}$ and $2p_{1/2}$ orbitals is not big enough to keep a neutron closed shell at $N = 40$, resulting in a $0_2^+$ state that is consistent with a two-neutron excitation from the $fp$ orbitals into the $1g_{9/2}$ orbital (spherical configuration), with the $0_1^+$ ground state consistent with a deformed state (Honma *et al.*, 2009). This gives rise to a spherical-deformed shape-coexisting situation in $^{72}$Ge.

The many approaches used in this particular mass region, starting from a HFB minimization with beyond mean-field extension, using (quasi-)RPA to build pairing vibrations and coupled to quadrupole vibrations, a bosonization of S pairs, large-scale shell-model studies using effective interactions, etc., lead to an "imposed" structure that will be somewhat
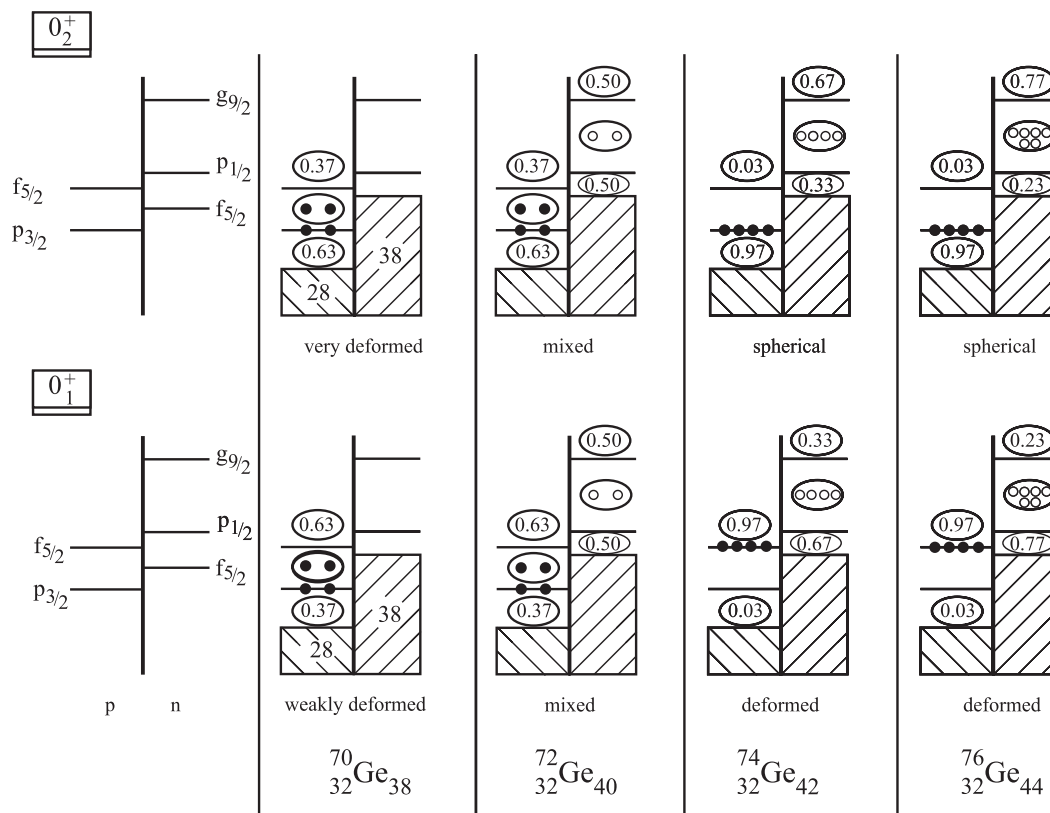


FIG. 37. The $\alpha_A^2$, $\beta_A^2$ values, from Table 3 in Van den Berg *et al.* (1982), and see text, Eq. (15), and the $\alpha_n^2$, $\beta_n^2$ values (with $n = 2$–6), from Table 3 in Becker *et al.* (1982), and see text, Eq. (16), respectively, describing the $0_1^+$ and $0_2^+$ states and separately describing the proton (Van den Berg *et al.*, 1982) and neutron (Becker *et al.*, 1982) parts of the wave functions in $^{70-76}$Ge. This illustrates the nucleon pairs in mixed shell-model configurations schematically using ovals around solid circles (protons) and open circles (neutrons).

different in each case and as such, not directly comparable, in any microscopic sense. Only by comparison with the data will it be possible to go beyond each of the various descriptions.

The odd-mass nuclei in this region appear to be either weakly deformed with decoupled bands or strongly deformed with rotational bands, with no evident occurrence of shape coexistence. Figure 38 shows a probable manifestation of the shape change and coexistence in the $N = 39$ isotones. The coexistence of prolate and oblate shapes in $^{75}$Kr and their mixing has been addressed by Skoda *et al.* (1990).

The evidence for coexisting prolate and oblate shapes in the $N = 39$ isotones is strongly supportive of wider searches for prolate-oblate coexistence in even-even nuclei in this region of $N$ and $Z$. Establishing the coexistence of oblate and prolate shapes in even-even nuclei is difficult because it requires the measurement of the signs of quadrupole moments. This is most easily carried out for $2^+$ states, but an intrinsic quadrupole moment for a $2^+$ state can be deduced only if the $K$ quantum number is known for the state: For first $2^+$ states this is reliably inferred to be $K = 0$, but for second excited $2^+$ states this can be ambiguous. We add some further details of spectroscopic results for this region that address issues of shape coexistence, but for which clarification is needed.

Figure 39 shows a selection of electric quadrupole, $E2$ properties for $^{74,76}$Kr, deduced from multistep Coulomb excitation (Clément *et al.*, 2007). We note that these isotopes are unstable, and obtaining such a detailed "map" of $E2$ properties (we do not show all those reported) represents, together with a similar study of $^{78}$Kr (see below), a first of its kind study. The $\langle Q^2 \rangle$ values for the ground and first-excited $0^+$ states strongly support shape coexistence. The diagonal $E2$ matrix elements for the first, second, and third $2^+$ states can be understood for $^{74}$Kr as revealing a prolate ($K = 0$) ground-state structure with an associated prolate $K = 2$ band, and an oblate ($K = 0$) excited $0^+$ state structure. However, the negative diagonal $E2$ matrix element for the second $2^+$

state in $^{76}$Kr, which appears to be a $K = 2$ excitation built on the ground state, is characteristic of an oblate intrinsic structure which contradicts the implied prolate intrinsic structure of the ground state.

The only sensible interpretation of $^{76}$Kr is that there must be strong mixing of coexisting prolate and oblate shapes. Strong $E0$ decays of the first-excited $0^+$ states in $^{72,74,76}$Kr (Chandler *et al.*, 1997; Wood *et al.*, 1999; Bouchez *et al.*, 2003; Giannatiempo *et al.*, 2005) unambiguously support mixing. Mixing has been suggested to explain energies in $^{72-78}$Kr and their deviation from rotor patterns (Korten, 2001; Bouchez *et al.*, 2003). To clarify this, it will be necessary to establish where there is $E0$ decay strength between $2^+$ states, as the $E0$ decay process has a $\Delta K = 0$ selection rule. In our earlier review (Wood *et al.*, 1992) we showed (Fig. 3.37), based on a comparison of yrast energies in $^{74,76}$Kr and $^{75}$Kr, that mixing must be occurring. We also caution that $\Delta K = 2$ mixing has a strong impact on diagonal $E2$ matrix elements (Allmond *et al.*, 2008).

Other multistep Coulomb excitation studies in the region include investigations of $^{70}$Se (Hurst *et al.*, 2007; Ljungvall *et al.*, 2008) and $^{78}$Kr (Becker *et al.*, 2006). The importance of triaxiality at low spin in this region was emphasized by Andrejtscheff and Petkov (1994), using model-independent arguments based on $E2$ matrix elements and the methods of Kumar (1972) and Cline (1986). These initiatives into the determination of nuclear shapes offer exciting prospects for establishing model-independent views of the more subtle aspects of nuclear collectivity in this region [cf. especially the multi-Coulex studies of Zielinska *et al.* (2002)].

Theoretical work that addresses shape coexistence centered on the Kr isotopes has been extensive. The variation after mean-field projection in realistic model spaces (VAMPIR) program made the Kr isotopes a focal point in a
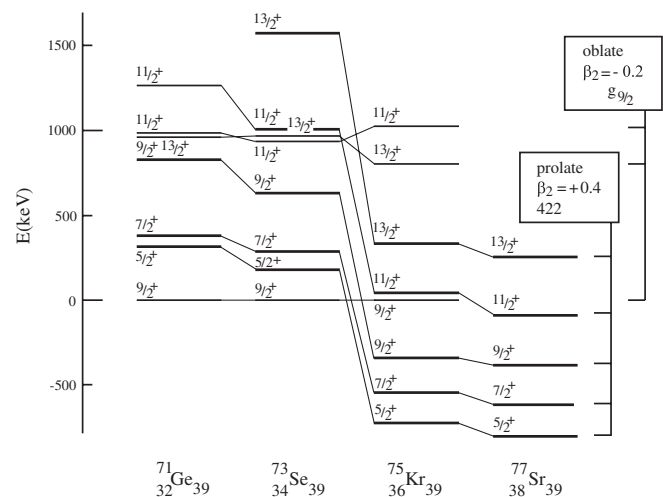


FIG. 38. Systematics of positive-parity states in the $N = 39$ isotones, arranged to reveal the probable occurrence of coexisting prolate and oblate shapes. Energies are given relative to $9/2_1^+$ in $^{71}$Ge ($E_x = 198$ keV), $^{73}$Se(gs), $9/2_2^+$ in $^{75}$Kr ($E_x = 726$ keV), arbitrarily offset in $^{77}$Sr. Band assignments are based on $\gamma$-decay branching ratios. The data are from Nuclear Data Sheets.
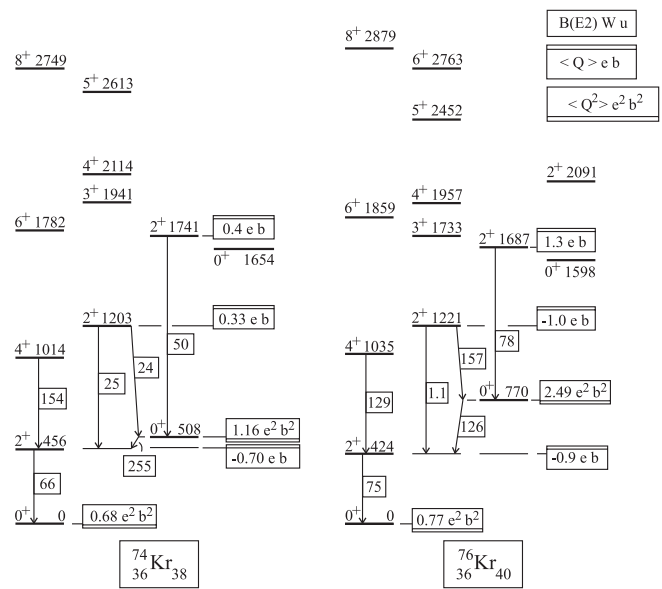


FIG. 39. Electric quadrupole collectivity in $^{74}$Kr and $^{76}$Kr. Arrows indicate selected transitions with their $B(E2)$ values. Boxes with a double underline give $\langle Q^2 \rangle$ values in units $e^2$ b$^2$ obtained by summing over squares of $E2$ matrix elements. Boxes with a double overline give the quadrupole moment $\langle Q \rangle$ in $e$ b. The data are from Clément *et al.* (2007) and Nuclear Data Sheets.

series of papers [earlier work in the VAMPIR program is given in our second review (Wood *et al.*, 1992)] (Petrovici, Schmid, and Faessler, 1992, 1996, 2000, 2002, 2003; Petrovici *et al.*, 2006). Work by the Madrid group (Sarriguren *et al.*, 1998; Sarriguren, Moya de Guerra, and Escuderos, 1999), while focused on $\beta$-decay strength, also provided valuable insight into prolate-oblate shape coexistence in this mass region. Other work includes Almehed and Walet (2004), Langanke, Dean, and Nazarewicz (2005), Hasegawa, Kaneko *et al.* (2007), Gaudefroy *et al.* (2009b), Girod *et al.* (2009), and Hinohara *et al.* (2009)).

## 6. Shape coexistence in heavy nuclei near other shells and subshells

The well-established presence of shape coexistence in the $Z \sim 50$, 82 midneutron shell regions but not in the $N \sim 50$, 82 midproton shell regions has its explanation in the subshell gaps at $Z = 40$, 64. As a consequence, intruder configurations are suppressed in the midproton shell regions at these closed-neutron shells. There is some evidence of low-energy intruder states at midsubshells such as $N \sim 50$, $Z \sim 32$, e.g., in the $N = 49$ isotones $^{81}$Ge and $^{83}$Se [see Fig. 3.25 in Heyde *et al.* (1983)]; but the issue of intruder states for $N \sim 50$, 82 nuclei remains virtually unexplored.

The emerging role of subshell gaps in giving rise to suppressed collectivity is an issue that needs to be investigated; here we point to some other regions or structures where hints to shape coexistence exist: Figure 40 shows two-proton transfer reaction strengths into even-Te and even-Xe isotopes. The second-excited $0^+$ states in these isotopes are strongly populated and may be the result of a proton subshell gap at $Z = 56$ or 58, or at $Z = 64$ [see Bloxham *et al.* (2010)].

## 7. Pairing isomers

The first hint of structures that have come to be known as pairing isomers was from the study of two-neutron transfer reactions in the actinide nuclei. There is a large asymmetry between $(p, t)$ and $(t, p)$ transfer strengths to low-lying 0+ states in Th, U, and Pu isotopes (Maher *et al.*, 1970, 1972; Casten *et al.*, 1972; Back *et al.*, 1973; Friedman *et al.*, 1974). This is explained by the concept of oblate and prolate orbitals between which there are reduced off-diagonal pairing matrix elements (Griffin, Jackson, and Volkov, 1971; Abdulvagabova, Ivanova, and Pyatov, 1972; Chasman, 1972; van Rij and Kahana, 1972; Immele and Struble, 1973; Sorensen, 1974; Abrosimov, 1979, 1981). [Chasman (1976) showed that a density-dependent delta interaction leads to off-diagonal pairing matrix elements in the actinides that vary by an order of magnitude.] Such a structure leads to different pair distributions about the Fermi energy: These can be viewed as different "deformations" of the Fermi surface.

The idea of different pairing deformations is similar to the idea of different shape deformations (in one and the same nucleus), hence the term pairing isomerism. The idea of pairing isomerism was developed by Ragnarsson and Broglia (1976). Indeed, consideration of the foregoing material in nuclei such as Zr, Mo, and Ge (see Figs. 29, 30, and 36, respectively) indicates that different shape isomers exhibit different pair structures and so shape isomers can also
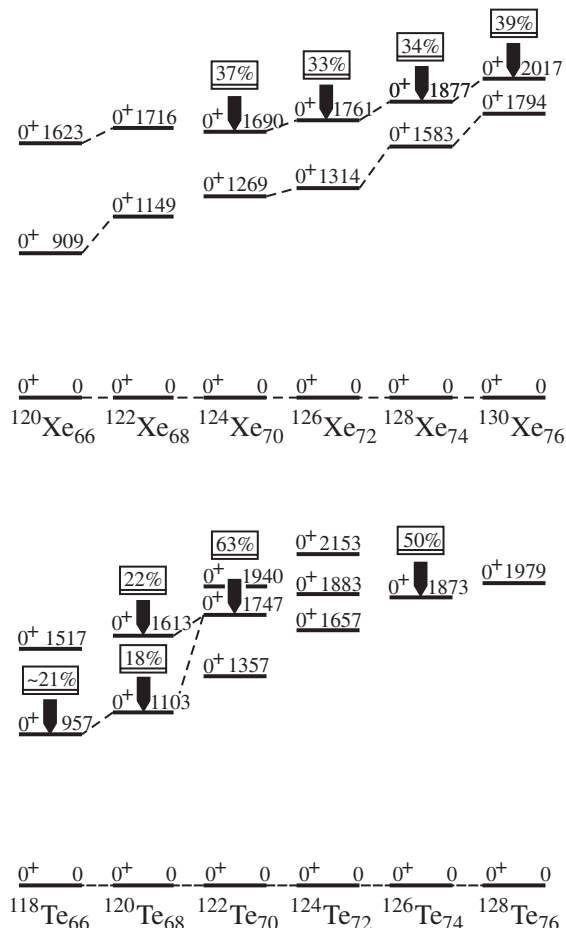


FIG. 40. Two-proton transfer data which indicate a pairing structure for $0_3^+$ states in the even-Te and even-Xe isotopes that support shape coexistence. The excited $0^+$ state populations are given as a percentage of the ground-state populations. The data are from Alford *et al.* (1979), Fielding *et al.* (1978), and Nuclear Data Sheets.

be regarded as pairing isomers. However, this raises the fundamental issue of the nature of low-lying $0^+$ states in deformed nuclei.

The interpretation of low-lying $0^+$ states in deformed nuclei, pairing isomerism aside, has been in terms of $\beta$ vibrations [see Garrett (2001) for a review] and microscopic $K^\pi = 0^+$ phonon structures, on the one hand [in the approach that was founded by Soloviev (1992), see, e.g., Lo Iudice, Sushkov, and Shirikova (2004) for a recent application], and, as couplings of $s$ and $d$ bosons to $J^\pi = 0^+$ on the other hand [see, e.g., the review by Casten and Warner (1988)]. An overall dominating view is that low-lying $0^+$ states must be collective because they lie below the pairing gap, which in deformed nuclei is nominally 2 MeV for both protons and neutrons. The evidence for pairing isomerism contradicts the concept of a single pairing gap for protons and for neutrons and, therefore, calls into question the simple view that all $0^+$ states below the pairing gap in deformed nuclei must be (quadrupole) collective [see also the review by Garrett (2001)].

There is a further issue with rotational bands built on excited $0^+$ states in deformed nuclei: They can show variations in rotational parameters, relative to the ground-state

band, of up to ±40%. Table I shows the largest differences known for the rare-earth region. In the table we show all known excited $K = 0$ bands with rotational energy spacing significantly different from the ground-state band. The "rank" $i$ of each band is indicated: $i = 1$, ground-state band; $i = 2$, first-excited $K = 0$ band, etc.; a missing rank number means that the $K = 0$ band has a similar rotational spacing to the ground-state band. The most extreme variations are indicated by ratios $r$ defined in the caption. Note that bands with rotational spacing significantly greater than the ground-state band, given at the end of the second column, all occur in nuclei at the "edges" of the deformed rare-earth region, i.e., they are consistent with the intrusion of less-deformed structures into a more deformed region.

The variation in rotational energy spacing of excited $K = 0$ bands in the rare-earth region was pointed out by a number of authors, see, e.g., Kuyucak and Morrison (1988), who note that such bands lie entirely outside of an IBM space, even with the commonly used extension employing $g$ and higher $L$ bosons. This point was also made by Bohr and Mottelson (1982). Indeed, while the spectroscopy involved can be demanding, a $K = 0$ band associated with two-neutron

TABLE I. The known cases of excited $K = 0$ bands in deformed rare-earth nuclei with rotational energy spacing significantly different from the ground-state band. The labeling $i$ is explained in the text; $\Delta E_{20}^i \equiv E_{2_i} - E_{0_i}$, $r \equiv (\Delta E_{20}^i)/(\Delta E_{20}^1)$, energies are given in keV, and the choice of cases for which $r$ is given is explained in the text. The data are from Nuclear Data Sheets.

| Isotope | $i$ | $\Delta E_{20}^i$ | $r$ | Isotope | $i$ | $\Delta E_{20}^i$ | $r$ |
|---|---|---|---|---|---|---|---|
| $^{156}$Gd | 1 | 89 | | $^{170}$Yb | 1 | 84 | |
| | 2 | 70 | | | 2 | 70 | |
| | 4 | 56 | 0.63 | $^{172}$Yb | 1 | 79 | |
| | 5 | 64 | | | 4 | 55 | 0.70 |
| $^{158}$Gd | 1 | 80 | | | 5 | 61 | 0.77 |
| | 2 | 64 | | $^{178}$Yb | 1 | 84 | |
| | 4 | 49 | 0.61 | | 2 | 72 | |
| $^{160}$Gd | 1 | 75 | | $^{172}$Hf | 1 | 91 | |
| | 2 | 51 | | | 4 | 61 | 0.67 |
| | 3 | 56 | | $^{176}$Hf | 1 | 88 | |
| $^{160}$Dy | 1 | 87 | | | 2 | 77 | |
| | 2 | 70 | | $^{178}$Hf | 1 | 93 | |
| | 5 | 59 | 0.68 | | 2 | 78 | |
| $^{164}$Er | 1 | 91 | | | 3 | 62 | |
| | 2 | 69 | | | 4 | 70 | |
| | 3 | 67 | | $^{178}$W | 1 | 106 | |
| $^{166}$Er | 1 | 81 | | | 2 | 86 | |
| | 2 | 68 | | $^{152}$Nd | 1 | 73 | |
| $^{168}$Er | 1 | 80 | | | 2 | 112 | 1.53 |
| | 2 | 59 | 0.75 | $^{182}$W | 1 | 100 | |
| | 4 | 59 | 0.75 | | 2 | 121 | 1.21 |
| $^{170}$Er | 1 | 79 | | $^{186}$W | 1 | 123 | |
| | 2 | 69 | | | 2 | 146 | 1.19 |
| | 3 | 61 | 0.75 | $^{184}$Os | 1 | 120 | |
| $^{164}$Yb | 1 | 123 | | | 2 | 163 | 1.36 |
| | 2 | 98 | | | | | |
| $^{168}$Yb | 1 | 88 | | | | | |
| | 4 | 62 | | | | | |

pair-transfer asymmetry characteristic of pairing isomerism and with considerably increased energy spacing, relative to the ground-state band, has been established in the $N = 90$ isotones, $^{154}$Gd (Kulp et al., 2003) and $^{152}$Sm (Kulp et al., 2005).

There is a further and interesting perspective on the role of pairing isomerism in deformed nuclei. Jänecke et al. (1981) observed that the $(d, {}^6\text{Li})$ $\alpha$ cluster transfer on selected actinide targets exhibits population of excited $0^+$ states with $>100\%$ of the ground-state strength. This indicates that there are strong proton-pair–neutron-pair correlations involved in these $0^+$ states. This is especially remarkable in that the $0^+$ states involved look completely ordinary with respect to other reported spectroscopic properties of these states. A further look at possible underlying structures of this type is explored by Wood (1984).

## 8. Superdeformation

Superdeformation (SD) has been a major facet of nuclear structure for over 40 years, at its inception in the guise of fission isomers (Polikanov et al., 1962; Metag, Habs, and Specht, 1980; Singh, Zywina, and Firestone, 2002) and followed by an explosive development due to its manifestation at high spin in the form of SD bands (Twin et al., 1986; Singh, Zywina, and Firestone, 2002). Although it is a dramatic form of shape coexistence, the topic has developed virtually in a completely independent manner from other investigations of shape coexistence, probably because the former were almost always in the high-spin regime and the latter in the low-spin regime. A serious obstacle to unifying the two has been the sparseness of information on absolute excitation energies and spins of SD bands because of the difficulty of elucidating patterns for their "draining," i.e., decay into low-spin regions. Achieving a unified description of SD band structures and low-spin coexistence structures remains a major unsolved problem in nuclear physics primarily because, while SD bands are amenable to semiclassical descriptions, such as the total Routhan surfaces (TRS) descriptions [see, e.g., Aberg, Flocard, and Nazarewicz (1990), Janssens and Khoo (1991), Nilsson and Ragnarsson (1995), Afanasjev et al. (1999), and Frauendorf (2001)], low-spin coexistence structures necessitate a fully quantum-mechanical description.

However, in contrast to the above rather pessimistic view, we point to a recent development that appears to offer some encouraging steps in the direction of a unified description of all shape coexistence, namely, the observation of many SD bands in the isotopes just above $^{56}$Ni (Svensson et al., 1997, 1998; Rudolph et al., 1998, 2001) with detailed information on patterns of draining. Indeed, the discovery of these bands comes with an extraordinary bonus: There are many draining paths that occur by prompt proton and $\alpha$-particle emission (Rudolph et al., 2005). This may be regarded as a completely new class of nuclear structure spectroscopy. Some bands may even have partial decay widths for proton emission that have led to the statement "...there even seems to be a kind of proton 'rain'." (Johansson et al., 2009). We return to this point below.

Table II gives a sampling of SD band properties. There is evidently a rather strong uniformity of excitation energies and inferred intrinsic quadrupole moments for SD bands, and a

few other bands in nuclei with $A \leq 56$ which are included and discussed in more detail in a following section. Indeed, we include nuclei for which SD bands extend all the way down to $J = 0$ to make a key point: The entire bands are seen when the low-energy level density is low. It is likely that many other SD bands involve $J = 0$ intrinsic configurations, but mixing substantially obscures the low-spin members because they are embedded in a dense, near continuum of other low-spin configurations. With the imminent arrival of next generation detector arrays (GRETINA, AGATA) this situation will soon change.

The observation of prompt charged particle decays from SD bands can be regarded as potentially a completely new spectroscopic fingerprint. It is in a sense an analog of single- and few-nucleon transfer reaction probes of rotational bands, so effectively developed in the deformed rare-earth and actinide nuclei and referred to as the "fingerprint of a band" (Elbek and Tjom, 1969; Rasmussen, 1970). Essentially, this found expression for rotations built on (deformed) Nilsson configurations as expansions in a spherical basis (to match the laboratory frame with respect to which the transfer reaction is occurring). The difference is that transfer reactions have to be reduced via a distorted-wave Born approximation (or a coupled-channels Born approximation), whereas the emission of charged particles has to be reduced via a barrier penetration approximation. Rotation alignment simplifies both processes, in the latter case being formulated as a two-dimensional barrier penetration problem (Rudolph *et al.*, 2005).

## B. Light nuclei

### 1. Shape coexistence in and near the $N = Z$ nuclei

Shape coexistence in nuclei had its historical origins in the doubly closed shell $N = Z$ isotopes $^{16}$O and $^{40}$Ca. Following

TABLE II. A selection of superdeformed band properties. Energies $E(J^{\pi})$ and energy differences $\Delta_{J,J'} = E(J) - E(J')$ are in keV. Transition quadrupole moments $Q_t$ are deduced from lifetime data. Some quadrupole deformation parameter values are given, assuming spheroidal nuclear shapes. Some features of these bands are discussed in the text. The data are from Johansson *et al.* (2009) ($^{58}$Ni), Svensson *et al.* (1999) ($^{60}$Zn), Rudolph *et al.* (2002b) ($^{58}$Cu), Andreoiu *et al.* (2002) ($^{59}$Cu), Yu *et al.* (1999), Andersson *et al.* (2009) ($^{61}$Zn), Svensson *et al.* (1997), Gellanki *et al.* (2009) ($^{62}$Zn), Singh, Zywina, and Firestone (2002) ($^{133}$Nd, $^{152}$Dy, $^{194}$Hg, $^{194}$Pb, $^{238}$U), and Wilson *et al.* (2003) ($^{192}$Hg).

| Isotope | $E(0^+)$ | $E(12^+)$ | $\Delta_{14,12}$ | $\|Q_t\|\ e\,\mathrm{b}$ | $\beta_2$ |
|---|---|---|---|---|---|
| $^{58}$Ni | $\cdots$ | 13 606 | 1688 | | |
| $^{60}$Zn | $\cdots$ | 12 132 | 1566 | $2.75^{45}$ | $0.47^7$ |
| | $J$ | $E(J)$ | $\Delta_{J+2,J}$ | | |
| $^{58}$Cu | 13 | 10 942 | 1576 | $\sim 2.5$ | |
| $^{59}$Cu | 29/2 | 13 351 | 1599 | $2.23^{27}_{22}$ | |
| $^{61}$Cu | 29/2 | 11 775 | 1509 | | |
| $^{61}$Zn | 29/2 | 12 802 | 1629 | $3.0^5_4$ | $0.50^7_6$ |
| | 41/2 | 18 363 | 2311 | | |
| $^{62}$Zn | 20 | 19 400 | 2214 | $2.7^4_3$ | $0.45^{10}_7$ |
| $^{133}$Nd | 17/2 | 2028 | 345 | $7.0^7$ | |
| $^{152}$Dy | 24 | 10 644 | 602 | $17.5^2$ | |
| $^{194}$Hg | 8 | 6416 | 212 | $16.8^7$ | |
| $^{192}$Pb | 8 | 4425 | 215 | | |
| $^{194}$Pb | 6 | 4878 | 170 | $20.6^{13}$ | |
| $^{238}$U | 0 | 2558 | $\sim 20$ | $29^3$ | |

Morinaga's original suggestion (Morinaga, 1956) that the first-excited state in $^{16}$O could (because it has spin zero and positive parity) only be understood by promotion of pairs of protons and pairs of neutrons across the $N$, $Z = 8$ closed shells, the nearly identical pattern of behavior in $^{40}$Ca was similarly explained (Brown, 1964; Brown and Green, 1966a, 1966b). The early history of the subject is detailed in our first review (Heyde *et al.*, 1983) and the status of coexistence in light, even-mass nuclei in 1992 is detailed in our second review (Wood *et al.*, 1992).

The occurrence of shape coexistence in the $N = Z$ nuclei $^{16}$O and $^{40}$Ca naturally suggests that it should occur also in $^{56}$Ni. Figure 41 shows the coexisting bands observed (Rudolph *et al.*, 1999) in $^{56}$Ni and an updated view of information (Ideguchi *et al.*, 2001) for $^{40}$Ca. Shape coexistence also occurs in nuclei neighboring $^{16}$O, $^{40}$Ca, and $^{56}$Ni. Table III shows the full extent of candidates for coexisting bands for even-even nuclei with $A$, $Z \leq 28$. Important further details can be found for some of these isotopes in our second review and the evidence for their multiparticle–multihole character has been discussed in a review by Fortune (1978).

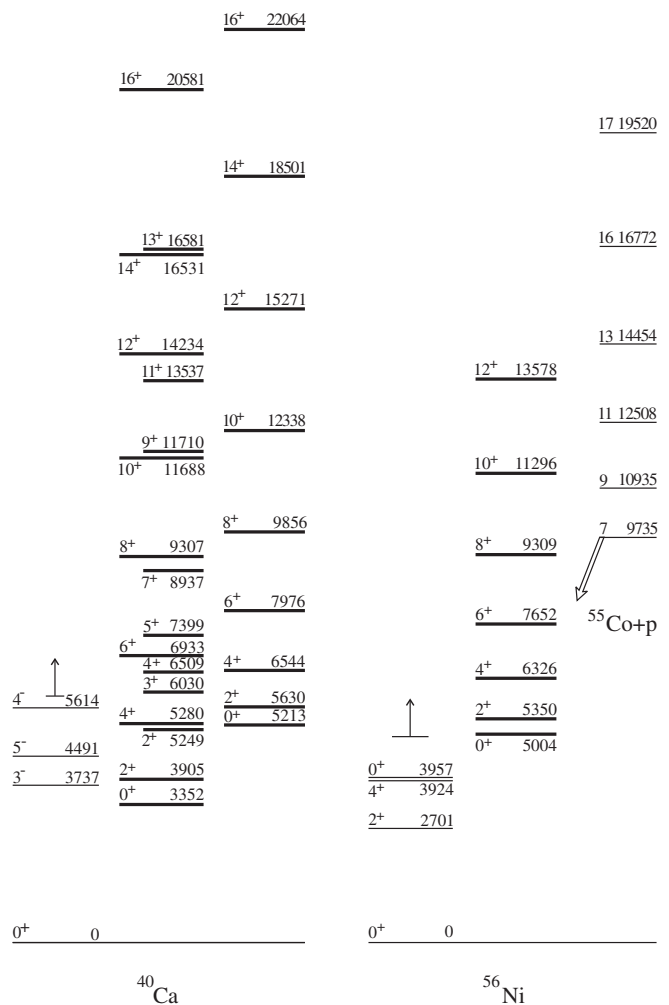

FIG. 41. Shape-coexisting bands in the $N = Z$ isotopes, $^{40}$Ca and $^{56}$Ni. The vertical arrows indicate excitation energies above which other excited states are observed. The state at 9735 keV in $^{56}$Ni decays by proton emission. The data are from Ideguchi *et al.* (2001), Johansson *et al.* (2008), and Nuclear Data Sheets.

The occurrence of shape coexistence in the $1f_{7/2}$ shell, manifested in the appearance at low energy of $s$-$d$ shell hole configurations in odd-mass nuclei, has been known for a long time [see, e.g., Styczen *et al.* (1976)]. In Fig. 42, we give an up-to-date perspective on this manifestation of coexistence. Detailed discussion of these structures can be found in Bednarczyk *et al.* (1997, and 1998). We emphasized that coexistence in this region probably involves multiparticle–multihole configurations [see, e.g., Wood *et al.* (1992), Fig. 3.9]. We note that these configurations are important for corrections to superallowed Fermi $\beta$ decay (Towner and Hardy, 2008).

### 2. Coexistence or islands of inversion? $(N, Z) \sim (8, 6)$, (20,12), and (28,14)

In recent years there has been a strong impetus toward the study of neutron-rich nuclei. This is motivated by the vast territory of isotopes which are predicted to be bound with respect to neutron emission, but for which there is little or no structural information. It is in this territory that answers to the question "Where do the heavy $(Z > 28)$ elements come from?" will be found, e.g., what is the isotopic path of the rapid neutron capture process in supernovae? It is also in neutron-rich regions that researchers are seeking the break-

down of shell structure [see, e.g., Dobaczewski *et al.* (1994), Hamamoto, Lukyanov, and Zhang (2001), Bender, Bertsch, and Heenen (2008), and Otsuka, Suzuki, Honma *et al.* (2010)] and pairing [see, e.g., Dobaczewski *et al.* (1996), Hebeler *et al.* (2009), and Baroni, Macchiavelli, and Schwenk, 2010]. The issue of shape coexistence and intruder states is central to this program of study. We observe that, particularly in light of the systematic view of intruder states and shape coexistence in heavy nuclei provided in this review, caution needs to be exercised in the interpretation of fragmentary information, most notably when it is tempting to announce departures from tenets of nuclear structure that have stood the test of some 60 years of wide and detailed spectroscopic study.

Figure 43 illustrates a remarkable similarity between the isotopic pairs $^{11}$Be/$^{12}$Be, $^{35}$S/$^{36}$S, $^{43}$S/$^{44}$S, $^{43}$K/$^{44}$Ca, $^{117}$In/$^{118}$Sn, and $^{189}$Tl/$^{190}$Pb. The pairs shown in Fig. 43(a) all lie at, or adjacent to, so-called "islands of inversion." The term island of inversion was first used by Warburton, Becker, and Brown (1990). The isotopes $^{12}$Be, $^{36}$S, and $^{44}$S are, conventionally, singly closed shell nuclei ($N = 8$, 20, 28). However, the isotopes $^{11}$Be, $^{35}$S, and $^{43}$S all exhibit low-lying intruder states. It is particularly the $N = 8$, 20, and 28 shells that have received attention regarding breakdown, as suggested to be evidenced by $^{12}$Be, $^{32}$Mg, and $^{44}$S [see, e.g.,

TABLE III. Coexistence in doubly even nuclei with $A \leq 56$: Deformed band energies are given in keV; $B(E2)$ values in W.u. [$B'_{20} \equiv B(E2; 2^+_{\text{def}} \to 0^+_{\text{def}})$] and $B_{20} \equiv B(E2; 2^+_1 \to 0^+_1))$. The data are from Ideguchi *et al.* (2010) and Nuclear Data Sheets.

| Isotope | $E(0^+)$ | $E(2^+)$ | $E(4^+)$ | $E(6^+)$ | to | $B'_{20}$ | $B'_{42}$ | $B'_{64}$ | $B_{20}$ |
|---|---|---|---|---|---|---|---|---|---|
| $^{14}_{6}$C$_8$ | 6589 | 8318 | 10736 | | | | | | |
| $^{14}_{8}$O$_6$ | 5920 | 7768 | 9915 | | | | | | |
| $^{16}_{8}$O$_8$ | 6049 | 6917 | 10355 | 16275 | | 27 | 65 | | $\cdots$ |
| $^{18}_{8}$O$_{10}$ | 3634 | 5255 | 7117 | | | 23 | | | 3.3 |
| $^{18}_{10}$Ne$_8$ | 3576 | 5106 | 7050 | | | | | | |
| $^{20}_{10}$Ne$_{10}$ | 6725 | 7422 | 9990 | | | | | | |
| | 7191 | 7833 | 9031 | 12317 | | | | | |
| $^{24}_{12}$Mg$_{12}$ | 6433 | 7849 | 8439 | | | | 39 | | 21 |
| $^{28}_{14}$Si$_{14}$ | 6691 | 7381 | 9165 | 11509 | | | 29 | | 13 |
| $^{32}_{16}$S$_{16}$ | 3778 | 5549 | | | | | | | |
| $^{36}_{18}$Ar$_{18}$ | 4329 | 4951 | 6137 | 7767 | $16^+$ | | 53 | 64 | 8.4 |
| $^{38}_{18}$Ar$_{20}$ | 3377 | 3937 | 5350 | 7288 | $16^+$ | | 29 | 31 | 3.3 |
| $^{40}_{18}$Ar$_{22}$ | 2121 | 2524 | 3515 | 4959 | $12^+$ | | 47 | 70 | 9.3 |
| $^{38}_{20}$Ca$_{18}$ | 3084 | 3684 | | | | | | | |
| $^{40}_{20}$Ca$_{20}$ | 3352 | 3905 | 5279 | 6930 | $16^+$ | 32 | 61 | 17 | $\cdots$ |
| | 5213 | 5630 | 6543 | 7976 | $16^+$ | | 170 | | $\cdots$ |
| $^{42}_{20}$Ca$_{22}$ | 1837 | 2424 | 3254 | 4715 | $8^+$ | | | | |
| $^{44}_{20}$Ca$_{24}$ | 1883 | 2656 | | | | | | | |
| $^{46}_{20}$Ca$_{26}$ | 2423 | 3024 | 3860 | | | | | | |
| $^{42}_{22}$Ti$_{20}$ | 1854 | 2396 | | | | | | | |
| $^{44}_{22}$Ti$_{22}$ | 1904 | 2531 | 3365 | 4500 | $12^+$ | 24 | 22 | | 13 |
| $^{52}_{24}$Cr$_{28}$ | 2647 | 2965 | 3415 | | | | | | |
| $^{54}_{26}$Fe$_{28}$ | 2562 | 2959 | | | | | | | |
| $^{56}_{28}$Ni$_{28}$ | 5002 | 5351 | 6327 | 7653 | $12^+$ | | | | |
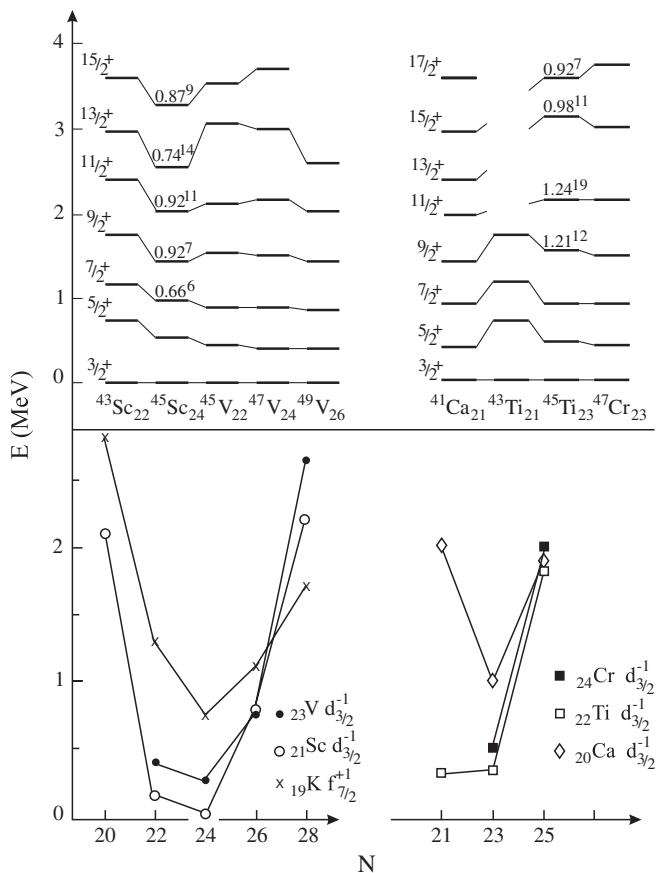
FIG. 42.   Systematics of the $d_{3/2}$ hole intruder orbital in the $f_{7/2}$ shell. The upper part shows the collective bands built on the configuration and the lower part shows the bandhead energies relative to the ground states (odd-proton cases on the left and odd-neutron cases on the right). The numbers given on the levels for $^{45}$Sc and $^{45}$Ti in the upper part of the figure are magnitudes of $Q_0$ in $e$ b (e.g., $0.66^6 = 0.66 \pm 0.06$), deduced from $B(E2)$ measurements by Bednarczyk et al. (1998). Energies are from Nuclear Data Sheets. The $3/2^+$ state in $^{45}$Sc is at 12.6 keV.

Sorlin and Porquet (2008)]. A comparison with the extensive data for even and odd nuclei in the $Z \sim 20$, 50, and 82 regions, a sample of which is given in Fig. 43(b), suggests that these isotopic pairs possess structures that can be placed in a unified framework involving intruder states and their connection to shape coexistence. Thus, the excited $0^+$ states in these even isotopes are all due to neutron- (proton-) pair excitations across neutron (proton) closed shells, and they are lowered in energy by the enormous gain in energy resulting from proton-pair–neutron-pair correlations.

The unified view provided above indicates that shape coexistence in these neutron-rich regions should occur for a spread in mass numbers. There is gathering evidence that this view is correct, albeit often realized only in the face of considerable experimental difficulties. Figure 44 shows the systematic features of low-lying excited states in the $N = 20$ isotones. The nucleus $^{32}$Mg has long been known (Détraz et al., 1979) to have a low-energy $2^+$ first-excited state. Lack of detailed spectroscopy has left this picture essentially unchanged for 30 years. Progress has been made in the neighboring isotopes $^{31}$Mg and $^{33}$Mg, where the characterization of ground-state spins and magnetic moments (Neyens et al.,

2005; Yordanov et al., 2007) provide strong evidence for intruder configurations becoming the ground state. The recognition that shape coexistence may be occurring in the neutron-rich $N \sim 28$ region is much more recent (Sarazin et al., 2000).

The close energy relationship between intruder states adjacent to closed shells and excited $0^+$ states in the neighboring singly closed shell nuclei, noted already for $Z = 82$, 50, can be demonstrated also for $N = 19$, 20, 21 and is shown in Fig. 45. We emphasize that it is the correlated pairs that appear to quantitatively explain the energy systematic. Clearly, the critical test of this picture will be the observation of low-energy excited $0^+$ states in $^{32}$Mg and $^{34}$Si, the former a spherical state and the latter a deformed state (with an associated rotational band). Recently, an excited $0^+$ state at an excitation energy of 1058 keV has been observed in $^{32}$Mg using a two-neutron transfer reaction in inverse kinematics at REX-ISOLDE (Wimmer et al., 2010), giving support to the proposed picture. Ibbotson et al. (1998) suggested that the $2_1^+$ state in $^{34}$Si is a $\nu$(2p-2h) configuration. It is this relationship which suggests that caution is needed in the language used to describe the structure at $N \sim 8$, 20, and 28: These structures are not due to a breakdown of the shell model, which is an independent-particle model; they are due to the correlation energies involved when pair excitations across closed shells occur. The term island of inversion refers to the fact that the 2p-2h states are below the 0p-0h closed-shell state. This implies inversions of states, in which phenomena are no different to the long known and widely characterized shape coexistence occurring in heavier nuclei and in $^{16}$O, $^{40}$Ca, and their neighbors. We add some discussion of evidence for shape coexistence in this region, with a measure of caution regarding what we point to being well established: The spectroscopy is difficult and progress in establishing a clear view of the structures involved is not smooth.



FIG. 43.   Selected pairs of nuclei showing a possible relationship between 1p-2h intruder states (marked with solid triangles) and low-lying excited $0^+$ states. The data are from Coenen (1985), Ajzenberg-Selove (1990), Endt (1998), Grévy et al. (2005), Shimoura et al. (2007), Gaudefroy et al. (2009a), and Nuclear Data Sheets.
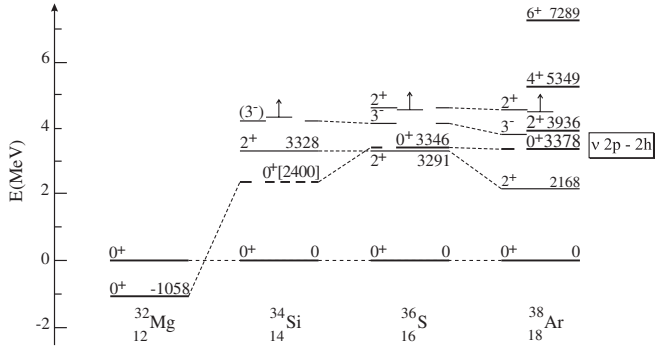
FIG. 44. Systematics of the even-mass $N = 20$ isotones. Known and possible $\nu$(2p-2h) states are shown. In $^{38}$Ar this structure gives rise to a deformed band. The extrapolation of this structure (see also Fig. 45) to explain the deformed states in $^{32}$Mg is discussed in the text. The estimate of the $0^+$ $\nu$(2p-2h) state at 2400 keV in $^{34}$Si is from Fig. 45 (and see the remark in the text on the $2^+_1$ state in $^{34}$Si). The data are from Endt (1998), Nummela et al. (2001a), Rudolph et al. (2002a), Wimmer et al. (2010), and Nuclear Data Sheets.

A key question with respect to the $N \sim 20$, 28 neutron-rich region is "To what degree do the $N = 20$ and 28 shell closures appear to survive?" Figure 46 shows the systematic pattern of the energy of the first-excited $2^+$ state as a function of $N$ and $Z$ in this region. This is always a leading indicator of nuclear structure in any mass region. We point, especially, to the strong asymmetry across the $N = 20$ line for the Ne and Mg isotopes, and the asymmetry across the shell; cf. $^{34}$Si and $^{42}$Si. Evidently, significant changes in structure are occurring.
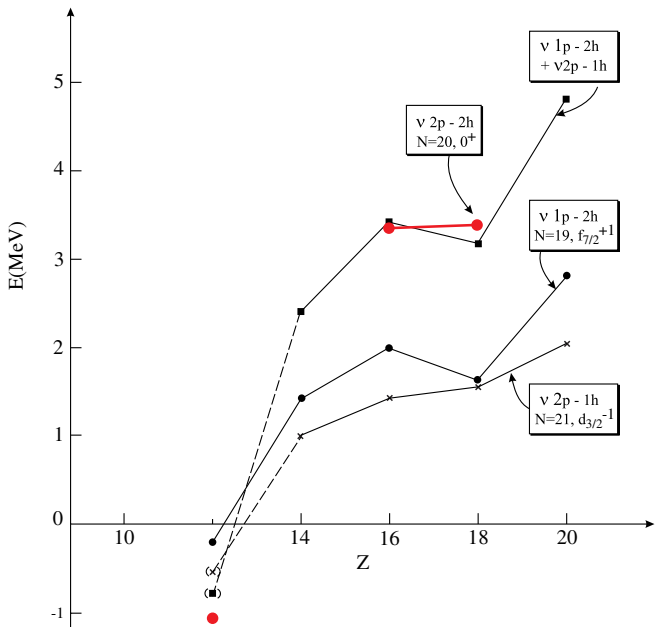
FIG. 45 (color online). Systematics of multiparticle–multihole states in the $N = 19$, 20, and 21 isotones. The sum of the $\nu$(1p-2h) and $\nu$(2p-1h) state energies strongly correlates with that of the $\nu$(2p-2h) state energies (cf. Figs. 17 and 24), supporting the extrapolation shown in $^{34}$Si and $^{32}$Mg. The $N = 21$ extrapolation from $^{35}$Si to $^{33}$Mg is assumed to be parallel to $N = 19$. The data are from Endt (1998), Nummela et al. (2002), Z. M. Wang et al. (2010b), Wimmer et al. (2010), and Nuclear Data Sheets.

We mention a few issues for which there are some encouraging answers. With regard to what is happening in $^{30-34}$Mg, a deformed structure has probably intruded to become the ground state at $^{32}$Mg: An excited $0^+$ state has been observed in $^{30}$Mg at 1789 keV by Schwerdtfeger et al. (2009), which may be the deformed intruding structure.

There has been emphasis placed on the importance of delineating the border of the island of inversion. Thus, there has been debate regarding whether the ground state of $^{33}$Al is inside or outside of the border (Himpe et al., 2006; Tripathi et al., 2008b). The debate hinges on the reliability of structural interpretation based on spins and parities deduced from $\log ft$ values (Tripathi et al., 2008b) versus magnetic moment values [see Yordanov et al. (2010)]. While the unequivocal resolution of these questions will provide a deeper insight into the structures underlying this region, it should be evident from the occurrence of shape coexistence in other mass regions that exactly which nuclei possess intruder ground states is interesting, but not profound: but for 12.6 keV (cf. Fig. 42), $^{45}$Sc would have been an island of inversion.

The importance of pairing structure in its role underlying shape coexistence has been emphasized for a number of mass regions in this review. We point to the use of "knockout" reactions as a promising fingerprint for exploration of intruder structures in this region. Following details of the underlying theory (Hansen and Tostevin, 2003; Tostevin et al., 2004; Tostevin and Brown, 2006), a number of applications have been made; see, e.g., Sauvan et al. (2000), Bazin et al. (2003), Fridmann et al. (2006), Yoneda et al. (2006), Diget et al. (2008), Gade et al. (2008), Terry et al. (2008), Miller et al. (2009), Nakamura et al. (2009), Simpson et al. (2009a, 2009b), Fallon et al. (2010), Gade and Tostevin (2010), and Kanungo et al. (2010). See also Catford et al. (2005), Gaudefroy et al. (2006, 2008), and Lee et al. (2010); and combined with in-beam $\gamma$-ray spectroscopy, for a recent

| | | N=18 | N=20 | N=22 | N=24 | N=26 | N=28 | N=30 | N=32 | N=34 | N=36 |
|---|---|---|---|---|---|---|---|---|---|---|---|
| Cr | 24 | | | 892 | 752 | 783 | 1434 | 835 | 1007 | 881 | 646 |
| Ti | 22 | | 1556 | 1083 | 889 | 983 | 1554 | 1050 | 1495 | 1129 | |
| Ca | 20 | 2213 | 3904 | 1525 | 1157 | 1346 | 3832 | 1026 | 2563 | | |
| Ar | 18 | 1970 | 2168 | 1461 | 1208 | 1158 | 1577 | 1037 | | | |
| S | 16 | 2127 | 3291 | 1292 | 904 | 890 | 1330 | 952 | | | |
| Si | 14 | 1941 | 3328 | 1399 | 1084 | 986 | 770 | | | | |
| Mg | 12 | 1483 | 886 | 660 | 660 | | | | | | |
| Ne | 10 | 1320 | 792 | 722 | | | | | | | |

FIG. 46. Energies of $2^+_1$ states for $N \geq 18$, $Z \leq 24$, illustrating the $N$, $Z = 20$, $N = 28$ shell closures and the neutron-drip line ($B_n \sim 0$). Some features are discussed in the text. The data are from Yanagisawa et al. (2003), Fornal et al. (2004), Liddick et al. (2004), Belleguic et al. (2005), Grévy et al. (2005), Iwasaki et al. (2005), Dombrádi et al. (2006), Doornenbal et al. (2009), and Nuclear Data Sheets.

review, see Gade and Glasmacher (2008), and also Gade et al. (2007, 2009).

A major difference between the manifestation of shape coexistence in light nuclei and heavy nuclei is the extent in mass number over which systematic study can be carried out. Systematic study, working from near stability to far from stability, played an essential role in elucidating shape coexistence in nuclei. If changes in structure as a function of mass number are too sudden, this makes the experimental task of spectroscopic characterization demanding. The only solution to this challenge is to conduct detailed spectroscopy: An excellent example of this is the work of Bednarczyk et al. (1998) in the $1f_{7/2}$ shell; cf. Fig. 42. Thus, it will be important in the study of shape coexistence at $N \sim 20$, 28 to carry out detailed spectroscopy of nuclei such as $^{33,34,35}$Si, $^{35,36,37}$S ($N = 19$, 20, 21) and $^{43,44,45}$S, $^{45,46,47}$Ar ($N = 27$, 28, 29), because further from stability detailed spectroscopy becomes increasingly challenging and ultimately impossible.

In our perusal of the literature for the neutron-rich $N \sim 20$, 28 region we encountered an active research frontier. While it is premature to present hard and fast interpretations of the emerging structure for these regions, we present a digest of the experimental literature to illustrate the techniques being used, organized by technique.

A major advance has become available in nuclear structure study with intense, high-energy radioactive beams and the large cross sections associated with Coulomb excitation. This provides access to probing the basic collectivity in nuclei far from stability with the determination of $2_1^+$ excitation energies and $B(E2; 2_1^+ \rightarrow 0_1^+)$ transition strengths in even-even nuclei. Examples of what has been achieved are found in a recent review by Görgen (2010), in an earlier review by Glasmacher (1998), and in Pritychenko et al. (2000, 2001), 2002), and Scheit et al. (2004).

Inelastic scattering and transfer reactions with radioactive beams (in inverse kinematics) also provide basic structural information; see, e.g., Maréchal et al. (1999, 2005), Chisté et al. (2001), Mittig et al. (2002), Yanagisawa et al. (2003), Iwasaki et al. (2005), Dombrádi et al. (2006), Elekes et al. (2006), Obertelli et al. (2006), Campbell et al. (2007), Doornenbal et al. (2009, 2010), and Takeuchi et al. (2009); and combined with in-beam $\gamma$-ray spectroscopy, Iwasa et al. (2003).

Grazing-incidence and deep-inelastic reactions provide access to medium-high spin states and, thus, via $\gamma$-ray spectroscopy information on band structure in neutron-rich nuclei; see the recent review by Gade and Glasmacher (2008), and Fornal et al. (1997, 2000), Liang et al. (2002a, 2002b), 2006), Sakurai (2002, 2005), Ollier et al. (2003, 2005), Belleguic et al. (2005), Krishichayan et al. (2006), Hodsdon et al. (2007), Tarasov et al. (2007, 2009), Bhattacharyya et al. (2008), Riley et al. (2008, 2009a, 2009b), Wiedeking et al. (2008), Moralles et al. (2009), Mengoni et al. (2010), O'Donnell et al. (2010), and Z. M. Wang et al. (2010a, 2010b). Some compound-nucleus evaporation reactions also provide access to these neutron-rich regions; see, e.g., Mason et al. (2005), Bender et al. (2009), Chakrabarti et al. (2009), Ionescu-Bujor et al. (2009), Deacon et al. (2010), and Force et al. (2010). An exciting prospect is direct observation of short-lived states

populated in fragmentation (Grévy et al., 2005). Among the more spectroscopically explicit probes is $\gamma$-ray spectroscopy following charge exchange reactions (Zegers et al., 2010).

Radioactive decay will always be a favored tool for far-from-stability study because it is less demanding on experimental setups. One bonus in neutron-rich nuclei is that excited states in a daughter nucleus can be populated in both $\beta$ decay and $\beta$-delayed neutron emission decay: This usually results in direct population of states in different spin ranges. Some examples of recent studies in the $N \sim 20$, 28 regions are found in Klotz et al. (1993), Winger et al. (2001), Nummela et al. (2001a, 2001b), 2002), Morton et al. (2002), Grévy et al. (2004), Weissman et al. (2004), Mach et al. (2005), Mantica (2005a, and 2005b), Maréchal et al. (2005), Padgett et al. (2005), Timis et al. (2005), Tripathi et al. (2005, 2006, 2007, Tripathi et al. (2008a, 2008b), Winger, Mantica, and Ronningen (2006), Mattoon et al. (2007), White et al. (2007), and Schwerdtfeger et al. (2009).

Ground- and isomeric-state properties, such as precision mass measurements and moments, often provide the first view of a newly accessible mass region. Recent mass measurements in the neutron-rich $N \sim 20$, 28 region include Sarazin et al. (2000); Lunney et al. (2001, 2006), Block et al. (2008a, 2008b), Gaulard et al. (2006), Jurado et al. (2007), Ringle et al. (2009), and Savajols et al. (2005). Recent moment measurements include Keim et al. (2000), Borremans et al. (2002), Neyens et al. (2005), Davies et al. (2006), Himpe et al. (2006, 2008), Speidel et al. (2006, 2008), Stuchbery et al. (2006), Kameda et al. (2007), Yordanov et al. (2007), Blaum et al. (2008), Kowalska et al. (2008), De Rydt et al. (2009, 2010), Gaudefroy et al. (2009a), Nagae et al. (2009), and Nagatomo et al. (2009).

Theoretical work that addresses structure in the $N \sim 20$, 28 region has particularly focused on shape coexistence and on shells and their survival in neutron-rich nuclei (see Secs. II.A and II.B for a more general discussion in the context of spherical shell-model and mean-field calculations).

A number of studies (Campi et al., 1975; Storm, Watt, and Whitehead, 1983; Poves and Retamosa, 1987; Heyde and Wood, 1991; Patra and Praharaj, 1991; Poves and Retamosa, 1994) have undertaken to explain the onset of deformation at $N \sim 20$, following the initial experimental work of Klapisch et al. (1973) and Thibault et al. (1975). Other investigations (Fukunishi, Otsuka, and Sebe, 1992; Otsuka and Fukunishi, 1996; Utsuno et al., 1999, 2001; 2004; Otsuka et al., 2001; Otsuka, Suzuki, Honma et al., 2010) have considered how the $N = 20$ shell gap could vanish. With the advent of large-scale shell-model calculations (Caurier et al., 1998; Caurier, Nowacki, and Poves, 2001), a detailed theoretical picture of this region is emerging. This has led to studies (Caurier, Nowacki, and Poves, 2004; Gaudefroy et al., 2006) [see Signoracci and Brown (2007) and Gaudefroy et al. (2007)], (Retamosa et al., 1997; Honma et al., 2004; Nowacki and Poves, 2009; Gaudefroy, 2010) of nuclei around $N \sim 28$, following indications (Sorlin et al., 1993; Sorlin et al., 1995) from unexpectedly short half-lives that the shell gap is weakened. Mean-field calculations (Werner et al., 1994, 1996; Terasaki et al., 1997; Lalazissis et al., 1999; Siiskonen, Lipas, and Rikovska, 1999; Peru, Girod, and

Berger, 2000; Rodríguez-Guzmán, Egido, and Robledo, 2000a, 2000b, 2002a, 2002b, 2003; Yamagami and Van Giai, 2004; Piekarewicz, 2007; Tarpanov *et al.*, 2008; Yoshida, 2009) directed at exploring deformation in $N \sim$ 20, 28 nuclei have also been carried out. Some consideration (Grasso *et al.*, 2009) to exotic structures has been given. Nilsson model structures have been investigated by Hamamoto (2007, 2009, 2010), from the perspective of the impact of the neutron-drip line and weak-binding potentials. Intruder structure has been investigated using antisymmetrized molecular dynamics (AMD), revealing specific $m$p-$n$h neutron configurations by Kimura (2007). A possible presence of specific three-body forces at the limits of the oxygen isotopes near $N \sim 20$ has been explored by Otsuka, Suzuki, Holt *et al.* (2010).

## 3. Clustering in nuclei

Clustering in nuclei is an excellent example of nuclear coexistence. The physics of cluster structures in nuclei has evolved to a sophisticated level, experimentally and theoretically, and there are a number of reviews (Freer and Merchant, 1997; von Oertzen, Freer, and Kanada-En'yo, 2006; Freer, 2007). We also note two recent papers by Funaki *et al.* (2010) and Horiuchi (2010). In view of this wealth of material, we limit our discussion to some more general remarks and refer the interested reader to the above-cited sources.

The issue of shape coexistence, as understood currently, starting either from the nuclear shell model or from beyond-mean-field calculations all point toward the fact that reordering nucleons to form multiparticle–multihole ($m$p-$n$h) configurations can show up in light nuclei, in particular, near $N \sim Z$ nuclei. Even starting at the cost of a large amount of energy to create such configurations, it turns out that these highly correlated configurations can give rise to low-lying intruder states or even interchange with the regular spherical ground-state configuration. Typical results as discussed before are $^{16}$O, $^{40}$Ca in which 4p-4h, 8p-8h excitations can give rise to highly deformed and superdeformed states, respectively.

There have been some early hints that $\alpha$-particle cluster formation may well be related to the fact that $^{16}$O and $^{12}$Ca exhibit relatively low first-excited $0^+$ states lying close to the decay threshold into an $\alpha$ particle. This then would point toward a competition between, on the one hand, the dominance of cluster correlations (localizing nucleons in two proton–two neutron entities) and, on the other hand, the nucleon-nucleon correlations inside the nucleus which lead to an average mean field.

In recent reviews, Freer and von Oertzen *et al.* discussed the subject of clustering and nuclear molecules in an $\alpha$-cluster model (also extending the application to neutron-rich nuclei) (von Oertzen, Freer, and Kanada-En'yo, 2006; Freer, 2007). The concepts underlying $\alpha$ clustering are connected to finding the particular arrangements of the nucleons inside the nucleus that maximize the number of interactions of an $\alpha$ cluster with its neighbors, optimizing the binding energy. An example is the fact that for binding energy, per nucleon, for the He, Be, C, O, Ne,... isotopes, this maximizes at the $1\alpha, 2\alpha, 3\alpha, 4\alpha, 5\alpha, ...$ nuclei. Early on, Ikeda, Takigawa, and Horiuchi (1968) and Brink and Castro

(1973) developed an appealing picture. This indicated that in $A = 4n$ ($n$ integer) nuclei, a family of configurations with increasing number of $\alpha$ clusters $A \rightarrow (A - \alpha)\alpha \rightarrow (A - 2\alpha)2\alpha \rightarrow \cdots (A/4)\alpha$ appears with increasing excitation energy [see the Ikeda diagram presented by von Oertzen, Freer, and Kanada-En'yo (2006)]. Therefore, one expects cluster structures to show up near the threshold for the corresponding cluster decay-$Q$ values.

There is another element which plays a particularly important role in the formation of cluster structures, which follows from the symmetry properties underlying the mean field, thereby influencing the possible geometrical arrangements of clusters. The degeneracies associated with the ordering in the single-particle energy spectrum, for given $N$ and $Z$ values, can largely enhance the preformation of $\alpha$ clusters in nuclei. This has been formulated within a three-dimensional harmonic oscillator potential with frequencies expressed as rational numbers (RHO) (Nazarewicz and Dobaczewski, 1992). A connection between the cluster model and the SU(3) coupling scheme for particles moving in a harmonic oscillator potential was shown by Bayman and Bohr (1959). This symmetry argument can also be made clear in calculating the nucleon densities in the deformed orbitals and it shows that these densities, for particular $N$ and $Z$ values, point toward a large overlap with localization of proton and neutron pairs into $\alpha$ particles.

Combining the Ikeda classification with degeneracies due to the symmetries and approximate degeneracies characterizing the deformed mean field, clear evidence for the presence of cluster structure in light nuclei such as $^{16}$O, $^{40}$Ca, and $^{40}$Ca has been discussed by Freer (2007). In the case of $^{16}$O, the 6.05 MeV $0^+$ state, which is described to be of mainly 4p-4h character, may well be related to the $^{12}$C + $\alpha$ state at 7.16 MeV ($Q$ value). This state has been associated with a quasiplanar structure. The experimental indication for a higher-lying cluster structure corresponding to an 8p-8h configuration, which would form a linear structure, is much less clear at present. In the case of $^{40}$Ca, two $0^+$ states appear at 3.35 and 5.21 MeV (cf. Fig. 41), respectively (Gerace and Green, 1967, 1969) which are mainly of a 4p-4h and 8p-8h nature, respectively. These states are associated with the $^{36}$Ar + $\alpha$ and $^{32}$S + $2\alpha$ cluster configurations, respectively.

It is possible to go away from $N = Z$ and study situations in nuclei where, besides a number of $\alpha$ clusters, a moderate number of extra neutrons will strongly influence the formation of molecularlike states. In particular, considering $^9$Be, where one might think of an $\alpha + \alpha + n$ configuration in which the system becomes bound through an exchange interaction where the neutron acts as mediator to produce covalent binding. These ideas go back to Hafstad and Teller (1938) and are reminiscent of the more recent ideas on halo nuclei with their Borromean structures. As such, the basis was formed to study nuclear molecular states (Hückel, 1930; Nordholm, Bäck, and Backsay, 2007).

There appears to be a whole arena where coexistence is implicit in nuclei, but much detailed spectroscopic work needs to be done: This is in the direction of the topic that has been termed "nuclear molecular resonances" [see miscellaneous papers in Treatise on Heavy-Ion Science, edited by D. A. Bromley (Plenum, New York, 1984)]. Recent work

on heavy-ion radiative capture [see, e.g., Jenkins *et al.* (2007)] suggests that a whole new direction for detailed studies in nuclear shape coexistence lies in the near future with the forthcoming large detector arrays such as GRETINA and AGATA.

The theoretical ideas that have been used derive mainly from rather schematic models. In order to describe and understand clustering in a more refined way, various models have been developed over the years. A starting point was the $\alpha$-cluster model approach in which the $\alpha$-particle states are described by means of a Gaussian form centered on each cluster. The $N\alpha$ wave function then becomes a Slater determinant for the $N$ clusters. The optimal localization is obtained variationally (Margenau, 1941; Brink and Boeker, 1967; Brink and Castro, 1973). One step further has been taken in constructing microscopic cluster models taking the internal structure of the $\alpha$ clusters into account. Thereby one has to use the generator coordinate method (GCM) and as such, the possibility of forming clusters differing from $\alpha$ clusters can be taken into account.

A major step beyond approaches in which clusters are entering was obtained using AMD (Ono *et al.*, 1992a, 1992b, 1993; Kanada-En'yo and Horiuchi, 1995). The model starts from the nucleon degrees of freedom solely, so no constraint on preformed $\alpha$ particles is imposed. The starting wave functions are taken as Gaussian wave packets (coupled to spin and isospin). The energy of the system is again computed variationally using an effective nucleon-nucleon interaction. This approach allows shell-model and cluster type states to show up in a natural way as a consequence of the interplay between the nucleon-nucleon correlations and the Pauli exclusion principle. This approach has been widened into the fermion molecular dynamics (FMD) approach, which allows for an improved description of both cluster and typical shell-model features of the nuclei (Feldmeier and Schnack, 2000; Neff, 2002; Neff and Feldmeier, 2003, 2004; Roth *et al.*, 2004).

Recently, relations between $\alpha$-cluster wave functions, derived from AMD and FMD, and symplectic states have been explored (Dytrych *et al.*, 2008; Horiuchi, 2010). This may lead to unifying clustering dynamics and shell-model dynamics in the future (see also Sec. III.C.7). For further insight see an entire journal issue devoted to the topic of clustering and containing some 50 papers (Int. J. Mod. Phys. E 17, No. 10, 2008).

## C. Unified perspectives for shape coexistence in nuclei

### 1. Global features of nuclear coexistence

Shape coexistence in nuclei is a remarkable phenomenon that has evolved into a widespread feature that may occur in nearly all nuclei. It is associated with the fundamental tendency of nuclei to deform, if not in their ground states, then in excited states, sometimes to large elongations.

To provide a unified perspective of nuclear shapes one needs to be free of imposed model-dependent interpretation of the data. Tables IV and V show $\langle Q^2 \rangle$ values constructed from $E2$ matrix elements obtained by multistep Coulomb excitation, where data are available for ground and excited $0^+$ states, in doubly even nuclei. The construction follows the

rules of Kumar (1972) and Cline (1986) and provides the necessary model-independent view of nuclear quadrupole deformation. For example, the rule used in Tables IV and V $\langle Q^2 \rangle_j \equiv \sum_i \langle 0_j^+ \| E2 \| 2_i^+ \rangle^2$ composes $\langle Q^2 \rangle$ values from measured $E2$ matrix elements (given for all known cases in the tables). These data suggest that one should carefully consider shape coexistence in a much wider context than just at and near closed shells and known subshells. Indeed, Fig. 47 shows that the majority of nuclei possess $E2$ properties that look rotational, even though the associated energies do not. (We note that many of the nuclei in the figure, that deviate significantly from the rotational line of $B_{42}/B_{20} = 1.429$, exhibit shape coexistence.)

It is useful to take a global view of what is known about the occurrence of shape coexistence across the mass surface. Figure 48 presents a perspective from which it is possible to better understand strongly deformed states appearing at low energy in doubly and singly closed shell nuclei and their neighbors. By adopting a "multishell" perspective, i.e., viewing more than one open-shell region as a single, larger shell region, the nuclei at and near the centers of these regions become candidates for exhibiting strongly deformed bands. Thus, by "suppressing" the lines corresponding to $N = 20$ and $Z = 20$ in Fig. 48, an open shell appears for $8 < N < 28$, $8 < Z < 28$ and nuclei in the region of $^{36}_{18}\text{Ar}_{18}$, pinpointed by intersecting diagonal lines in the figure, become candidates for exhibiting strongly deformed states. The superscript notation $^{36}_{18}\text{Ar}_{18}^{[2,2]}$ expresses the multiplicity of shells, i.e., two proton and two neutron shells, involved. Note that this view points to, e.g., the region around $^{154}_{66}\text{Dy}_{88}$ and $^{186}_{82}\text{Pb}_{104}$, where strongly deformed structures, even superdeformed, are observed (cf. discussion of Figs. 22 and 23, Sec. III.A.1, and Table II).

### 2. How to look: Spectroscopic fingerprints

A major goal of this review is to illustrate the spectroscopic fingerprints that most strongly support shape coexistence in atomic nuclei. These fingerprints can be roughly divided into "direct," "indirect," and "hints."

The best direct fingerprints of nuclear deformation are diagonal $E2$ matrix elements. Diagonal $E2$ matrix elements require the measurement of $\gamma$-ray yields in multistep Coulomb excitation and the experiments are demanding. Examples of such data are presented in Figs. 32 and 39. We anticipate that there will be advances in this direction with the arrival of high-energy radioactive beams: This will permit multistep Coulomb excitation of beams of rare isotopes, i.e., inverse Coulomb excitation [for a recent review, see Görgen (2010)].

The next best fingerprints of nuclear deformation are $B(E2)$ values, although these do not distinguish between static and dynamic deformation. However, Fig. 47 shows how to distinguish using $B_{42}$ vs $B_{20}$ plots. The determinations of $B(E2)$ values are widely achieved via lifetime measurements, particularly Doppler line-shape broadening and fast electronic timing, but can also be extracted from Coulomb excitation $\gamma$-ray yields. A subtle but critical issue is that often the highly collective transitions are low energy and are between levels at high excitation which incurs, via the

TABLE IV. Reduced $E2$ matrix elements $\langle \| \, E2 \, \| \rangle$ ($e$ b) for the $0_1^+$ and $0_2^+$ states to the $2_i^+$ states ($i = 1, 2, \dots$) where known. The boldface numbers denote the corresponding $\langle Q^2 \rangle \equiv \sum_i \langle 0_j^+ \, \| \, E2 \, \| \, 2_i^+ \rangle^2$ (for $j = 1$ and 2) (in units $e^2$ b$^2$). The upper (or upper and lower) index for the matrix element denotes the error bar.

| Isotope | $0_1$–$2_1$ | $0_1$–$2_2$ | $0_1$–$2_i$ | $0_2$–$2_1$ | $0_2$–$2_2$ | $0_2$–$2_3$ | $0_2$–$2_i$ | Reference |
|---|---|---|---|---|---|---|---|---|
| $^{66}$Zn | $0.3766^7$ **0.142** | $0.016^3$ | | | | | | Koizumi $et\ al.$, 2003 |
| $^{68}$Zn | $0.359^{11}$ **0.134** | $0.069^3$ | $0.034^3$ $i=3$ | $0.091^7$ **0.214** | $0.25^9$ | $0.379^{45}$ | | Koizumi $et\ al.$, 2004 |
| $^{70}$Ge | $0.424^3$ **0.182** | $0.037^{14}_{-0.0434^{13}}$ | $0.027^3$ $i=3$ | $0.272^{11}$ **0.641** | $0.25^2$ | $-0.71^{13}$ | | Sugawara $et\ al.$, 2003 |
| $^{72}$Ge | $0.46^1$ **0.213** | $0.034^5$ | $\leq 0.022$ $i=3$ | $0.36^4$ **0.147** | $0.019^5$ | $\leq 0.13$ | | Kotlinski $et\ al.$, 1990b |
| $^{74}$Ge | $0.551^2$ **0.307** | $0.058^{10}$ | | $0.14^4$ **0.020** | $0.00^{11}$ | | | Toh $et\ al.$, 2000 |
| $^{76}$Ge | $0.522^4$ **0.277** | $0.069^{10}$ | | $-0.08^3$ **0.010** | $0.06^2$ | | | Toh $et\ al.$, 2001 |
| $^{76}$Se | $0.647^{33}$ **0.432** | $0.112^6$ | $0.02_4$ $i=3$ | $0.47^{11}_{10}$ **0.592** | $0.15^8_{18}$ | $0.59^{30}_{74}$ | | Kavka $et\ al.$, 1995 |
| $^{78}$Se | $0.57^4$ **0.331** | $0.08^1$ | | $0.18^6$ **0.032** | | | | Hayakawa $et\ al.$, 2003 |
| $^{80}$Se | $0.486^{26}$ **0.249** | $0.106^6$ | $0.034^4_6$ $i=3$ <br> $0.03^1$ $i=4$ | $0.12^1$ **0.246** | $-0.05^1_5$ | $0.23^5_{16}$ | $0.42^4_{13}$ $i=4$ | Kavka $et\ al.$, 1995 |
| $^{82}$Se | $0.423^{22}$ **0.197** | $0.120^6$ | $0.060^6_8$ $i=3$ | $-0.11^2_1$ **0.069** | $0.06^{17}_4$ | $0.23^7_{35}$ | | Kavka $et\ al.$, 1995 |
| $^{74}$Kr | $0.782^7$ **0.681** | $-0.199^{18}_{11}$ | $-0.172^{21}_{14}$ $i=3$ | $0.68^4_3$ **1.155** | $-0.48^3_4$ | $0.68^{27}$ | | Clément $et\ al.$, 2007 |
| $^{76}$Kr | $0.849^6$ **0.769** | $0.183^8_6$ | $0.121^4_5$ $i=3$ | $-0.490^{11}_8$ **2.485** | $1.22^8_4$ | $0.87^4_2$ | | Clément $et\ al.$, 2007 |
| $^{78}$Kr | $0.82^2$ **0.729** | $0.157^3_4$ | $0.18^7_8$ $i=3$ | $0.30^1$ **0.159** | $-0.03^2_1$ | $0.26^1$ | | Becker $et\ al.$, 2006 |
| $^{82}$Kr | $0.474^{10}$ **0.233** | $-0.035^{11}_8$ | $0.061^{18}$ $i=3$ <br> $0.056^{10}$ $i=4$ | $0.18^3$ **0.122** | | | $0.30^5$ $i=4$ | Brüssermann $et\ al.$, 1985 |
| $^{84}$Kr | $0.35^5$ **0.151** | $0.17^2$ | | | | | | Osa $et\ al.$, 2002 |
| $^{98}$Mo | $0.526^8_6$ **0.292** | $0.123^3_4$ | $-0.021^1$ $i=3$ | $0.36^2_5$ **0.289** | $0.251^9$ | $0.311^6$ | | Zielinska $et\ al.$, 2002 |
| $^{100}$Mo | $0.725^{18}$ **0.536** | $0.097^4$ | $<0.03$ $i=3$ | $-0.50^3$ **0.644** | $<0.1$ | $0.62^{13}$ | | Mundy $et\ al.$, 1985 |
| $^{104}$Ru | $0.917^{25}$ **0.875** | $-0.156^2$ | $-0.105$ $i=3$ | $-0.304^{10}$ **0.603** | $0.08^3$ | $0.71^4$ | | Srebrny $et\ al.$, 2006 |
| $^{106}$Pd | $0.79^4$ **0.641** | $-0.114^6$ | $0.045^3$ $i=3$ <br> $0.012^1$ $i=4$ <br> $-0.033^2$ $i=5$ | $0.36^2$ **0.874** | $0.24^4_2$ | $0.76^4$ | $0.33^5$ $i=5$ | Svensson $et\ al.$, 1995; Svensson, 1989 |
| $^{108}$Pd | $0.87^6_4$ **0.772** | $-0.098^5$ | $0.038^2_3$ $i=3$ <br> $0.022^2_1$ $i=4$ <br> $0.056^{15}_{10}$ $i=5$ | $0.40^2$ **1.207** | $0.38^2_5$ | $0.95^6_5$ | | Svensson $et\ al.$, 1995; Svensson, 1989 |
| $^{110}$Pd | $0.919^{12}_{35}$ **0.863** | $-0.096^2_3$ | $0.069^2_4$ $i=3$ <br> $-0.017^2_4$ $i=4$ <br> $-0.065^{11}_7$ $i=5$ | $0.297^{13}_3$ **1.337** | $0.44^{10}_6$ | $0.97^3_5$ | $-0.28^{16}_8$ $i=4$ <br> $0.19^{14}_3$ $i=5$ | Svensson, 1989 |

$(\Delta E_\gamma)^5$ factor, a large attenuation of the observable: the $\gamma$-decay branching ratio. In multistep Coulomb excitation, direct observation is not necessary because the matrix element in question will have a high virtual weight in the analysis of the $\gamma$-ray yield and can be extracted from a multichannel fit. From lifetime measurements, while the total lifetime is straightforwardly determined from a strong decay branch, determination of the collective $B(E2)$ of interest necessitates the direct observation of a weak $\gamma$ ray: Considerable progress has been made recently [see, e.g.,

Kulp $et\ al.$ (2006) and Green $et\ al.$ (2009)] using radioactive decay with large arrays of Compton-suppressed Ge detectors.

Indirect fingerprints depend on just how reliably shape coexistence can be inferred from the measured quantity. In light of the examples presented in this review, we suggest that two leading candidates for considering the presence of shape coexistence are strong $E0$ transitions and particle-core coupling patterns.

The strengths of $E0$ transitions depend on the mixing of configurations with different mean-square charge radii.

TABLE V.  See caption to Table IV. *Note that $\langle Q^2 \rangle$ is not given because data are incomplete (no $0_2$–$2_3, \ldots,$ data).

| Isotope | $0_1$–$2_1$ | $0_1$–$2_2$ | $0_1$–$2_i$ | $0_2$–$2_1$ | $0_2$–$2_2$ | $0_2$–$2_3$ | $0_2$–$2_i$ | Reference |
|---|---|---|---|---|---|---|---|---|
| $^{114}$Cd | $0.714^{21}$ | $0.091^{3}$ | $0.073^{3}_{2}$ $i=3$ <br> $0.056^{5}_{3}$ $i=4$ <br> $0.042^{3}_{9}$ $i=5$ | $0.300^{7}_{9}$ | $-0.17^{4}_{2}$ | $0.51^{3}$ | $0.86^{5}$ $i=4$ | Fahlander et al., 1988 |
| | **0.528** | | | **1.119** | | | | |
| $^{148}$Nd | $1.138^{26}_{27}$ | $0.123^{5}_{4}$ | $0.271^{6}$ $i=3$ | $0.352^{9}_{8}$ | $0.915^{37}$ | | | Ibbotson et al., 1997 |
| | **1.384** | | | **0.961** | | | | |
| $^{150}$Nd | $1.627^{18}_{6}$ | $0.066^{2}_{5}$ | $0.276^{1}_{4}$ $i=3$ | $0.339^{3}_{6}$ | $1.145^{34}_{20}$ | | | Zielinska, 2004 |
| | **2.728** | | | **1.426** | | | | |
| $^{156}$Gd | $2.1^{1}$ | $0.14_{20}$ | $0.25^{1}$ $i=3$ <br> $0.087^{3}_{4}$ $i=4$ | $0.079^{4}_{70}$ | $2.1^{1}_{1.4}$ | | | Varnestig, 1987 |
| | **4.438** | | | **4.42** | | | | |
| $^{166}$Er | $2.28^{11}$ | $0.372^{19}$ | | | | | | Fahlander et al., 1992a |
| | **5.337** | | | | | | | |
| $^{168}$Er | $2.43^{7}$ | $0.34^{1}$ | $<\vert 0.2 \vert$ $i=3$ | $<\vert 0.2 \vert$ | $<\vert 0.3 \vert$ | | | Kotlinski et al., 1990a |
| | **6.061** | | | | | | | |
| $^{172}$Yb | $2.45^{12}$ | $0.090^{9}$ | $0.208^{10}_{40}$ $i=3$ | $0.166^{18}$ | $3.02^{80}_{25}$ | | | Fahlander et al., 1992b |
| | **6.054** | | | **9.148** | | | | |
| $^{182}$W | $1.94^{4}$ | $0.326^{4}$ | | | | | | Wu et al., 1991 |
| | **3.87** | | | | | | | |
| $^{184}$W | $1.89^{4}$ | $0.358^{7}$ | | | | | | Wu et al., 1991 |
| | **3.70** | | | | | | | |
| $^{186}$Os | $1.674^{25}_{21}$ | $0.545^{13}_{7}$ | | | $0.40^{11}_{8}$ | | | Wu et al., 1996 |
| | **2.75** | | | * | | | | |
| $^{188}$Os | $1.585^{10}$ | $0.483^{2}_{9}$ | | $\pm0.078^{2}$ | $0.165^{6}_{4}$ | | | Wu et al., 1996 |
| | **2.746** | | | * | | | | |
| $^{190}$Os | $1.530^{20}_{11}$ | $0.444^{9}_{7}$ | | $\pm0.119^{10}$ | $0.384^{37}_{32}$ | | | Wu et al., 1996 |
| | **2.538** | | | * | | | | |
| $^{192}$Os | $1.456^{8}_{9}$ | $0.430^{8}_{4}$ | | $\pm0.063^{8}_{10}$ | $0.449^{21}$ | | | Wu et al., 1996 |
| | **2.305** | | | * | | | | |
| $^{194}$Pt | $1.208^{49}_{17}$ | $0.0888^{12}$ | | $\pm0.070^{9}_{15}$ | $0.231^{30}_{21}$ | | | Wu et al., 1996 |
| | **1.467** | | | * | | | | |
| $^{196}$Pt | $1.1697^{13}$ | $0.000$ | | $0.167^{15}$ | $-0.35^{70}$ | | | Mauthofer et al., 1990 |
| | **1.368** | | | * | | | | |

Examples are shown in Figs. 27, 31, and 34. The observables are conversion electron line intensities and lifetime measurements. A subtle difficulty that arises is that the states involved are usually low spin and are not populated strongly in reactions (excepting inelastic neutron scattering, which requires large amounts of stable target material): Therefore Doppler line broadening is not generally available and electronic timing is usually necessary.

Particle-core coupling patterns may reveal shape coexistence through strongly coupled ($\Delta I = 1$) and decoupled ($\Delta I = 2$) spin sequences, as shown, for example, in Figs. 18, 20, and 38. Caution is needed because the coupling is sensitive to the location of the Fermi energy. The clearest examples are for "unique-parity" orbitals and the theory is presented by Stephens (1975), Meyer-Ter-Vehn (1975a, 1975b), and see Wood et al. (1976).

Hints to shape coexistence come from quantities such as changes in mean-square radii (isotope and isomer shifts), changes in masses (two-nucleon separation energies), and changes in pair occupancies (direct nucleon pair-transfer reaction cross sections). From more direct spectroscopic fingerprints, detailed above, the association of systematic patterns of change in some mass regions (see, e.g., Figs. 9, 29, 30, 33, and 36) provides strong indications of how radii, masses, and transfer strengths can be used to obtain hints of shape coexistence. These signatures are often the way in which regions far from stability are first accessed spectroscopically. This was the case for the neutron-deficient Hg isotopes (Bonn et al., 1972) and the neutron-rich Na isotopes ($N = 20$) (Thibault et al., 1975; Huber et al., 1978). Transfer reaction spectroscopy is beginning to be used in extreme neutron-rich nuclei to infer shape changes [see, e.g., Hansen and Tostevin (2003), Terry et al. (2008), and Fallon et al. (2010)]. We also note that $\alpha$ decay in the $Z \sim 82$ region provides strong identification of similar configurations through low hindrance factor decay branches, as shown in Figs. 14 and 15, but this depends on establishing details of the structures involved by more direct spectroscopic methods.

There are many suggested instances of shape coexistence, too numerous to be included in this review. A leading basis for such suggestions is phenomenological band mixing analyses. Useful presentations of such analyses can be found by Dracoulis (1994), Kibédi et al. (1994, 2001), and Davidson et al. (1999).

### 3. Difficulties in understanding low-lying (excited) $0^+$ states in nuclei

The structure of $0^+$ states in nuclei is believed to be well understood for the ground states of doubly even nuclei: They are variously spherical or deformed and they variously have
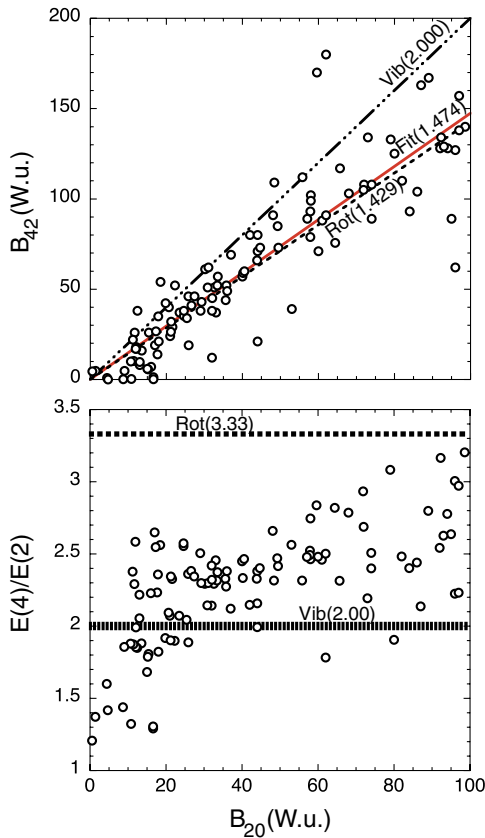
FIG. 47 (color online). Global systematics for the quantities $B_{42} := B(E2; 4^+ \rightarrow 2^+)/B(E2; 2^+ \rightarrow 0^+)$ and $E(4^+)/E(2^+)$ plotted against $B_{20} := B(E2; 2^+ \rightarrow 0^+)$ in W.u. The $E(4^+)/E(2^+)$ values are characteristic of nonrotational nuclei and yet the $B_{42}$ ratios are characteristic of a rigid rotor. Uncertainties in $B_{20}$ and $B_{42}$ are not shown as they would clutter the figure. The data are from Nuclear Data Sheets.

sharp or diffuse Fermi surfaces depending on the strength of pairing correlations and the proximity of shell (or subshell) energy gaps. However, the details presented in the foregoing sections reveal that excited $0^+$ states can be the result of the interplay of important interactions which may produce structures different from the ground state. In this section we present a perspective on $0^+$ states which shows that much work needs to be done to achieve a unified perspective.

The structure of singly closed shell nuclei is well described by the seniority pair-coupling scheme when it is dominated by a single-$j$ subshell [see, e.g., Talmi (1993) and Rowe and Rosensteel (2001)]. However, when there are multiple active $j$ subshells, the simple seniority scheme will in general be modified in a major way. The examples of $^{68}$Ni and $^{90}$Zr are shown in Figs. 49 and 50, respectively. It is clear from the systematic of the seniority-two states that the ground state and first-excited $0^+$ state in each case result from strong mixing of two underlying $0^+$ configurations. This is because each of these nuclei possesses a $j = 1/2$ configuration close to the Fermi energy. A $j = 1/2$ pair can only have seniority zero and so the seniority-two states form a uniformly spaced multiplet.

The situations shown in Figs. 49 and 50 can be misinterpreted if the energies of the $2^+$ states are used to deduce

structure: A naive conclusion would be that $^{68}$Ni and $^{90}$Zr have (weak) doubly closed shell character because of the high $2^+$ energies. One must then conclude from the energies of the first-excited $2^+$ states in neighboring nuclei (which are significantly lower) that the closed subshell structure collapses. The answer is clear from Figs. 49 and 50: the $j = 1/2$ orbital, which is nearly degenerate with the higher-$j$ orbital, is responsible and there is not an energy gap as would occur for a doubly closed shell. Further discussion of the structure of $^{68}$Ni and $^{90}$Zr, particularly the $0^+$ state at 2512 keV in $^{68}$Ni, can be found in Pauwels *et al.* (2010). The nuclei $^{14}$C, $^{14}$O, $^{146}$Gd and probably $^{24}$O are other examples where $j = 1/2$ orbitals produce unusually high first-excited $2^+$ state energies. [The nucleus $^{24}$O has recently received attention (Hoffman *et al.*, 2009; Janssens, 2009; Kanungo *et al.*, 2009) as a potential new doubly closed shell candidate.]

Nuclei adjacent to closed shells have been conventionally viewed as spherical and soft with the consequence that first-excited $0^+$ states in such nuclei are regarded as two-phonon quadrupole vibrational excitations. In the event that the first-excited $0^+$ state is a deformed intruder state, then the view is that the second-excited $0^+$ state is the two-phonon state. The Cd isotopes have been adopted as a textbook example of this. Recent experimental work, reviewed by Garrett and Wood (2010), revealed that the $0^+$ states in $^{110,112,114,116}$Cd, long held to be two-phonon vibrational states, do not exhibit the strong two-phonon to one-phonon $B(E2)$ strengths characteristic of a quadrupole vibrator. Failure of the vibrational description of these isotopes also at the three-phonon level leads to the conclusion (Garrett and Wood, 2010) that the description is inapplicable. This raises the question: What is the nature of the $0^+$ states in $^{110,112,114,116}$Cd that have been interpreted as two-phonon states? A likely answer comes from ($^3$He, $d$) one-proton transfer (Auble *et al.*, 1972) which strongly populates this $0^+$ state in $^{110}$Cd. This suggests that these states involve a different proton pair distribution relative to the ground state. Based on the ground-state configurations of the $^{107,109}$Ag target nuclei, this is likely due to the $2p_{1/2}$ and $1g_{9/2}$ proton orbits forming separate $0^+$ configurations.

The data presented in Secs. III.A and III.B illustrate a wide range of examples where caution needs to be exercised in the interpretation of excited $0^+$ states in nuclei. An overview of $0^+$ states is presented in Tables IV and V: They show $\langle Q^2 \rangle$ values, constructed from $E2$ matrix elements obtained by multistep Coulomb excitation, where data are available for ground and excited $0^+$ states in doubly even nuclei. Values of $\langle Q^2 \rangle$ for excited $0^+$ states different from ground states could be interpreted as due to vibrational fluctuations. However, results in the Cd isotopes (Garrett and Wood, 2010) and in the $N = 90$ isotones [see Sec. III.A.4 and Kulp *et al.* (2008)] show no evidence for vibrations and strongly suggest that a broader view is necessary.

An important spectroscopic fingerprint that needs to be widely employed in the interpretation of excited $0^+$ states is $E0$ transition strengths. The strength of $E0$ transitions gives a model-independent view of the mean-square radii of the $0^+$ configurations underlying the transition (Wood *et al.*, 1999). It also provides a measure of the mixing strength of the configurations (see Sec. III.A.1). These are both fundamental
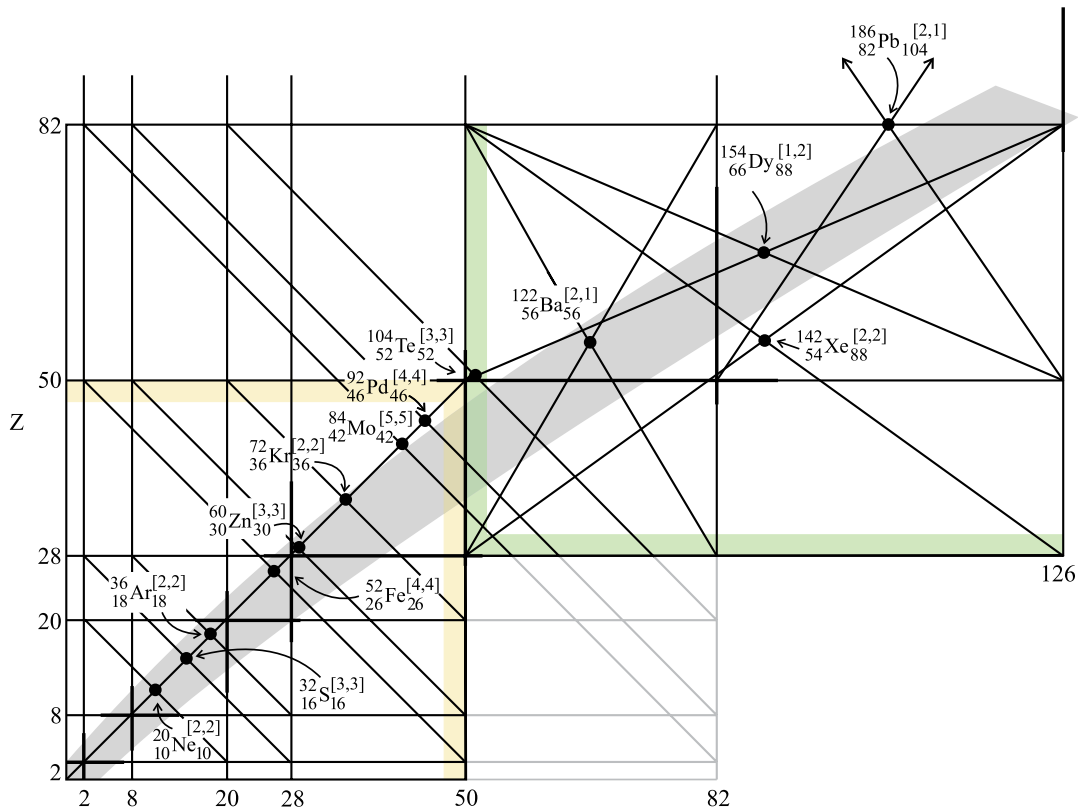
FIG. 48 (color online).   Illustration of the concept of "multishells." Removal of a closed-shell "line" between two open-shell regions creates an open multishell region. For $Z = 82$ this provides an explanation of the extreme deformation associated with the coexisting states observed in the Hg and Pb isotopes. This perspective may also provide an explanation of the mass regions where superdeformation is observed. The superscripts, e.g., [2, 1] attached to $^{186}$Pb[2,1], indicate the number of proton and neutron "regular" shells forming the multishells as shown by the diagonal lines passing through the location of the isotope. The region boxed in the lower left-hand corner contains mainly $N = Z$ line cases, i.e., "symmetric" cases; the region boxed in the upper right-hand corner contains only asymmetric cases.
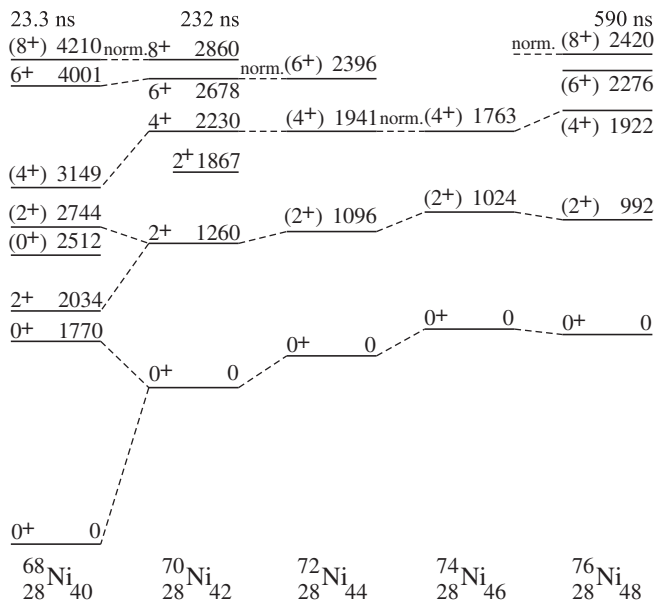


FIG. 49.   Systematics of the low-lying positive-parity states in $^{68-76}$Ni shown relative to the $(1g_{9/2})^n$, $J = 8$ states. The pattern shows that in $^{68}$Ni the $0_2^+$ state results from a strong mixing between configurations involving different pair occupancies of the $1g_{9/2}$ and $2p_{1/2}$, $2p_{3/2}$, and $1f_{5/2}$ orbitals (cf. Fig. 37). The data are from Nuclear Data Sheets.

to understanding $0^+$ states in nuclei. Table VI shows a sample of mixing strengths across the mass surface, deduced from various spectroscopic data. As for the $E0$ transition rates, an expression for the $B(E2)$ reduced transition probability can be derived using a simple two-level model as described in Sec. III.A.1 which can be used to extract a mixing matrix element. Combining the known experimental data such as the excitation energy, $B(M1)$, $B(E2)$, $\rho^2(E0)$ values, and transfer data, it is possible to extract a mixing matrix element. Differences in mean-square radii for the mixing configurations can sometimes be deduced from isotope shifts, cf. Figs. 26 and 33, and occasionally from isomer shifts (Wu and Wilets, 1969). To fully understand $0^+$ states in nuclei, a systematic mapping of $E0$ transition strength is needed (this should also include $\Delta J = 0$ transitions between states with $J \neq 0$).

Other spectroscopic fingerprints that need to be considered in the interpretation of excited $0^+$ states are one-, two-, and four-nucleon transfer reactions. Examples of two- and four-nucleon transfer data are shown in Figs. 29, 30, and 36. One-nucleon transfer data have hardly ever been considered, although strong warnings have been given regarding their importance, e.g., for the $N = 90$ nucleus $^{154}$Gd (Burke, Waddington, and Jolly, 2001; Garrett, 2001), cf. Sec. III.A.4, and note the above-cited example of $^{110}$Cd. Indeed, what is really needed for an understanding of $0^+$ states are maps of

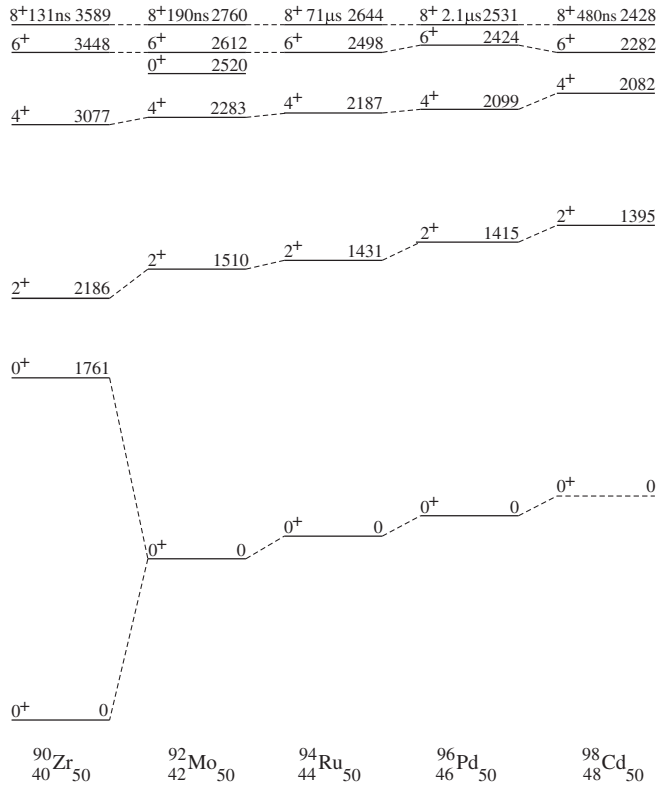FIG. 50. A similar pattern, as the one in Fig. 49 (the Ni isotopes) for the $N = 50$ isotones, also involving the same shell-model orbitals. The data are from Nuclear Data Sheets.

subshell occupancies, such as presented in Fig. 37 for the Ge isotopes. [We note that transition densities deduced from inelastic electron scattering also can reveal important information about differences in the structure of $0^+$ configurations

(Bazantay *et al.*, 1985).] It is evident that the concept of a single pairing condensate (single vacuum) upon which all collectivity is built is probably never realized in nuclei.

A useful overall view of excited $0^+$ states in nuclei is presented in Table VII which shows the lowest known cases across the mass surface. In particular, many of these cases lie in regions of established shape coexistence and, indeed, have been identified as coexisting structures.

### 4. Where to look

Shape coexistence at low energy has now emerged in a widely spread number of mass regions as the result of a variety of dominant structural factors. We suggest criteria for further searches below, but we caution that the historical record has been rather full of surprises.

The overriding factor that appears to be needed for the appearance of shape coexistence at low energy is a competition between an energy gap and a residual interaction that lowers the energy of configurations involving promotion of nucleons across the gap.

The occurrence of the "gap and interaction" mechanism most commonly can arise in singly closed shell regions near midshell (for the other kind of nucleon) and $V_{\pi,\nu}$. The $Z = 50$ and 82 regions near $N = 66$ and 104, respectively, are clear manifestations of this. But this rule needs an exception for the $N = 50$ and 82 regions near $Z = 39$ and 66 where low-energy shape coexistence is not observed: The *suppression effect* of subshell gaps at $Z = 40$ and 64 appears to be the answer. The most valuable data in support of this idea are those at $Z \sim 40$, $N \sim 60$ as manifested in Figs. 27 and 28 which show that nuclei at and close to double-subshell gaps can exhibit shape coexistence via the suppression of ground-state collectivity. Thus, shape coexistence in the $N = 50$ and 82 regions needs

TABLE VI. Mixing strength (in units of keV) used in the description of energy, decay, and transfer reaction properties of coexisting structures.

| Isotope | $V_{\mathrm{mix}}$ | Quantities fitted | Reference |
|---|---|---|---|
| $^{72}$Kr | 310 | $E$ | Becker *et al.*, 1999; Korten, 2001; Bouchez *et al.*, 2003 |
| $^{74}$Kr | 340 | $E$ | Becker *et al.*, 1999; Korten, 2001; Bouchez *et al.*, 2003 |
| $^{76}$Kr | 250 | $E$ | Becker *et al.*, 1999; Korten, 2001; Bouchez *et al.*, 2003 |
| $^{78}$Kr | 200 | $E$ | Becker *et al.*, 1999; Korten, 2001; Bouchez *et al.*, 2003 |
| $^{98}$Sr | 67 | $E$, $B(E2)$, $\rho^2(E0)$ | Mach *et al.*, 1989 |
|  | 34 | $B(E2)$, $\rho^2(E0)$ | Wu, Hua, and Cline, 2003 |
| $^{100}$Zr | 115 | $E$, $B(E2)$, $\rho^2(E0)$ | Mach *et al.*, 1989 |
|  | 88 | $B(E2)$, $\rho^2(E0)$ | Wu, Hua, and Cline, 2003 |
| $^{98}$Mo | 326 | $B(M1)$ | Rusev *et al.*, 2005 |
| $^{100}$Mo | 321 | $B(M1)$ | Rusev *et al.*, 2005 |
| $^{112,114}$Cd | 297 | $\sigma(t, p)$ | O'Donnell, Kotwal, and Fortune, 1988 |
| $^{152}$Sm | 310 | $\rho^2(E0)$ | Kulp *et al.*, 2007 |
| $^{176}$Pt | 180 | $E$ | Dracoulis *et al.*, 1986 |
| $^{178}$Pt | 210 | $E$ | Dracoulis *et al.*, 1986 |
| $^{180}$Pt | 220 | $E$ | Dracoulis *et al.*, 1986 |
| $^{182}$Pt | 230 | $E$ | Dracoulis *et al.*, 1986 |
| $^{184}$Pt | 240 | $E$ | Dracoulis *et al.*, 1986 |
| $^{186}$Pt | 220 | $E$ | Dracoulis *et al.*, 1986 |
| $^{188}$Pt | 400 | $E$ | Dracoulis *et al.*, 1986 |
| $^{192}$Pb | 52 | $B(E2)$, $\rho^2(E0)$ | Van Duppen, Huyse, and Wood, 1990 |
| $^{194}$Pb | 51 | $B(E2)$, $\rho^2(E0)$ | Van Duppen, Huyse, and Wood, 1990 |

TABLE VII.   The nuclei with the lowest known $E(0_2^+)$ energies and the related $2^+$ state energies. A classification into different groups, according to $(N, Z)$ values is given: A ($N \sim 60$, $Z \sim 40$); B ($N \sim 104$, $Z \sim 82$); C ($N \sim 40$, $Z \sim 36$); D ($N \sim 90$, $Z \sim 64$); E ($N \sim 140$, $Z \sim 92$); and F ($N \sim 118$, $Z \sim 76$). The symbol # marks those nuclei in which the $2_2^+$ states are interpreted as axially asymmetric rotor states. The data are from Nuclear Data Sheets.

| Isotope | $E(0_2^+)$ | $E(2_2^+) - E(0_2^+)$ | $E(2_1^+)$ | | Isotope | $E(0_2^+)$ | $E(2_2^+) - E(0_2^+)$ | $E(2_1^+)$ | |
|---|---|---|---|---|---|---|---|---|---|
| $^{98}$Sr | 215 | 656 | 145 | A | $^{154}$Gd | 681 | 134 | 123 | D |
| $^{182}$Hg | 328 | 221 | 351 | B | $^{152}$Sm | 685 | 125 | 122 | D |
| $^{100}$Zr | 331 | 548 | 213 | A | $^{72}$Ge | 691 | 773 | 834 | C |
| $^{184}$Hg | 375 | 160 | 367 | B | $^{232}$U | 691 | 44 | 48 | E |
| $^{178}$Pt | 422 | $\cdots$ # | 171 | B | $^{100}$Mo | 695 | 369 | 536 | A |
| $^{176}$Pt | 443 | $\cdots$ | 264 | B | $^{166}$Hf | (695) | 116 | 159 | |
| $^{186}$Pt | 472 | 326 # | 192 | B | $^{194}$Os | 696 | $\cdots$ | 219 | F |
| $^{180}$Pt | 478 | 382 # | 153 | B | $^{102}$Mo | 697 | 552 | 296 | A |
| $^{184}$Pt | 493 | 352 # | 163 | B | $^{228}$Ra | 721 | 50 | 64 | E |
| $^{182}$Pt | 500 | 355 # | 155 | B | $^{188}$Pb | 725$(0_3^+)$ | 228 | 724 | B |
| $^{74}$Kr | 508 | 1233 | 456 | C | $^{232}$Th | 730 | 44 | 49 | E |
| $^{186}$Hg | 523 | 99 | 406 | B | $^{98}$Mo | 735 | 697 | 787 | A |
| $^{186}$Pb | 532 | 130 | 662 | B | $^{180}$Os | 737 | 94 | 132 | B |
| $^{174}$Os | 545 | 146 | 159 | B | $^{150}$Sm | 740 | 306 | 334 | D |
| $^{196}$Po | 558 | 301 | 463 | B | $^{172}$Os | 758 | 52 | 228 | B |
| $^{184}$Pb | 570 | 132 | 702 | B | $^{172}$W | 762 | 105 | 123 | B |
| $^{188}$Pb | 591 | 133 | 724 | B | $^{192}$Pb | 769 | 469 | 854 | B |
| $^{176}$Os | 601 | 141 | 135 | B | $^{76}$Kr | 770 | 917 | 424 | C |
| $^{152}$Gd | 615 | 316 | 344 | D | $^{148}$Ce | 770 | 166 | 159 | D |
| $^{230}$Th | 635 | 43 | 53 | E | $^{152}$Dy | (775) | (424) | 614 | D |
| $^{186}$Pb | 650$(0_3^+)$ | 295 | 662 | B | $^{174}$W | 792 | 98 | 113 | B |
| $^{178}$Os | 650 | 121 | 132 | B | $^{188}$Pt | 798 | 317 | 266 | B |
| $^{190}$Pb | 658 | 116 | 1162 | B | | | | | |
| $^{154}$Dy | 661 | 244 | 335 | D | | | | | |
| $^{72}$Kr | 671 | $\cdots$ | 709 | C | | | | | |
| $^{156}$Dy | 676 | 153 | 138 | D | | | | | |
| $^{150}$Nd | 676 | 176 | 130 | D | | | | | |

to be sought near $Z = 33$, 45 and 58, 74, respectively. We note that the $N \sim 50$, $Z \sim 33$ region was shown in our first review [cf. Fig. 3.25 in Heyde *et al.* (1983)] to have low-energy shape coexistence and has been pointed out by Bender, Bertsch, and Heenen (2008) to have a decreased energy gap.

The consideration of gaps as meaning not only major shell gaps but also subshell gaps appears to offer a fairly widely applicable organizing principle. Thus, the $N = 20$ (shell), $Z = 16$ (subshell) gaps appear to control the region around $^{32}$Mg, cf. Figs. 44 and 45; we conjecture that the $N \sim 40$, $Z \sim 40$ region is influenced by a double-subshell gap, although the subshell gap structure may not be strongly associated with $N$, $Z = 40$, i.e., gaps at other nucleon numbers may be important (this would appear to be an open question).

The extraordinary structures of $^{16}$O, $^{40}$Ca, and $^{56}$Ni show the special properties of $N = Z$ nuclei with respect to shape coexistence. This is presumably due to the exceptional effectiveness of $V_{\pi,\nu}$ with respect to identical proton and neutron configurations. Certainly, $^{100}$Sn will be an interesting nucleus for study. But we suggest that the entire $N \sim Z$ region needs more detailed study. For example, $^{40}$Ca exhibits three

coexisting shapes, but $^{56}$Ni exhibits only two. Shell-model calculations for $^{40}$Ca (Caurier *et al.*, 2007) and $^{56}$Ni (Horoi *et al.*, 2006) appear to support this difference. However, note that the deformed band in $^{56}$Ni is similar to the more-deformed band in $^{40}$Ca (cf. Fig. 41). This suggests that a less-deformed band remains to be discovered in $^{56}$Ni. Possibly it is associated with the $0^+$ state at 3957 keV and is nonyrast already at low spin with respect to the observed deformed band. We already noted above the incomplete view of the $N$, $Z \sim 40$ region. The interplay of subshells for $N \sim Z$ appears to be deserving of detailed study.

Nuclei adjacent to the $N = Z$ line also need careful study. Table III shows that shape coexistence around the $N = Z$ line has a "parentage" that needs careful systematic study with respect to the generic structures in $^{16}$O, $^{40}$Ca, and $^{56}$Ni. For example, many of the excited states in $^{41}$Ca and $^{41}$Sc can be classified into quasirotational bands built on Nilsson states (Röpke, 2004). A similar situation may be occurring around $^{56}$Ni (Rudolph *et al.*, 1999). We point out the recent studies of prompt charged particle emission as an exciting new tool (Rudolph *et al.*, 2005).

The implication of subshell structures as playing an important role in the regions expected to exhibit shape

coexistence raises the deeper question of just where can we expect new subshells? We note that deformed shell gaps are often proposed to explain SD band excitations. However, these are unrelated to the issue here, which is the effect of the energy gap on the suppression of collectivity.

Pairing isomerism also is a situation controlled by an energy gap and an interaction. The energy gap is with respect to Nilsson configurations (and as a result $V_{\pi,\nu}$ is implicit through its deformation producing effect in the underlying structure). The interaction is the pairing interaction and its attenuation with respect to upsloping (oblate) and downsloping (prolate) orbitals. This mechanism appears to need more extensive exploration, especially when considering the different rotational band parameters in Table I.

## 5. New insights

The most important new insight since the last review in 1992 is the likelihood that shape coexistence occurs in all nuclei except the lightest. It is also likely that there are hierarchies of coexisting structures, i.e., many structures with a whole range of deformations. Indeed, we adopt the view that spherical shapes are just one particular deformation that dominates structure only when shell gaps suppress the natural tendency of nuclei to deform.

New data since the last review clearly show that subshells can behave just as major shells in giving rise to coexisting structures. However, mixing will often obscure the direct spectroscopic fingerprints such as states with different quadrupole deformations; but mixing produces $E0$ transition strength and this is a strong indication of underlying coexisting structures.

The nature of the low-lying excited states in nuclei much depends on the structure of the mean field (single-particle energies) at and near to the Fermi level. This monopole part, in particular, its evolution with changing $A(Z, N)$ when moving away from the stable nuclei, is responsible for describing the correct saturation properties of nuclei (global effect), but also describes local changes in the single-particle energies and as such the well-known shell gaps at $Z$ (or $N$) = 8, 20, 28, 50, 82.

In general, $m$p-$n$h excitations across these closed shells can be formed at the cost of the monopole field which preserves the closed-shell situation with corresponding spherical nuclear shapes. However, there are strong correlations (multipole forces, pairing correlations) associated with the $m$p-$n$h excitations that are the origin of important lowering in energy of these configurations. It is the balance between these two counteracting effects that determines which energy component dominates and whether the ground state (excited state) has a closed-shell configuration or becomes an mp-nh structure. We especially point to the paper by Bender, Bertsch, and Heenen (2008) as providing valuable insight into the issue of energy gaps in mean-field descriptions.

After all there exist only a limited number of spherical nuclei in the presence of a strong quadrupole-quadrupole interaction energy because only in a limited number of situations ($Z = 8$ at $N = 8$, $Z = 20$ at $N = 20$, etc.) are the energy gaps in the mean field large enough to prevent the development of deformed ground states. Therefore, we speak of ''suppressed collectivity.''

## 6. Unsolved problems

The result in the Cd isotopes that vibrational behavior at low energy is refuted (Garrett and Wood, 2010) opens the entire issue of the nature of excited $0^+$ states in nuclei. A reliable characterization of the first few excited $0^+$ states in all nuclei is needed. Too often interpretations have been based on energies and relative $B(E2)$'s. An illustration of ambiguity in interpretation is provided by the neutron-deficient Pt isotopes in which it is possible to describe a limited set of observables [$E_x$, $B(E2)$'s] in these isotopes without any need for shape coexistence [see McCutchan, Casten, and Zamfir (2005) and Garcia-Ramos and Heyde (2009)]. We note that the basis on which shape coexistence is deduced for the Pt isotopes, given by Wood  et al. (1992), did not involve $E_x$ and $B(E2)$. Besides $E2$ matrix elements, both diagonal and transitional, it is evident that data from the little-used spectroscopic fingerprint of transfer reactions are much needed.

Too little is yet known about the structure of the correlations involved in $0^+$ states in nuclei. Often, the language used is in terms of particle pairs and hole pairs with the implication that these are Cooper pairs. This language is for convenience but is too simplistic.

Mixing of coexisting structures always occurs but with widely varying strengths. These strengths (cf. Table VI) need to be systematized. Particularly, we need to quantify the degree to which mixing occurs for various differences in deformation between the mixing configurations. The fact that we observe clear manifestations of coexisting shapes shows that the mixing is not that strong. But in certain cases it is evident that mixing is near maximal such as in $N = 90$ nuclei near $Z = 62$.

An issue that is central to the above, unsolved problems is the strength of pairing in deformed nuclei. Diagonal pairing in a deformed nucleus is made up of two parts: that due to the twofold, so-called Kramers degeneracy of orbitals in a deformed, reflection-symmetric field; and that due to short-ranged components of the residual nucleon-nucleon interaction. To our knowledge, these two contributions to pairing have not been deconvoluted in a quantitative manner; however, see Yoshida and Takigawa (1997), Satula, Dobaczewski, and Nazarewicz (1998), Sugawara-Tanabe, Arima, and Yoshida (1999), Xu, Wyss, and Walker (1999), Duguet et al. (2001), and Venkova  et al. (2005). The off-diagonal pairing in deformed nuclei is known to be highly variable and is often quantified globally by invoking monopole-plus-quadrupole pairing [see, e.g., Chu  et al. (1995a; 1995b) and Shihab-Eldin  et al. (1995)]. Direct experimental evidence comes from anomalous orbital occupancies [see, e.g., Peterson and Garrett (1984)]. Detailed theoretical estimates of matrix elements have been made (Chasman, 1976). However, there is no systematic study known to us.

A related issue to variable pairing in nuclei is the importance of proton-pair–neutron-pair correlations. There is strong evidence for this from $\alpha$-cluster transfer reaction spectroscopy; cf. remarks in Sec. III.A.7 and Figs. 29, 30, and 36. This naturally extends to the issue of $\alpha$ clustering in nuclei. These data strongly suggest that the coexistence of different pair distributions for one kind of nucleon induce the different pair distributions for the other kind of nucleon. This

is explicit in Fig. 37. An actual $\alpha$ cluster would be an extreme example of this.

A factor in the occurrence of shape coexistence is the location of shell and subshell gaps: This issue will be a leading one in the future exploration of shape coexistence and intruder states. At present there is evidently a lack of a unified view on just where shell structure survives. A recent review undertakes to explore where shells have appeared or disappeared (Sorlin and Porquet, 2008), but we hold the view that a more unified perspective is needed. A recent paper by Bender, Bertsch, and Heenen (2008) provided perspective on quenching of signatures for shell structures; in particular, they showed that at $N \sim 50$ there is a clear favoring of intruder structures around $Z \sim 32$; cf. our remarks in Sec. III.A.6. There is also the issue, rather well phrased, by Zeldes, Dimitrescu, and Köhler (1983), of the "mutual support of magicities" which is clearly occurring at $Z \sim 40$, and $N \sim 56$.

We pointed to the fundamental parabolic pattern exhibited by intruder states and shape-coexisting structures. It is tempting to interpret this parabolic variation in the associated states with varying deformation and to describe the states as arising from "deformation-driving" orbitals; except that, where data exist which reveal the deformations of these structures, their deformation is changing only slightly, or not at all (cf. Figs. 18 and 20). We suggest that a fundamental change of perspective is likely needed, namely, to invert the parabolas and regard spherical structures as being the intruding structures.

The inverted parabola view emphasizes that spherical ground states occur only rarely across the mass surface, and often the first- or second-excited state in such nuclei is deformed. There has been a natural adherence to spherical shapes as the reference shape, because a shell-model basis is only weakly mixed in such nuclei. Indeed, calculations using deformed bases are not favored because arriving at states of good angular momentum is not easy.

With respect to the origin of the parabolic patterns, if the variation in deformation of the more-deformed structures is insufficient to explain the patterns, we note that Bender, Bertsch, and Heenen (2008) emphasized the importance of collective contributions to ground-state structures of nuclei at and near closed shells: We need to determine the contributions from both the more-deformed and less-deformed structures to the parabolic energy patterns. It is often forgotten that we usually plot nuclear data, setting the ground-state energy at the zero of the chosen energy scale, so that we blind ourselves to variations in ground-state energies (cf. Figs. 49 and 50).

### 7. Suggestions for future theory

In making suggestions for a comprehensive description of shape coexistence, one should start from a critical consideration of both successes and limitations of mean-field and shell-model approaches.

In the mean-field approach, one starts from an effective nucleon-nucleon force and uses self-consistent HF + BCS or HFB methods to construct an optimized nuclear many-body wave function built from independent (quasi)particles. The introduction of nuclear shapes is through constraints on the multipole moments obtained from these methods so that they take on specific values (Bender, Heenen, and Reinhard, 2003).

As a consequence of recent developments (largely due to the rapid increase in computing power and the construction of efficient algorithms), steady progress has been made to go beyond the standard (relativistic) mean-field approximation. Restoring the symmetries broken in the intrinsic frame and including dynamical correlations through solving the Hill-Wheeler-Griffin equations (GCM) (Hill and Wheeler, 1953; Griffin and Wheeler, 1957) has resulted in major improvements over the early studies in many mass regions (Bender and Heenen, 2008; Rodríguez and Egido, 2010; Yao et al., 2010). Systematic studies of nuclear low-lying collective properties have also been carried out using (relativistic) mean-field theory in order to calculate the deformation dependence of the parameters that determine the dynamics of the 5DCH (see also Sec. II.B) (Nikšić et al., 2009; Delaroche et al., 2010; Li et al., 2010). A consistent approach to derive the inertial functions that determine the dynamics of this 5DCH has recently been described by Hinohara et al. (2010), making use of the adiabatic time-dependent HFB theory, and has been applied to the study of shape coexistence in the proton-rich $^{68,70,72}$Se nuclei.

Limitations come from the fact that the effective forces used (Skyrme, Gogny) have been fitted so as to describe nuclear global properties such as binding energies, charge and matter radii, and densities. Up to now, pairing properties have been parametrized in phenomenological ways (Bender, Heenen, and Reinhard, 2003). Only recently have efforts been made to construct nonempirical pairing interactions (Hebeler et al., 2009; Baroni, Macchiavelli, and Schwenk, 2010). An issue that is not well understood as yet concerns the coupling of the collective excitations, arising naturally from mean-field studies, with specific few-nucleon excitations near to closed shells.

In the spherical shell-model approach all nuclear many-body states, built from a limited set of single-particle orbitals near the Fermi level, are taken into account (mainly a complete $0\hbar\omega$ harmonic oscillator shell-model basis) to solve the Schrödinger equation or the equivalent energy eigenvalue problem. The nucleon-nucleon forces used result either from realistic nucleon-nucleon interactions, fitted to free nucleon scattering observables, from which an in-medium G matrix is constructed (Kuo and Brown, 1966, 1968; Hjorth-Jensen, Kuo, and Osnes, 1995), or from a fit of the corresponding two-body matrix elements to nuclear data within a restricted ($0\hbar\omega$, $1\hbar\omega$) region of the nuclear mass surface (Richter, Mkhize, and Brown, 2008; Honma et al., 2009; Nowacki and Poves, 2009). Hence, within the spherical shell-model approach, all correlations consistent with the starting nucleon-nucleon force are included within the chosen model space.

It has turned out that in order to describe collective phenomena, such as shape coexistence, many-particle many-hole ($m$p-$n$h) excitations relative to a $0\hbar\omega$ model space need to be incorporated explicitly (Poves and Retamosa, 1987; Warburton, Becker, and Brown, 1990; Heyde and Wood, 1991; Poves and Retamosa, 1994). As a consequence, and in order to describe these collective phenomena alongside

typical few-nucleon excitations in a consistent way, extended model spaces such as $1p_{1/2,3/2}$-$2s_{1/2}1d_{3/2,5/2}$, $2s_{1/2}1d_{3/2,5/2}$-$2p_{1/2,3/2}1f_{5/2,7/2}$, and $1f_{5/2}2p_{1/2,3/2}1g_{9/2}$ have been considered. Here one is close to reaching the present limits of computing possibilities. Benchmark calculations for, e.g., $^{40}$Ca (Caurier *et al.*, 2007) and $^{56}$Ni (Horoi *et al.*, 2006) have given rise to a consistent description of the lowest-lying spherical states, deformed states, and even superdeformed structures that appear at low excitation energy. Even though large-scale shell-model calculations can produce low-lying collective states [energy, $B(E2)$ values, $Q$ moment], an obvious insight is hampered because of the complexity of the shell-model wave functions. Still, effective charges are needed with typical values of $e_\pi = 1.5e$ and $e_\nu = 0.5e$. A relation to quasi-SU(3) and to quasipseudo-SU(3) has been addressed (Caurier *et al.*, 2005) but has not been developed in a systematic way.

Uncovering symmetries present within the huge shell-model Hilbert space should allow for an extraction of the collective dynamics, starting from microscopic effective nucleon-nucleon forces.

Theoretical prediction of shape coexistence in nuclei has largely evolved using separate descriptions of their intrinsic and collective structure, i.e., intrinsic structures have been calculated using constrained HF(B) theory and collective structure has been imposed (either by fiat or by beyond-mean-field techniques). However, a unified description is available using the symplectic shell model (Rosensteel and Rowe, 1977; Rowe, 1985, 1996). We say that, in reflecting on the substance of this review, experiment has "caught up" to the symplectic shell model which provides the fundamental theoretical framework for understanding shape coexistence in atomic nuclei. We suggest that this time lag has been because it has taken 30 years to move the experimental perspective of shape coexistence from an exotic rarity to a near-universal property of nuclei.

From a symplectic perspective, configurations associated with spherical shapes are just a small subset of a large number of possible nuclear configurations. This suggests that we can invert the intruder parabolas to emphasize that the occurrence of spherical structures at doubly and singly closed shells is the manifestation of just a few of the many possibilities for structures in such nuclei. We depict this new perspective in Fig. 51.

Figure 52 gives a schematic view of the way in which the Hilbert space of a nucleus is viewed from a symplectic Sp(3, R) model perspective: Each "tower" in Fig. 52 is a symplectic irrep or collective band labeled by the quantum numbers $\lambda$, $\mu$ of the Sp(3, R) subgroup, SU(3). Symplectic $(2\hbar\omega)$ raising and lowering operators, acting within each Sp(3, R) irrep are indicated. This "vertical" perspective reflects a remarkable and fundamental property of Sp(3, R): It contains the Bohr model as a submodel. Indeed, at its inception (Rosensteel and Rowe, 1977), Sp(3, R) was the result of a search for the microscopic shell-model basis of the Bohr model. It is the configurations contained in the towers that are necessary to microscopically generate the large collective strengths observed at low energy in nearly all nuclei.

From a shell-model perspective, one views the Hilbert space of a nucleus in terms of a valence energy shell together with a few shells below and above, i.e., from a "horizontal" perspective. Most of this review used this perspective to organize data. Microscopic, shell-model based theory followed this way of looking at nuclear collectivity. However, one cannot describe the highly deformed states of rotational nuclei in a conventional spherical shell-model basis without using unphysically large effective charges.

From a mean-field perspective, the observed deformations of nuclei can be generated from the Hilbert space when major shell mixing is allowed. However, the details of the intrinsic structure of each of these deformed minima is obscured because beyond-mean-field methods impose the collective dynamics, i.e., the view of nuclear collectivity that results is limited.

From a symplectic perspective, each SU(3) irrep $(\lambda, \mu)$ is an intrinsic state with $\lambda$ and $\mu$ values determined by the number of oscillator quanta $N$ carried by the collectively active nucleons in the nucleus. A simple way to make this connection is via the partitioning of the $N$ quanta over $n_x$, $n_y$, and $n_z$, and the relationships $N = n_x + n_y + n_z$, $\lambda = 2n_z - n_x - n_y$, and $\mu = n_x - n_y$. The values of $\lambda$ and $\mu$ are related to the Bohr model parameters $\beta$ and $\gamma$ (Rowe, 1985; Castanos, Draayer, and Leschber, 1988).

Collectivity can emerge from a $(\lambda, \mu)$ irrep directly as an SU(3) dynamical symmetry through a nucleon-nucleon interaction of the quadrupole-quadrupole type of the Elliott
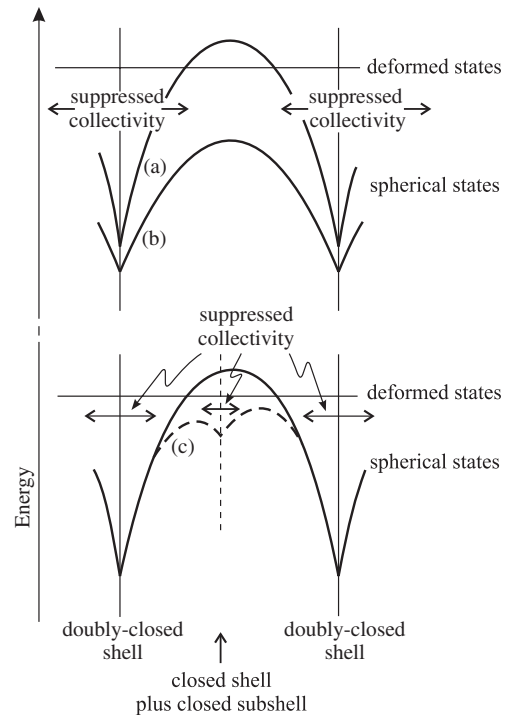


FIG. 51. A schematic view of the intruder-state "parabolas," shown to dramatize the way that shells and subshells suppress the emergence of low-energy collectivity in nuclei. (a) The situation where deformed structures intrude to become the ground state at the middle of a singly closed shell, e.g., $^{32}$Mg; (b) where the ground states for a sequence of singly closed shell nuclei remain spherical, but deformed structures form excited intruder bands, e.g., the Sn and Pb isotopes; (c) where a subshell may suppress intrusion of a deformed structure from becoming the ground state or a low-lying excited band, e.g., $N = 50$, 82.
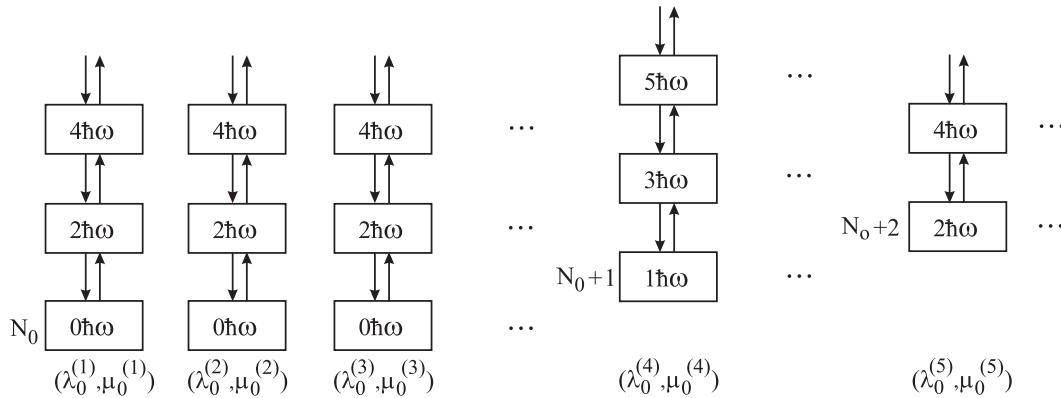
FIG. 52.    The vertical shells of the symplectic collective model, labeled by the number of oscillator quanta and the quantum numbers of the SU(3) subgroup of the model. Some details are discussed in the text. Adapted from Rowe (1985) and Carvalho *et al.* (1986).

model, or by mixing of $(\lambda, \mu)$ irreps [see, e.g., Thiamova, Rowe, and Wood (2006)], or by mixing of Sp(3, R) irreps [see, e.g., Rowe, Vassanji, and Carvalho (1989)]. Mixing within an Sp(3, R) irrep is of particular interest because it retains Sp(3, R) as a dynamical symmetry (with all of its algebraic structure available for the calculation of matrix elements), but can produce observed collective quadrupole strength without the need for effective charges. Indeed, this allows one to restrict the full microscopic shell-model space of the nucleus to the most important modes of collective dynamics.

A doubly closed shell nucleus, such as $^{16}$O, possesses the ground-state irrep $(\lambda, \mu) = (0, 0)$ and its Sp(3, R) collective degrees of freedom are restricted to just the giant monopole and quadrupole resonances. However, the first-excited state is $(\lambda, \mu) = (8, 4)$ (Rowe, Thiamova, and Wood, 2006) and it possesses a highly collective band.

A leading challenge for the symplectic collective model and its SU(3) submodel is identifying the lowest-energy irreps in a given nucleus when the nucleon number is large. This is a trivial task in the rotor model, and in the interacting boson model it is dictated by a simple recipe [the number of SU(6) bosons is given by counting the number of valence nucleon pairs from the nearest closed shells]. An effective way to address this challenge for strongly deformed structures has been put forward by Jarrio, Wood, and Rowe (1991) and Carvalho and Rowe (1992), and ways to extend this method to weakly deformed structures have been suggested by Hess *et al.* (2002). Following ideas by Cseh and Scheid (1992), extension to cluster structures may also be in reach.

From the perspective of the Bohr model and its full algebraic realization, the algebraic collective model (ACM) (Rowe, Welsh, and Caprio, 2009; Rowe and Wood, 2010), Sp(3, R) provides the means to look beyond this foundational model of nuclear structure.

We add a few more observations regarding where we see developments occurring:

• The rapid advances in achieving a unified perspective of nuclear structure in low-*A* nuclei via no-core shell-model techniques and the prospect of carrying out calculations in all nuclei with the symplectic no-core shell model (Dytrych *et al.*, 2008) promises an exciting future for nuclear structure theory. Indeed, such
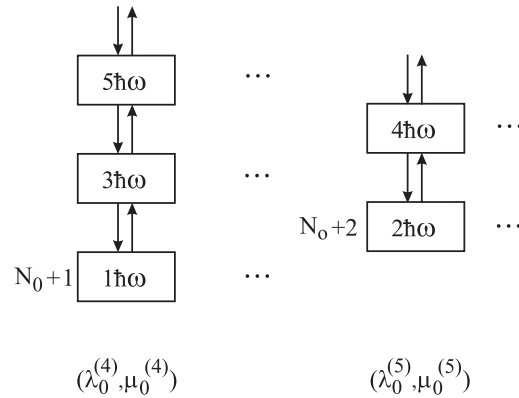
theoretical developments will be highly demanding of experimental techniques for identifying such structures.

• Mean-field techniques are reaching unimagined levels of sophistication from the perspective of our earlier reviews. These techniques can straightforwardly suggest some of the shapes expected in mass regions far from stability.

• The nuclear shell model has reached an extraordinarily high level of sophistication, combining the construction of highly efficient algorithms with increased computing power, to obtain the energies and wave functions of the lowest-lying excited states, even going up to high-spin values. There is clearly room for exploring new truncation methods to the nuclear eigenvalue problem.

• A topic for future investigation of nuclear structures involving different shapes is the correlations involved. Pairing is not naturally incorporated into the symplectic models. Mean-field techniques emphasize independent-particle degrees of freedom in their use of Slater determinants. Indeed, we have undertaken in this review to point to correlations (cf. Figs. 29, 30, 36, and 37) that may well be indicators of important components of coexisting structures.

• To carry out symplectic model calculations for comparison with data in heavy nuclei requires the identification of the SU(3) irreps that dominate low-lying collective structures in heavy nuclei and the important interactions that mix these irreps. The application of such a program to shape coexistence in heavy nuclei is a leading research challenge for nuclear structure. There is an important role to be played by phenomenological band mixing applied to data, e.g., in the analysis of interband *E*0 and *E*2 transition strengths in the first steps of such a program to reveal details of the underlying coexisting structures.

## IV. CONCLUSIONS AND OUTLOOK

There has been a shift in perspective on shape coexistence since ∼30 years ago (the first review was in 1983) from an exotic phenomenon occurring in just a few mass regions to its presence in almost all nuclei. The balance between shell and subshell energy gaps (an independent-particle effect) and

large correlation energy (due mainly to pairing and quadrupole two-body forces) is at the heart of understanding the presence of shape coexistence in nuclei. We point to the need for considerable care in separating these completely different factors.

Two major thrusts in experimental techniques particularly contributed to advances in the identification of shape coexistence in nuclei. The first is the range of techniques used far from stability, where low event rates are the leading challenge. The second is the development of detailed spectroscopy, of various "standard" types, applied at and near stability, which reveal more subtle manifestations of coexistence and which have previously been ascribed to other types of structure.

For future experimental work we emphasize the importance of study far from stability and detailed study near stability using not only standard fingerprints, such as $B(E2)$, $\rho^2(E0)$, and quadrupole data, but also transfer reaction data, both single and multinucleon.

Theoretically, we suggest that a major revolution is underway. The semiclassical approaches and phenomenological models have largely been superseded. Fully quantum-mechanical microscopic approaches with predictive power are now beginning to be used. It is here that there is much to be learned about many-nucleon systems and their separate independent-particle and correlated-particle behaviors, revealed through shape coexistence.

## ACKNOWLEDGMENTS

## REFERENCES

Abdulvagabova, S. K., S. P. Ivanova, and N. I. Pyatov, 1972, Phys. Lett. B **38**, 215.

Aberg, S., H. Flocard, and W. Nazarewicz, 1990, Annu. Rev. Nucl. Part. Sci. **40**, 439.

Abrosimov, V., 1979, Z. Phys. A **293**, 17.

Abrosimov, V., 1981, Sov. J. Nucl. Phys. **31**, 348.

Afanasjev, A. V., D. B. Fossan, G. J. Lane, and I. Ragnarsson, 1999, Phys. Rep. **322**, 1.

Ahalpara, D. P., and K. H. Bhatt, 1982, Phys. Rev. C **25**, 2072.

Ajzenberg-Selove, F., 1990, Nucl. Phys. A **506**, 1.

Alford, W. P., R. E. Anderson, P. A. Batay-Scorba, R. A. Emigh, D. A. Lind, P. A. Smith, and C. D. Zafiratos, 1979, Nucl. Phys. A **323**, 339.

Allmond, J. M., R. Zaballa, A. M. Oros-Peusquens, W. D. Kulp, and J. L. Wood, 2008, Phys. Rev. C **78**, 014302.

Almehed, D., and N. R. Walet, 2004, Phys. Lett. B **604**, 163.

Andersson, L.-L., et al., 2009, Phys. Rev. C **79**, 024312.

Andrejtscheff, W., and P. Petkov, 1994, Phys. Lett. B **329**, 1.

Andreoiu, C., et al., 2002, Eur. Phys. J. A **14**, 317.

Andreyev, A. N., et al., 2009a, Phys. Rev. C **80**, 054322.

Andreyev, A. N., et al., 2009b, Phys. Rev. C **80**, 044334.

Andreyev, A. N., et al., 2006, Phys. Rev. C **73**, 044324.

Andreyev, A. N., et al., 2000, Nature (London) **405**, 430.

Andreyev, A. N., et al., 2002, Phys. Rev. C **66**, 014313.

Anguiano, M., J. L. Egido, and L. M. Robledo, 2002, Phys. Lett. B **545**, 62.

Ardouin, D., D. L. Hanson, and N. Stein, 1980, Phys. Rev. C **22**, 2253.

Ardouin, D., C. Lebrun, F. Guilbault, B. Remaud, E. R. Flynn, D. L. Hanson, S. D. Orbesen, M. N. Vergnes, G. Rotbard, and K. Kumar, 1978a, Phys. Rev. C **18**, 1201.

Ardouin, D., B. Remaud, K. Kumar, F. Guilbault, P. Avignon, R. Seltz, M. Vergnes, and G. Rotbard, 1978b, Phys. Rev. C **18**, 2739.

Ardouin, D., R. Tamisier, G. Berrier, J. Kalifa, G. Rotbard, and M. Vergnes, 1975a, Phys. Rev. C **11**, 1649.

Ardouin, D., R. Tamisier, M. Vergnes, G. Rotbard, J. Kalifa, G. Berrier, and B. Grammaticos, 1975b, Phys. Rev. C **12**, 1745.

Auble, R. L., D. J. Horen, F. E. Bertrand, and J. B. Ball, 1972, Phys. Rev. C **6**, 2223.

Audi, G., A. H. Wapstra, and C. Thibault, 2003, Nucl. Phys. A **729**, 337.

Back, B. B., E. R. Flynn, O. Hansen, R. F. Casten, and J. D. Garrett, 1973, Nucl. Phys. A **217**, 116.

Bansal, R. K., and J. B. French, 1964, Phys. Lett. **11**, 145.

Baranger, M., and K. Kumar, 1968, Nucl. Phys. A **110**, 490.

Barfield, A. F., and B. R. Barrett, 1984, Phys. Lett. B **149**, 277.

Barfield, A. F., B. R. Barrett, K. A. Sage, and P. D. Duval, 1983, Z. Phys. A **311**, 205.

Baroni, S., A. O. Macchiavelli, and A. Schwenk, 2010, Phys. Rev. C **81**, 064308.

Baxter, A. M., A. P. Byrne, G. D. Dracoulis, P. M. Davidson, T. Kibédi, R. V. F. Janssens, M. P. Carpenter, C. N. Davids, T. L. Khoo, and T. Lauritsen, 2005, Phys. Rev. C **71**, 054302.

Bayman, B. F., and A. Bohr, 1959, Nucl. Phys. **9**, 596.

Bazantay, J. P., et al., 1985, Phys. Rev. Lett. **54**, 643.

Bazin, D., et al., 2003, Phys. Rev. Lett. **91**, 012501.

Becker, F., C. Alderliesten, E. A. Bakkum, K. Van der Borg, C. P. M. Van Engelen, L. Zybert, and R. Kamermans, 1982, Nucl. Phys. A **388**, 477.

Becker, F., et al., 1999, Eur. Phys. J. A **4**, 103.

Becker, F., et al., 2006, Nucl. Phys. A **770**, 107.

Bednarczyk, P., et al., 1998, Eur. Phys. J. A **2**, 157.

Bednarczyk, P., et al., 1997, Phys. Lett. B **393**, 285.

Belleguic, M., et al., 2005, Phys. Rev. C **72**, 054316.

Belyaev, S. T., 1961, Nucl. Phys. **24**, 322.

Bender, M., G. F. Bertsch, and P.-H. Heenen, 2008, Phys. Rev. C **78**, 054312.

Bender, M., P. Bonche, T. Duguet, and P.-H. Heenen, 2004, Phys. Rev. C **69**, 064303.

Bender, M., P. Bonche, and P.-H. Heenen, 2006, Phys. Rev. C **74**, 024312.

Bender, M., T. Cornelius, G. A. Lalazissis, J. A. Maruhn, W. Nazarewicz, and P.-G. Reinhard, 2002, Eur. Phys. J. A **14**, 23.

Bender, M., H. Flocard, and P.-H. Heenen, 2003, Phys. Rev. C **68**, 044321.

Bender, M., and P.-H. Heenen, 2005, Eur. Phys. J. A **25**, 519.

Bender, M., and P.-H. Heenen, 2008, Phys. Rev. C **78**, 024309.

Bender, M., P.-H. Heenen, and P.-G. Reinhard, 2003, Rev. Mod. Phys. **75**, 121.

Bender, P. C., et al., 2009, Phys. Rev. C **80**, 014302.

Berger, J.-F., M. Girod, and D. Gogny, 1984, Nucl. Phys. A **428**, 23.

Berger, J.-F., M. Girod, and D. Gogny, 1991, Comput. Phys. Commun. **63**, 365.

Bhattacharyya, S., et al., 2008, Phys. Rev. Lett. **101**, 032501.

Blaum, K., W. Geithner, J. Lassen, P. Lievens, K. Marinova, and R. Neugart, 2008, Nucl. Phys. A **799**, 30.

Block, M., et al., 2008a, Phys. Rev. Lett. **100**, 132501.

Block, M., et al., 2008b, Phys. Rev. Lett. **101**, 059901.

Bloxham, T., et al., 2010, Phys. Rev. C **82**, 027308.

Bohr, A., and B. R. Mottelson, 1982, Phys. Scr. **25**, 28.

Bohr, A., B. R. Mottelson, and D. Pines, 1958, Phys. Rev. **110**, 936.

Bonn, J., G. Huber, H.-J. Kluge, L. Kugler, and E. W. Otten, 1972, Phys. Lett. B **38**, 308.

Borremans, D., et al., 2002, Phys. Lett. B **537**, 45.

Boucenna, A., L. Kraus, I. Linck, and T. U. Chan, 1990, Phys. Rev. C **42**, 1297.

Bouchez, E., et al., 2003, Phys. Rev. Lett. **90**, 082502.

Brink, D. M., and E. Boeker, 1967, Nucl. Phys. A **91**, 1.

Brink, D. M., and R. A. Broglia, 2005, *Nuclear Superfluidity: Pairing in Finite Systems*, Cambridge Monographs on Particle Physics, Nuclear Physics and Cosmology Vol. 24 (Cambridge University Press, Cambridge).

Brink, D. M., and J. J. Castro, 1973, Nucl. Phys. A **216**, 109.

Bron, J., W. Hesselink, A. V. Poelgeest, J. Zalmstra, M. J. Uitzinger, H. Verheul, K. Heyde, M. Waroquier, H. Vincx, and P. V. Isacker, 1979, Nucl. Phys. A **318**, 335.

Brown, B. A., 2002, Nucl. Phys. A **704**, 11.

Brown, B. A., and W. D. M. Rae, 2007, NUSHELL@MSU, MSUNSCL Report 2007 (unpublished) [http://www.nscl.msu.edu/~brown/].

Brown, B. A., and W. A. Richter, 2006, Phys. Rev. C **74**, 034315.

Brown, B. A., and B. H. Wildenthal, 1988, Annu. Rev. Nucl. Part. Sci. **38**, 29.

Brown, G. E., 1964, in *Comptes Rendus du Congres International de Physique Nucléaire de Paris* (Editions du Centre National de la Recherche Scientifique, Paris), Vol. 1, p. 129.

Brown, G. E., and A. M. Green, 1966a, Nucl. Phys. **75**, 401.

Brown, G. E., and A. M. Green, 1966b, Nucl. Phys. **85**, 87.

Brüssermann, S., K. P. Lieb, P. Sona, H. Emling, E. Grosse, and J. Stachel, 1985, Phys. Rev. C **32**, 1521.

Burke, D. G., J. C. Waddington, and O. P. Jolly, 2001, Nucl. Phys. A **688**, 716.

Campbell, C., et al., 2007, Phys. Lett. B **652**, 169.

Campi, X., H. Flocard, A. K. Kerman, and S. Koonin, 1975, Nucl. Phys. A **251**, 193.

Carchidi, M., and H. T. Fortune, 1985, Phys. Rev. C **31**, 853.

Carchidi, M., and H. T. Fortune, 1986, J. Math. Phys. (N.Y.) **27**, 633.

Carchidi, M., and H. T. Fortune, 1988a, Phys. Rev. C **37**, 556.

Carchidi, M., and H. T. Fortune, 1988b, Phys. Rev. C **38**, 1403.

Carchidi, M., H. T. Fortune, and M. Burlein, 1989, Phys. Rev. C **39**, 795.

Carchidi, M., H. T. Fortune, G. S. F. Stephans, and L. C. Bland, 1984, Phys. Rev. C **30**, 1293.

Carpenter, M. P., et al., 2009, in *FUSION08: New Aspects of Heavy Ion Collisions Near the Coulomb Barrier*, edited by K. E. Rehm, B. B. Back, H. Esbensen, and C. J. Lister (American Institute of Physics, New York), Vol. CP1098, p. 58.

Carvalho, J., R. L. Blanc, M. G. Vassanji, D. J. Rowe, and J. B. McGrory, 1986, Nucl. Phys. A **452**, 240.

Carvalho, J., and D. J. Rowe, 1992, Nucl. Phys. A **548**, 1.

Castanos, O., J. P. Draayer, and Y. Leschber, 1988, Z. Phys. A **329**, 33.

Casten, R. F., E. R. Flynn, J. D. Garrett, O. Hansen, T. J. Mulligan, D. R. Bés, R. A. Broglia, and B. Nilsson, 1972, Phys. Lett. B **40**, 333.

Casten, R. F., and D. D. Warner, 1988, Rev. Mod. Phys. **60**, 389.

Catford, W. N., R. C. Lemmon, M. Labiche, C. N. Timis, N. A. Orr, L. Caballero, R. Chapman, M. Chartier, M. Rejmund, H. Savajols, and the TIARA Collaboration, 2005, Eur. Phys. J. A **25**, 245.

Caurier, E., G. Martínez-Pinedo, F. Nowacki, A. Poves, and A. P. Zuker, 2005, Rev. Mod. Phys. **77**, 427.

Caurier, E., J. Menéndez, F. Nowacki, and A. Poves, 2007, Phys. Rev. C **75**, 054317.

Caurier, E., F. Nowacki, and A. Poves, 2001, Nucl. Phys. A **693**, 374.

Caurier, E., F. Nowacki, and A. Poves, 2004, Nucl. Phys. A **742**, 14.

Caurier, E., F. Nowacki, and A. Poves, 2005, Phys. Rev. Lett. **95**, 042502.

Caurier, E., F. Nowacki, A. Poves, and J. Retamosa, 1998, Phys. Rev. C **58**, 2033.

Chabanat, E., P. Bonche, P. Haensel, J. Meyer, and R. Schaeffer, 1998, Nucl. Phys. A **635**, 231.

Chakrabarti, R., et al., 2009, Phys. Rev. C **80**, 034326.

Chakrawarthy, R. S., P. von Brentano, J. Gableske, A. Dewald, R. Wirowski, S. Albers, and M. Schimmer, 1998, Eur. Phys. J. A **2**, 323.

Chamoli, S. K., P. Joshi, A. Kumar, R. Kumar, R. P. Singh, S. Muralithar, R. K. Bhowmik, and I. M. Govil, 2005, Phys. Rev. C **71**, 054324.

Chandler, C., et al., 1997, Phys. Rev. C **56**, R2924.

Chasman, R. R., 1972, Phys. Rev. Lett. **28**, 1275.

Chasman, R. R., 1976, Phys. Rev. C **14**, 1935.

Chasman, R. R., J. L. Egido, and L. M. Robledo, 2001, Phys. Lett. B **513**, 325.

Cheifetz, E., R. C. Jared, S. G. Thompson, and J. B. Wilhelmy, 1970, Phys. Rev. Lett. **25**, 38.

Chen, J.-Q., 1997, Nucl. Phys. A **626**, 686.

Chisté, V., et al., 2001, Phys. Lett. B **514**, 233.

Chu, S. Y., J. O. Rasmussen, M. A. Stoyer, L. F. Canto, R. Donangelo, and P. Ring, 1995a, Phys. Rev. C **52**, 685.

Chu, S. Y., J. O. Rasmussen, M. A. Stoyer, P. Ring, and L. F. Canto, 1995b, Phys. Rev. C **52**, 1407.

Clément, E., et al., 2007, Phys. Rev. C **75**, 054313.

Cline, D., 1986, Annu. Rev. Nucl. Part. Sci. **36**, 683.

Cocolios, T. E., et al., 2011, Phys. Rev. Lett. **106**, 052503.

Coenen, E., 1985, Ph.D. thesis, University of Leuven.

Coenen, E., K. Deneffe, M. Huyse, P. V. Duppen, and J. L. Wood, 1985, Phys. Rev. Lett. **54**, 1783.

Cole, J. D., et al., 1976, Phys. Rev. Lett. **37**, 1185.

Cseh, J., and W. Scheid, 1992, J. Phys. G **18**, 1419.

Davidson, P. M., G. D. Dracoulis, T. Kibédi, A. P. Byrne, S. S. Anderssen, A. M. Baxter, B. Fabricius, G. J. Lane, and A. E. Stuchbery, 1994, Nucl. Phys. A **568**, 90.

Davidson, P. M., G. D. Dracoulis, T. Kibédi, A. P. Byrne, S. S. Anderssen, A. M. Baxter, B. Fabricius, G. J. Lane, and A. E. Stuchbery, 1999, Nucl. Phys. A **657**, 219.

Davies, A. D., *et al.*, 2006, Phys. Rev. Lett. **96**, 112503.

Deacon, A. N., *et al.*, 2010, Phys. Rev. C **82**, 034305.

Decharg\u00e9, J., and D. Gogny, 1980, Phys. Rev. C **21**, 1568.

De Coster, C., B. Decroix, and K. Heyde, 1996, Phys. Lett. B **379**, 20.

De Coster, C., B. Decroix, K. Heyde, J. Jolie, H. Lehmann, and J. L. Wood, 1999, Nucl. Phys. A **651**, 31.

De Coster, C., B. Decroix, K. Heyde, J. L. Wood, J. Jolie, and H. Lehmann, 1997, Nucl. Phys. A **621**, 802.

De Coster, C., K. Heyde, B. Decroix, P. V. Isacker, J. Jolie, H. Lehmann, and J. L. Wood, 1996, Nucl. Phys. A **600**, 251.

Delaroche, J. P., M. Girod, J. Libert, and I. Deloncle, 1989, Phys. Lett. B **232**, 145.

Delaroche, J. P., M. Girod, J. Libert, H. Goutte, S. Hilaire, S. P\u00e9ru, N. Pillet, and G. F. Bertsch, 2010, Phys. Rev. C **81**, 014303.

De Rydt, M., *et al.*, 2010, Phys. Rev. C **81**, 034308.

De Rydt, M., *et al.*, 2009, Phys. Lett. B **678**, 344.

D\u00e9traz, C., D. Guillemaud, G. Huber, R. Klapisch, M. Langevin, F. Naulin, C. Thibault, L. C. Carraz, and F. Touchard, 1979, Phys. Rev. C **19**, 164.

Dewald, A., *et al.*, 2003, Phys. Rev. C **68**, 034314.

Didong, M., H. M\u00fcther, K. Goeke, and A. Faessler, 1976, Phys. Rev. C **14**, 1189.

Diget, C. A., *et al.*, 2008, Phys. Rev. C **77**, 064309.

Dobaczewski, J., I. Hamamoto, W. Nazarewicz, and J. A. Sheikh, 1994, Phys. Rev. Lett. **72**, 981.

Dobaczewski, J., W. Nazarewicz, T. R. Werner, J. F. Berger, C. R. Chinn, and J. Decharg\u00e9, 1996, Phys. Rev. C **53**, 2809.

Dombr\u00e1di, Z., *et al.*, 2006, Phys. Rev. Lett. **96**, 182501.

Doornenbal, P., *et al.*, 2009, Phys. Rev. Lett. **103**, 032501.

Doornenbal, P., *et al.*, 2010, Phys. Rev. C **81**, 041305.

Dracoulis, G., *et al.*, 2006, Phys. Lett. B **635**, 200.

Dracoulis, G. D., 1994, Phys. Rev. C **49**, 3324.

Dracoulis, G. D., 2000, Phys. Scr. **T88**, 54.

Dracoulis, G. D., G. J. Lane, A. P. Byrne, A. M. Baxter, T. Kib\u00e9di, A. O. Macchiavelli, P. Fallon, and R. M. Clark, 2003, Phys. Rev. C **67**, 051301.

Dracoulis, G. D., G. J. Lane, A. P. Byrne, T. Kib\u00e9di, A. M. Baxter, A. O. Macchiav\u00e8lli, P. Fallon, and R. M. Clark, 2004, Phys. Rev. C **69**, 054318.

Dracoulis, G. D., G. J. Lane, T. Kib\u00e9di, and P. Nieminen, 2009, Phys. Rev. C **79**, 031302.

Dracoulis, G. D., G. J. Lane, T. M. Peaty, A. P. Byrne, A. M. Baxter, P. M. Davidson, A. N. Wilson, T. Kib\u00e9di, and F. R. Xu, 2005, Phys. Rev. C **72**, 064319.

Dracoulis, G. D., A. E. Stuchbery, A. P. Byrne, A. R. Poletti, S. J. Poletti, J. Gerl, and R. A. Bark, 1986, J. Phys. G **12**, L97.

Dufour, M., and A. P. Zuker, 1996, Phys. Rev. C **54**, 1641.

Duguet, T., M. Bender, P. Bonche, and P.-H. Heenen, 2003, Phys. Lett. B **559**, 201.

Duguet, T., P. Bonche, P.-H. Heenen, and J. Meyer, 2001, Phys. Rev. C **65**, 014311.

Duval, P. D., and B. R. Barrett, 1981, Phys. Lett. B **100**, 223.

Duval, P. D., and B. R. Barrett, 1982, Nucl. Phys. A **376**, 213.

Dytrych, T., K. D. Sviratcheva, J. P. Draayer, C. Bahri, and J. P. Vary, 2008, J. Phys. G **35**, 123101.

Egido, J. L., L. M. Robledo, and R. R. Rodr\u00edguez-Guzm\u00e1n, 2004, Phys. Rev. Lett. **93**, 082502.

Elbek, B., and P. O. Tjom, 1969, *Advances in Nuclear Physics* (Plenum Press, New York), Vol. 3, p. 259.

Elekes, Z., *et al.*, 2006, Phys. Rev. C **73**, 044314.

Endt, P., 1998, Nucl. Phys. A **633**, 1.

Fahlander, C., *et al.*, 1988, Nucl. Phys. A **485**, 327.

Fahlander, C., *et al.*, 1992a, Nucl. Phys. A **537**, 183.

Fahlander, C., B. Varnestig, A. B\u00e4cklin, L. E. Svensson, D. Disdier, L. Kraus, I. Linck, N. Schulz, and J. Pedersen, 1992b, Nucl. Phys. A **541**, 157.

Fallon, P., *et al.*, 2010, Phys. Rev. C **81**, 041302.

Federman, P., and S. Pittel, 1977, Phys. Lett. B **69**, 385.

Federman, P., and S. Pittel, 1979, Phys. Rev. C **20**, 820.

Feldmeier, H., and J. Schnack, 2000, Rev. Mod. Phys. **72**, 655.

Fielding, H. W., R. E. Anderson, P. D. Kunz, D. A. Lind, C. D. Zafiratos, and W. P. Alford, 1978, Nucl. Phys. A **304**, 520.

Force, C., *et al.*, 2010, Phys. Rev. Lett. **105**, 102501.

Fornal, B., *et al.*, 2000, Eur. Phys. J. A **7**, 147.

Fornal, B., *et al.*, 1997, Phys. Rev. C **55**, 762.

Fornal, B., *et al.*, 2004, Phys. Rev. C **70**, 064304.

Fortune, H. T., and M. Carchidi, 1985, J. Phys. G **11**, L193.

Fortune, H. T., and M. Carchidi, 1987, Phys. Rev. C **36**, 2584.

Fortune, H. T., M. Carchidi, and S. Mordechai, 1984, Phys. Lett. B **145**, 4.

Fortune, H. T., C. Ogilvie, R. Gilman, J. D. Zumbro, D. L. Watson, M. J. Smithson, M. D. Cohler, A. Ghazarian, R. Wadsworth, and J. O'Donnell, 1987, Phys. Rev. C **35**, 1603.

Fortune, T., 1978, in *Proceedings of the International Conference on Nuclear Structure, Tokyo, 1977* [J. Phys. Soc. Jpn., 44, Suppl., p. 99].

Fossion, R., K. Heyde, G. Thiamova, and P. Van Isacker, 2003, Phys. Rev. C **67**, 024306.

Frank, A., and P. Van Isacker, 1994, *Algebraic Methods in Molecular and Nuclear Structure Physics* (Wiley, New York).

Frank, A., P. Van Isacker, and C. E. Vargas, 2004, Phys. Rev. C **69**, 034323.

Frauendorf, S., 2001, Rev. Mod. Phys. **73**, 463.

Freer, M., 2007, Rep. Prog. Phys. **70**, 2149.

Freer, M., and A. C. Merchant, 1997, J. Phys. G **23**, 261.

Fridmann, J., *et al.*, 2006, Phys. Rev. C **74**, 034313.

Friedman, A. M., K. Katori, D. Albright, and J. P. Schiffer, 1974, Phys. Rev. C **9**, 760.

Fukunishi, N., T. Otsuka, and T. Sebe, 1992, Phys. Lett. B **296**, 279.

Funaki, Y., M. Girod, H. Horiuchi, G. R\u00f6pke, P. Schuck, A. Tohsaki, and T. Yamada, 2010, J. Phys. G **37**, 064012.

Gableske, J., *et al.*, 2001, Nucl. Phys. A **691**, 551.

Gade, A., and T. Glasmacher, 2008, Prog. Part. Nucl. Phys. **60**, 161.

Gade, A., and J. Tostevin, 2010, Nucl. Phys. News **20**, 11.

Gade, A., *et al.*, 2007, Phys. Rev. Lett. **99**, 072502.

Gade, A., *et al.*, 2008, Phys. Rev. C **77**, 044306.

Gade, A., *et al.*, 2009, Phys. Rev. Lett. **102**, 182502.

Gangopadhyay, G., 1999, Phys. Rev. C **59**, 2541.

Gangopadhyay, G., *et al.*, 1995, Z. Phys. A **351**, 1.

Ganguly, S., P. Banerjee, I. Ray, R. Kshetri, R. Raut, S. Bhattacharya, M. Saha-Sarkar, A. Goswami, and S. K. Basu, 2008, Phys. Rev. C **78**, 037301.

Ganguly, S., *et al.*, 2007, Nucl. Phys. A **789**, 1.

Garcia-Ramos, J.-E., and K. Heyde, 2009, Nucl. Phys. A **825**, 39.

Garrett, P. E., 2001, J. Phys. G **27**, R1.

Garrett, P. E., *et al.*, 2009, Phys. Rev. Lett. **103**, 062501.

Garrett, P. E., and J. L. Wood, 2010, J. Phys. G **37**, 064028.

Gaudefroy, L., 2010, Phys. Rev. C **81**, 064329.

Gaudefroy, L., *et al.*, 2009a, Phys. Rev. Lett. **102**, 092501.

Gaudefroy, L., A. Obertelli, S. P\u00e9ru, N. Pillet, S. Hilaire, J. P. Delaroche, M. Girod, and J. Libert, 2009b, Phys. Rev. C **80**, 064313.

Gaudefroy, L., *et al.*, 2006, Phys. Rev. Lett. **97**, 092501.

Gaudefroy, L., *et al.*, 2007, Phys. Rev. Lett. **99**, 099202.

Gaudefroy, L., *et al.*, 2008, Phys. Rev. C **78**, 034307.

Gaulard, C., G. Audi, C. Bachelet, D. Lunney, M. de Saint Simon, C. Thibault, and N. Vieira, 2006, Nucl. Phys. A **766**, 52.

Gellanki, J., *et al.*, 2009, Phys. Rev. C **80**, 051304.

Gerace, W. J., and A. M. Green, 1967, Nucl. Phys. A **93**, 110.

Gerace, W. J., and A. M. Green, 1969, Nucl. Phys. A **123**, 241.

Giannatiempo, A., *et al.*, 2005, Phys. Rev. C **72**, 044308.

Girod, M., J. P. Delaroche, D. Gogny, and J. F. Berger, 1989, Phys. Rev. Lett. **62**, 2452.

Girod, M., J.-P. Delaroche, A. Görgen, and A. Obertelli, 2009, Phys. Lett. B **676**, 39.

Girod, M., and B. Grammaticos, 1979, Nucl. Phys. A **330**, 40.

Girod, M., and P.-G. Reinhard, 1982, Phys. Lett. B **117**, 1.

Glasmacher, T., 1998, Annu. Rev. Nucl. Part. Sci. **48**, 1.

Gogny, D., 1973, in *Proceedings of the International Conference on Nuclear Physics*, edited by J. de Boer and H. J. Mang (North-Holland, Amsterdam), p. 48.

Gogny, D., 1975, in *Proceedings of the International Conference on Nuclear Self-Consistent Fields*, edited by G. Ripka and M. Porneuf (North-Holland, Amsterdam), p. 333.

Görgen, A., 2010, J. Phys. G **37**, 103101.

Grahn, T., *et al.*, 2006, Phys. Rev. Lett. **97**, 062501.

Grahn, T., *et al.*, 2008, Nucl. Phys. A **801**, 83.

Grahn, T., *et al.*, 2009, Phys. Rev. C **80**, 014324.

Grasso, M., L. Gaudefroy, E. Khan, T. Nikšić, J. Piekarewicz, O. Sorlin, N. V. Giai, and D. Vretenar, 2009, Phys. Rev. C **79**, 034318.

Green, K. L., *et al.*, 2009, Phys. Rev. C **80**, 032502.

Grévy, S., *et al.*, 2004, Phys. Lett. B **594**, 252.

Grévy, S., *et al.*, 2005, Eur. Phys. J. A **25**, 111.

Griffin, J. C., R. A. Braga, R. W. Fink, J. L. Wood, H. K. Carter, R. L. Mlekodaj, C. R. Bingham, E. Coenen, M. Huyse, and P. V. Duppen, 1991, Nucl. Phys. A **530**, 401.

Griffin, J. J., and J. A. Wheeler, 1957, Phys. Rev. **108**, 311.

Griffin, R. E., A. D. Jackson, and A. B. Volkov, 1971, Phys. Lett. B **36**, 281.

Guilbault, F., D. Ardouin, J. Uzureau, P. Avignon, R. Tamisier, G. Rotbard, M. Vergnes, Y. Deschamps, G. Berrier, and R. Seltz, 1977, Phys. Rev. C **16**, 1840.

Guo, L., J. A. Maruhn, and P.-G. Reinhard, 2007, Phys. Rev. C **76**, 034317.

Hafstad, L. R., and E. Teller, 1938, Phys. Rev. **54**, 681.

Hager, U., *et al.*, 2007, Nucl. Phys. A **793**, 20.

Hamamoto, I., 2007, Phys. Rev. C **76**, 054319.

Hamamoto, I., 2009, Phys. Rev. C **79**, 014307.

Hamamoto, I., 2010, J. Phys. G **37**, 055102.

Hamamoto, I., S. V. Lukyanov, and X. Z. Zhang, 2001, Nucl. Phys. A **683**, 255.

Hamilton, J. H., *et al.*, 1975, Phys. Rev. Lett. **35**, 562.

Hamilton, J. H., A. V. Ramayya, W. T. Pinkston, R. M. Ronningen, G. Garcia-Bermudez, H. K. Carter, R. L. Robinson, H. J. Kim, and R. O. Sayer, 1974, Phys. Rev. Lett. **32**, 239.

Hansen, P. G., and J. A. Tostevin, 2003, Annu. Rev. Nucl. Part. Sci. **53**, 219.

Harder, M. K., K. T. Tang, and P. V. Isacker, 1997, Phys. Lett. B **405**, 25.

Hasegawa, M., K. Kaneko, T. Mizusaki, and Y. Sun, 2007, Phys. Lett. B **656**, 51.

Hasegawa, M., T. Mizusaki, K. Kaneko, and Y. Sun, 2007, Nucl. Phys. A **789**, 46.

Hayakawa, T., *et al.*, 2003, Phys. Rev. C **67**, 064310.

Hebeler, K., T. Duguet, T. Lesinski, and A. Schwenk, 2009, Phys. Rev. C **80**, 044321.

Heenen, P.-H., A. Valor, M. Bender, P. Bonche, and H. Flocard, 2001, Eur. Phys. J. A **11**, 393.

Helariutta, K., *et al.*, 1999, Eur. Phys. J. A **6**, 289.

Hellemans, V., S. D. Baerdemacker, and K. Heyde, 2008, Phys. Rev. C **77**, 064324.

Hellemans, V., R. Fossion, S. De Baerdemacker, and K. Heyde, 2005, Phys. Rev. C **71**, 034308.

Hess, P. O., A. Algora, M. Hunyadi, and J. Cseh, 2002, Eur. Phys. J. A **15**, 449.

Heyde, K., C. De Coster, J. Jolie, and J. L. Wood, 1992, Phys. Rev. C **46**, 541.

Heyde, K., P. V. Isacker, M. Waroquier, J. L. Wood, and R. A. Meyer, 1983, Phys. Rep. **102**, 291.

Heyde, K., J. Jolie, H. Lehmann, C. De Coster, and J. L. Wood, 1995, Nucl. Phys. A **586**, 1.

Heyde, K., K. Jolie, J. Moreau, J. Ryckebusch, M. Waroquier, P. Van Duppen, M. Huyse, and J. L. Wood, 1987, Nucl. Phys. A **466**, 189.

Heyde, K., and R. A. Meyer, 1988, Phys. Rev. C **37**, 2170.

Heyde, K., and J. L. Wood, 1991, J. Phys. G **17**, 135.

Hill, D. L., and J. A. Wheeler, 1953, Phys. Rev. **89**, 1102.

Himpe, P., *et al.*, 2006, Phys. Lett. B **643**, 257.

Himpe, P., *et al.*, 2008, Phys. Lett. B **658**, 203.

Hinohara, N., T. Nakatsukasa, M. Matsuo, and K. Matsuyanagi, 2009, Phys. Rev. C **80**, 014305.

Hinohara, N., K. Sato, T. Nakatsukasa, M. Matsuo, and K. Matsuyanagi, 2010, Phys. Rev. C **82**, 064313.

Hjorth-Jensen, M., T. T. S. Kuo, and E. Osnes, 1995, Phys. Rep. **261**, 125.

Hodsdon, A., *et al.*, 2007, Phys. Rev. C **75**, 034313.

Hoffman, C., *et al.*, 2009, Phys. Lett. B **672**, 17.

Honma, M., T. Otsuka, B. A. Brown, and T. Mizusaki, 2004, Phys. Rev. C **69**, 034335.

Honma, M., T. Otsuka, T. Mizusaki, and M. Hjorth-Jensen, 2009, Phys. Rev. C **80**, 064323.

Horiuchi, H., 2010, J. Phys. G **37**, 064021.

Horoi, M., B. A. Brown, T. Otsuka, M. Honma, and T. Mizusaki, 2006, Phys. Rev. C **73**, 061305.

Huber, G., *et al.*, 1978, Phys. Rev. C **18**, 2342.

Hückel, E., 1930, Z. Phys. **60**, 423.

Hurst, A. M., *et al.*, 2007, Phys. Rev. Lett. **98**, 072501.

Iachello, F., and A. Arima, 1987, *The Interacting Boson Model* (Cambridge University, New York).

Iachello, F., and P. Van Isacker, 1991, *The Interacting Boson-Fermion Model* (Cambridge University, New York).

Ibbotson, R. W., *et al.*, 1998, Phys. Rev. Lett. **80**, 2081.

Ibbotson, R. W., *et al.*, 1997, Nucl. Phys. A **619**, 213.

Ideguchi, E., *et al.*, 2010, Phys. Lett. B **686**, 18.

Ideguchi, E., *et al.*, 2001, Phys. Rev. Lett. **87**, 222501.

Ikeda, K., N. Takigawa, and H. Horiuchi, 1968, Prog. Theor. Phys. Suppl., **E68**, 464 [http://ptp.ipap.jp/link?PTPS/E68/464/].

Immele, J. D., and G. L. Struble, 1973, Lett. Nuovo Cimento **7**, 41.

Inglis, D. R., 1956, Phys. Rev. **103**, 1786.

Ionescu-Bujor, M., *et al.*, 2009, Phys. Rev. C **80**, 034314.

Ionescu-Bujor, M., *et al.*, 2007, Phys. Lett. B **650**, 141.

Ionescu-Bujor, M., *et al.*, 2010, Phys. Rev. C **81**, 024323.

Iwasa, N., *et al.*, 2003, Phys. Rev. C **67**, 064315.

Iwasaki, H., *et al.*, 2005, Phys. Lett. B **620**, 118.

Iwasaki, S., T. Marumori, F. Sakata, and K. Takada, 1976, Prog. Theor. Phys. **56**, 1140.

Jänecke, J., F. D. Becchetti, D. Overway, J. D. Cossairt, and R. L. Spross, 1981, Phys. Rev. C **23**, 101.

Janssens, R., 2009, Nature (London) **459**, 1069.

Janssens, R. V. F., and T. L. Khoo, 1991, Annu. Rev. Nucl. Part. Sci. **41**, 321.

Jarrio, M., J. L. Wood, and D. J. Rowe, 1991, Nucl. Phys. A **528**, 409.

Jenkins, D. G., *et al.*, 2002, Phys. Rev. C **66**, 011301.

Jenkins, D. G., *et al.*, 2007, Phys. Rev. C **76**, 044310.

Johansson, E. K., *et al.*, 2008, Phys. Rev. C **77**, 064316.

Johansson, E. K., *et al.*, 2009, Phys. Rev. C **80**, 014321.

Johnstone, I. P., and B. Castel, 1986, Phys. Rev. C **33**, 1086.

Jolie, J., and K. Heyde, 1990, Phys. Rev. C **42**, 2034.

Jolie, J., and H. Lehmann, 1995, Phys. Lett. B **342**, 1.

Joshi, P., A. Kumar, I. M. Govil, R. P. Singh, G. Mukherjee, S. Muralithar, R. K. Bhowmik, and U. Garg, 2004, Phys. Rev. C **69**, 044304.

Joshi, P., A. Kumar, G. Mukherjee, R. P. Singh, S. Muralithar, U. Garg, R. K. Bhowmik, and I. M. Govil, 2002, Phys. Rev. C **66**, 044306.

Joubert, J., F. J. W. Hahne, P. Navrátil, and H. B. Geyer, 1994, Phys. Rev. C **50**, 177.

Julin, R., K. Helariutta, and M. Muikku, 2001, J. Phys. G **27**, R109.

Jurado, B., *et al.*, 2007, Phys. Lett. B **649**, 43.

Juutinen, S., *et al.*, 1997, Nucl. Phys. A **617**, 74.

Kameda, D., *et al.*, 2007, Phys. Lett. B **647**, 93.

Kanada-En'yo, Y., and H. Horiuchi, 1995, Prog. Theor. Phys. **93**, 115.

Kanungo, R., *et al.*, 2009, Phys. Rev. Lett. **102**, 152501.

Kanungo, R., *et al.*, 2010, Phys. Lett. B **685**, 253.

Kavka, A. E., *et al.*, 1995, Nucl. Phys. A **593**, 177.

Kay, B. P., *et al.*, 2009, Phys. Rev. C **79**, 021301.

Keim, M., U. Georg, A. Klein, R. Neugart, M. Neuroth, S. Wilbert, P. Lievens, L. Vermeeren, B. Brown, and the ISOLDE Collaboration, 2000, Eur. Phys. J. A **8**, 31.

Kettunen, H., *et al.*, 2003, Eur. Phys. J. A **17**, 537.

Kibédi, T., G. D. Dracoulis, A. P. Byrne, and P. M. Davidson, 2001, Nucl. Phys. A **688**, 669.

Kibédi, T., G. D. Dracoulis, A. P. Byrne, P. M. Davidson, and S. Kuyucak, 1994, Nucl. Phys. A **567**, 183.

Kibédi, T., and R. H. Spear, 2005, At. Data Nucl. Data Tables **89**, 77.

Kilcher, P., *et al.*, 1988, in *Nuclei Far from Stability: Fifth International Conference*, edited by I. Towner, AIP Conf. Proc. No. 164 (AIP, New York), p. 517.

Kimura, M., 2007, Phys. Rev. C **75**, 041302.

Klapisch, R., R. Prieels, C. Thibault, A. M. Poskanzer, C. Rigaud, and E. Roeckl, 1973, Phys. Rev. Lett. **31**, 118.

Klotz, G., P. Baumann, M. Bounajma, A. Huck, A. Knipper, G. Walter, G. Marguier, C. Richard-Serre, A. Poves, and J. Retamosa, 1993, Phys. Rev. C **47**, 2502.

Klug, T., A. Dewald, V. Werner, P. von Brentano, and R. F. Casten, 2000, Phys. Lett. B **495**, 55.

Klüge, H.-J., and W. Nötershäuser, 2003, Spectrochim. Acta, Part B: At. Spectrosc. **58**, 1031.

Koizumi, M., *et al.*, 2004, Nucl. Phys. A **730**, 46.

Koizumi, M., *et al.*, 2003, Eur. Phys. J. A **18**, 87.

Kondev, F. G., *et al.*, 2002, Phys. Lett. B **528**, 221.

Kondev, F. G., *et al.*, 2001, Phys. Lett. B **512**, 268.

Koopman, T., 1934, Physica (Amsterdam) **1**, 104.

Kortelahti, M. O., E. F. Zganjar, H. K. Carter, C. D. Papanicolopulos, M. A. Grimm, and J. L. Wood, 1988, J. Phys. G **14**, 1361.

Korten, W., 2001, Acta Phys. Pol. B **32**, 729.

Kotlinski, B., *et al.*, 1990a, Nucl. Phys. A **517**, 365.

Kotlinski, B., T. Czosnyka, D. Cline, J. Srebrny, C. Y. Wu, A. Bäcklin, L. Hasselgren, L. Westerberg, C. Baktash, and S. G. Steadman, 1990b, Nucl. Phys. A **519**, 646.

Kowalska, M., D. T. Yordanov, K. Blaum, P. Himpe, P. Lievens, S. Mallion, R. Neugart, G. Neyens, and N. Vermeulen, 2008, Phys. Rev. C **77**, 034307.

Krishichayan, *et al.*, 2006, Eur. Phys. J. A **29**, 151.

Kulp, W. D., 2009 (private communication).

Kulp, W. D., J. M. Allmond, P. Hatcher, J. L. Wood, J. Loats, P. Schmelzenbach, C. J. Stapels, K. S. Krane, R.-M. Larimer, and E. B. Norman, 2006, Phys. Rev. C **73**, 014308.

Kulp, W. D., *et al.*, 2007, arXiv:0706.4129.

Kulp, W. D., *et al.*, 2005, Phys. Rev. C **71**, 041303.

Kulp, W. D., *et al.*, 2008, Phys. Rev. C **77**, 061301.

Kulp, W. D., J. L. Wood, K. S. Krane, J. Loats, P. Schmelzenbach, C. J. Stapels, R.-M. Larimer, and E. B. Norman, 2003, Phys. Rev. Lett. **91**, 102501.

Kumar, K., 1972, Phys. Rev. Lett. **28**, 249.

Kumar, K., 1974, Nucl. Phys. A **231**, 189.

Kumar, K., 1978, J. Phys. G **4**, 849.

Kuo, T. T. S., and G. E. Brown, 1966, Nucl. Phys. **85**, 40.

Kuo, T. T. S., and G. E. Brown, 1968, Nucl. Phys. A **114**, 241.

Kuyucak, S., and I. Morrison, 1988, Phys. Rev. C **38**, 2482.

LaFosse, D. R., *et al.*, 1995, Phys. Rev. C **51**, R2876.

Lafrance, S., S. Mordechai, H. T. Fortune, and R. Middleton, 1978, Nucl. Phys. A **307**, 52.

Lalazissis, G. A., D. Vretenar, P. Ring, M. Stoitsov, and L. M. Robledo, 1999, Phys. Rev. C **60**, 014310.

Langanke, K., D. J. Dean, and W. Nazarewicz, 2005, Nucl. Phys. A **757**, 360.

Lebrun, C., F. Guilbault, D. Ardouin, E. R. Flynn, D. L. Hanson, S. D. Orbesen, R. Rotbard, and M. N. Vergnes, 1979, Phys. Rev. C **19**, 1224.

Lee, J., *et al.*, 2010, Phys. Rev. Lett. **104**, 112701.

Lehmann, H., and J. Jolie, 1995, Nucl. Phys. A **588**, 623.

Lehmann, H., J. Jolie, C. D. Coster, B. Decroix, K. Heyde, and J. L. Wood, 1997, Nucl. Phys. A **621**, 767.

Li, Z. P., T. Nikšić, D. Vretenar, and J. Meng, 2010, Phys. Rev. C **81**, 034316.

Liang, X., *et al.*, 2006, Phys. Rev. C **74**, 014311.

Liang, X., *et al.*, 2002a, Phys. Rev. C **66**, 037301.

Liang, X., *et al.*, 2002b, Phys. Rev. C **66**, 014302.

Libert, J., M. Girod, and J.-P. Delaroche, 1999, Phys. Rev. C **60**, 054301.

Liddick, S. N., *et al.*, 2004, Phys. Rev. C **70**, 064303.

Ljungvall, J., *et al.*, 2008, Phys. Rev. Lett. **100**, 102502.

Lo Iudice, N., A. V. Sushkov, and N. Y. Shirikova, 2004, Phys. Rev. C **70**, 064316.

Lunney, D., G. Audi, M. de Saint Simon, C. Gaulard, C. Thibault, and N. Vieira, 2006, Eur. Phys. J. A **28**, 129.

Lunney, D., G. Audi, H. Doubre, S. Henry, C. Monsanglant, M. de Saint Simon, C. Thibault, C. Toader, C. Borcea, and G. Bollen, 2001, Phys. Rev. C **64**, 054311.

Mach, H., *et al.*, 2005, Eur. Phys. J. A **25**, Supplement 1, 105.

Mach, H., M. Moszynski, R. L. Gill, F. K. Wohn, J. A. Winger, J. C. Hill, G. Molnar, and K. Sistemich, 1989, Phys. Lett. B **230**, 21.

Maher, J. V., J. R. Erskine, A. M. Friedman, J. P. Schiffer, and R. H. Siemssen, 1970, Phys. Rev. Lett. **25**, 302.

Maher, J. V., J. R. Erskine, A. M. Friedman, R. H. Siemssen, and J. P. Schiffer, 1972, Phys. Rev. C **5**, 1380.

Mantica, P., 2005a, J. Phys. G **31**, S1617.

Mantica, P., 2005b, Eur. Phys. J. A **25**, 83.

Maréchal, F., *et al.*, 2005, Phys. Rev. C **72**, 044314.

Maréchal, F., *et al.*, 1999, Phys. Rev. C **60**, 034615.

Margenau, H., 1941, Phys. Rev. **59**, 37.

Mason, P., *et al.*, 2005, Phys. Rev. C **71**, 014316.

Mateja, J. F., L. R. Medsker, H. T. Fortune, R. Middleton, G. E. Moore, M. E. Cobern, S. Mordechai, J. D. Zumbro, and C. P. Browne, 1978, Phys. Rev. C **17**, 2047.

Mattoon, C. M., *et al.*, 2007, Phys. Rev. C **75**, 017302.

Mauthofer, A., K. Stelzer, J. Idzko, T. W. Elze, H. J. Wollersheim, H. Emling, P. Fuchs, E. Grosse, and D. Schwalm, 1990, Z. Phys. A **336**, 263.

McCutchan, E. A., R. F. Casten, V. Werner, R. Winkler, R. B. Cakirli, G. Gürdal, X. Liang, and E. Williams, 2008, Phys. Rev. C **78**, 014320.

McCutchan, E. A., R. F. Casten, and N. V. Zamfir, 2005, Phys. Rev. C **71**, 061301.

Menéndez, J., A. Poves, E. Caurier, and F. Nowacki, 2009, Phys. Rev. C **80**, 048501.

Mengoni, D., et al., 2010, Nucl. Phys. A **834**, 69c.

Metag, V., D. Habs, and H. J. Specht, 1980, Phys. Rep. **65**, 1.

Meyer-Ter-Vehn, J., 1975a, Nucl. Phys. A **249**, 111.

Meyer-Ter-Vehn, J., 1975b, Nucl. Phys. A **249**, 141.

Miller, D., P. Adrich, B. A. Brown, V. Moeller, A. Ratkiewicz, W. Rother, K. Starosta, J. A. Tostevin, C. Vaman, and P. Voss, 2009, Phys. Rev. C **79**, 054306.

Mittig, W., et al., 2002, Eur. Phys. J. A **15**, 157.

Möller, O., et al., 2006, Phys. Rev. C **74**, 024313.

Morales, I. O., A. Frank, C. E. Vargas, and P. V. Isacker, 2008, Phys. Rev. C **78**, 024303.

Moralles, M., P. Jänker, K. E. G. Löbner, and P. R. Pascholati, 2009, Phys. Rev. C **79**, 037302.

Mordechai, S., H. T. Fortune, R. Middleton, and G. Stephans, 1978, Phys. Rev. C **18**, 2498.

Mordechai, S., H. T. Fortune, R. Middleton, and G. Stephans, 1979, Phys. Rev. C **19**, 1733.

Moreno, O., E. Moya de Guerra, P. Sarriguren, and A. Faessler, 2010, Phys. Rev. C **81**, 041303.

Morinaga, H., 1956, Phys. Rev. **101**, 254.

Morton, A. C., et al., 2002, Phys. Lett. B **544**, 274.

Mueller, W. F., et al., 2004, Phys. Rev. C **69**, 064315.

Mundy, S. J., W. Gelletly, J. Lukasiak, W. R. Phillips, and B. J. Varley, 1985, Nucl. Phys. A **441**, 534.

Nadjakov, E. G., K. P. Marinova, and Y. P. Gangrsky, 1994, At. Data Nucl. Data Tables **56**, 133.

Nagae, D., et al., 2009, Phys. Rev. C **79**, 027301.

Nagatomo, T., et al., 2009, Eur. Phys. J. A **42**, 383.

Nakamura, T., et al., 2009, Phys. Rev. Lett. **103**, 262501.

Nazarewicz, W., 1993, Phys. Lett. B **305**, 195.

Nazarewicz, W., and J. Dobaczewski, 1992, Phys. Rev. Lett. **68**, 154.

Ncapayi, N. J., et al., 2005, Eur. Phys. J. A **26**, 265.

Neff, T., 2002, Ph.D. thesis, Technische Universität Darmstadt.

Neff, T., and H. Feldmeier, 2003, Nucl. Phys. A **713**, 311.

Neff, T., and H. Feldmeier, 2004, Nucl. Phys. A **738**, 357.

Neyens, G., 2003, Rep. Prog. Phys. **66**, 633.

Neyens, G., et al., 2005, Phys. Rev. Lett. **94**, 022501.

Nikšić, T., Z. P. Li, D. Vretenar, L. Próchniak, J. Meng, and P. Ring, 2009, Phys. Rev. C **79**, 034303.

Nikšić, T., P. Ring, D. Vretenar, Y. Tian, and Z.-y. Ma, 2010, Phys. Rev. C **81**, 054318.

Nikšić, T., D. Vretenar, and P. Ring, 2006a, Phys. Rev. C **73**, 034308.

Nikšić, T., D. Vretenar, and P. Ring, 2006b, Phys. Rev. C **74**, 064309.

Nikšić, T., D. Vretenar, P. Ring, and G. A. Lalazissis, 2002, Phys. Rev. C **65**, 054320.

Nilsson, S. G., and I. Ragnarsson, 1995, *Shapes and Shells in Nuclear Structure* (Cambridge University Press, Cambridge).

Nordholm, S., A. Bäck, and G. B. Backsay, 2007, J. Chem. Educ. **84**, 1201.

Nowacki, F., and A. Poves, 2009, Phys. Rev. C **79**, 014310.

Nummela, S., et al., 2002, Nucl. Phys. A **701**, 410.

Nummela, S., et al., 2001a, Phys. Rev. C **63**, 044316.

Nummela, S., et al., 2001b, Phys. Rev. C **64**, 054313.

Obertelli, A., S. Péru, J. P. Delaroche, A. Gillibert, M. Girod, and H. Goutte, 2005, Phys. Rev. C **71**, 024304.

Obertelli, A., et al., 2006, Phys. Rev. C **74**, 064305.

O'Donnell, D., et al., 2010, Phys. Rev. C **81**, 024318.

O'Donnell, J. M., A. Kotwal, and H. T. Fortune, 1988, Phys. Rev. C **38**, 2047.

Ollier, J., et al., 2005, Phys. Rev. C **71**, 034316.

Ollier, J., et al., 2003, Phys. Rev. C **67**, 024302.

Ono, A., H. Horiuchi, T. Maruyama, and A. Ohnishi, 1992a, Phys. Rev. Lett. **68**, 2898.

Ono, A., H. Horiuchi, T. Maruyama, and A. Ohnishi, 1992b, Prog. Theor. Phys. **87**, 1185.

Ono, A., H. Horiuchi, T. Maruyama, and A. Ohnishi, 1993, Phys. Rev. C **47**, 2652.

Oros, A., K. Heyde, C. D. Coster, B. Decroix, R. Wyss, B. R. Barrett, and P. Navratil, 1999, Nucl. Phys. A **645**, 107.

Osa, A., et al., 2002, Phys. Lett. B **546**, 48.

Otsuka, T., R. Fujimoto, Y. Utsuno, B. A. Brown, M. Honma, and T. Mizusaki, 2001, Phys. Rev. Lett. **87**, 082502.

Otsuka, T., and N. Fukunishi, 1996, Phys. Rep. **264**, 297.

Otsuka, T., T. Suzuki, J. D. Holt, A. Schwenk, and Y. Akaishi, 2010, Phys. Rev. Lett. **105**, 032501.

Otsuka, T., T. Suzuki, M. Honma, Y. Utsuno, N. Tsunoda, K. Tsukiyama, and M. Hjorth-Jensen, 2010, Phys. Rev. Lett. **104**, 012501.

Otten, E., 1989, in *Treatise on Heavy-Ion Science*, edited by D. A. Bromley (Plenum Press, New York), Vol. 8, p. 517.

Padgett, S. W., et al., 2005, Phys. Rev. C **72**, 064330.

Pakarinen, J., et al., 2007, Phys. Rev. C **75**, 014302.

Papanicolopoulos, C. D., M. A. Grimm, J. L. Wood, E. F. Zganjar, M. O. Kortelahti, J. D. Cole, and H. K. Carter, 1988, Z. Phys. A **330**, 371.

Patra, S. K., and C. R. Praharaj, 1991, Phys. Lett. B **273**, 13.

Paul, E. S., et al., 1995, Phys. Rev. C **51**, 78.

Pauwels, D., J. L. Wood, K. Heyde, M. Huyse, R. Julin, and P. Van Duppen, 2010, Phys. Rev. C **82**, 027304.

Peierls, R. E., and J. Yoccoz, 1957, Proc. Phys. Soc. London Sect. A **70**, 381.

Peru, S., M. Girod, and J. F. Berger, 2000, Eur. Phys. J. A **9**, 35.

Peterson, R. J., and J. D. Garrett, 1984, Nucl. Phys. A **414**, 59.

Petrovici, A., K. Schmid, O. Radu, and A. Faessler, 2006, J. Phys. G **32**, 583.

Petrovici, A., K. W. Schmid, and A. Faessler, 1992, Nucl. Phys. A **549**, 352.

Petrovici, A., K. W. Schmid, and A. Faessler, 1996, Nucl. Phys. A **605**, 290.

Petrovici, A., K. W. Schmid, and A. Faessler, 2000, Nucl. Phys. A **665**, 333.

Petrovici, A., K. W. Schmid, and A. Faessler, 2002, Nucl. Phys. A **708**, 190.

Petrovici, A., K. W. Schmid, and A. Faessler, 2003, Nucl. Phys. A **728**, 396.

Piekarewicz, J., 2007, J. Phys. G **34**, 467.

Podolyák, Z., et al., 2004, Int. J. Mod. Phys. E **13**, 123.

Polikanov, S. M., V. A. Druin, V. A. Karnaukhov, V. L. Mikheev, A. A. Pleve, N. K. Skobelov, V. G. Subbottin, G. M. Ter-Akopyan, and V. A. Fomichev, 1962, Sov. Phys. JETP **15**, 1016.

Poves, A., and J. Retamosa, 1987, Phys. Lett. B **184**, 311.

Poves, A., and J. Retamosa, 1994, Nucl. Phys. A **571**, 221.

Poves, A., and A. Zuker, 1981, Phys. Rep. **70**, 235.

Pritychenko, B. V., T. Glasmacher, B. A. Brown, P. D. Cottle, R. W. Ibbotson, K. W. Kemper, and H. Scheit, 2000, Phys. Rev. C **62**, 051601.

Pritychenko, B. V., T. Glasmacher, B. A. Brown, P. D. Cottle, R. W. Ibbotson, K. W. Kemper, and H. Scheit, 2001, Phys. Rev. C **63**, 047308.

Pritychenko, B. V., T. Glasmacher, P. D. Cottle, R. W. Ibbotson, K. W. Kemper, L. A. Riley, A. Sakharuk, H. Scheit, M. Steiner, and V. Zelevinsky, 2002, Phys. Rev. C **65**, 061304.

Proetel, D., R. M. Diamond, and F. S. Stephens, 1974, Phys. Lett. B **48**, 102.

Raddon, P. M., *et al.*, 2004, Phys. Rev. C **70**, 064308.

Ragnarsson, I., and R. A. Broglia, 1976, Nucl. Phys. A **263**, 315.

Rahkila, P., *et al.*, 2010, Phys. Rev. C **82**, 011303.

Rasmussen, J. O., 1970, Acc. Chem. Res. **3**, 166.

Reinhard, P.-G., 1989, Rep. Prog. Phys. **52**, 439.

Reinhard, P.-G., D. J. Dean, W. Nazarewicz, J. Dobaczewski, J. A. Maruhn, and M. R. Strayer, 1999, Phys. Rev. C **60**, 014316.

Retamosa, J., E. Caurier, F. Nowacki, and A. Poves, 1997, Phys. Rev. C **55**, 1266.

Richter, W. A., S. Mkhize, and B. Brown, 2008, Phys. Rev. C **78**, 064302.

Rigollet, C., P. Bonche, H. Flocard, and P.-H. Heenen, 1999, Phys. Rev. C **59**, 3120.

Rikovska, J., N. J. Stone, P. M. Walker, and W. B. Walters, 1989, Nucl. Phys. A **505**, 145.

Riley, L. A., *et al.*, 2009a, Phys. Rev. C **79**, 051303.

Riley, L. A., *et al.*, 2008, Phys. Rev. C **78**, 011303.

Riley, L. A., *et al.*, 2009b, Phys. Rev. C **80**, 037305.

Ring, P., 1996, Prog. Part. Nucl. Phys. **37**, 193.

Ring, P., and P. Schuck, 1980, *The Nuclear Many-Body Problem* (Springer-Verlag, New York).

Ringle, R., *et al.*, 2009, Phys. Rev. C **80**, 064321.

Robinson, S. J. Q., L. Zamick, and Y. Y. Sharon, 2011, Phys. Rev. C **83**, 027302.

Robledo, L. M., R. R. Rodríguez-Guzmán, and P. Sarriguren, 2008, Phys. Rev. C **78**, 034314.

Rodríguez, T. R., and J. L. Egido, 2007, Phys. Rev. Lett. **99**, 062501.

Rodríguez, T. R., and J. L. Egido, 2008, Phys. Lett. B **663**, 49.

Rodríguez, T. R., and J. L. Egido, 2010, Phys. Rev. C **81**, 064323.

Rodríguez, T. R., J. L. Egido, and A. Jungclaus, 2008, Phys. Lett. B **668**, 410.

Rodríguez-Guzmán, R., J. L. Egido, and L. M. Robledo, 2000a, Phys. Lett. B **474**, 15.

Rodríguez-Guzmán, R., P. Sarriguren, L. M. Robledo, and J. E. García-Ramos, 2010, Phys. Rev. C **81**, 024310.

Rodríguez-Guzmán, R. R., J. L. Egido, and L. M. Robledo, 2000b, Phys. Rev. C **62**, 054319.

Rodríguez-Guzmán, R. R., J. L. Egido, and L. M. Robledo, 2002a, Phys. Rev. C **65**, 024304.

Rodríguez-Guzmán, R. R., J. L. Egido, and L. M. Robledo, 2002b, Nucl. Phys. A **709**, 201.

Rodríguez-Guzmán, R. R., J. L. Egido, and L. M. Robledo, 2003, Eur. Phys. J. A **17**, 37.

Rodríguez-Guzmán, R. R., J. L. Egido, and L. M. Robledo, 2004, Phys. Rev. C **69**, 054319.

Röpke, H., 2004, Eur. Phys. J. A **22**, 213.

Rosensteel, G., and D. J. Rowe, 1977, Phys. Rev. Lett. **38**, 10.

Rotbard, G., G. La Rana, M. Vergnes, G. Berrier, J. Kalifa, F. Guilbault, and R. Tamisier, 1978, Phys. Rev. C **18**, 86.

Rotbard, G., M. Vergnes, G. Berrier-Ronsin, and J. Vernotte, 1980, Phys. Rev. C **21**, 2293.

Rotbard, G., M. Vergnes, G. La Rana, J. Vernotte, J. Kalifa, G. Berrier, F. Guilbault, R. Tamisier, and J. F. A. van Hienen, 1977, Phys. Rev. C **16**, 1825.

Roth, R., T. Neff, H. Hergert, and H. Feldmeier, 2004, Nucl. Phys. A **745**, 3.

Roussiére, B., *et al.*, 1998, Nucl. Phys. A **643**, 331.

Rowe, D., 1985, Rep. Prog. Phys. **48**, 1419.

Rowe, D., 1996, Prog. Part. Nucl. Phys. **37**, 265.

Rowe, D. J., and G. Rosensteel, 2001, Phys. Rev. Lett. **87**, 172501.

Rowe, D. J., G. Thiamova, and J. L. Wood, 2006, Phys. Rev. Lett. **97**, 202501.

Rowe, D. J., M. G. Vassanji, and J. Carvalho, 1989, Nucl. Phys. A **504**, 76.

Rowe, D. J., T. A. Welsh, and M. A. Caprio, 2009, Phys. Rev. C **79**, 054304.

Rowe, D. J., and J. L. Wood, 2010, *Fundamentals of Nuclear Models Foundational Models* (World Scientific, Singapore).

Rud, N., D. Ward, H. R. Andrews, R. L. Graham, and J. S. Geiger, 1973, Phys. Rev. Lett. **31**, 1421.

Rudolph, D., *et al.*, 1999, Phys. Rev. Lett. **82**, 3763.

Rudolph, D., C. Baktash, M. Devlin, D. R. LaFosse, L. L. Riedinger, D. G. Sarantites, and C.-H. Yu, 2001, Phys. Rev. Lett. **86**, 1450.

Rudolph, D., *et al.*, 1998, Phys. Rev. Lett. **80**, 3018.

Rudolph, D., E. K. Johansson, L.-L. Andersson, J. Ekman, C. Fahlander, and R. du Rietz, 2005, Nucl. Phys. A **752**, 241.

Rudolph, D., *et al.*, 2002a, Phys. Rev. C **65**, 034305.

Rudolph, D., *et al.*, 2002b, Eur. Phys. J. A **14**, 137.

Rupnik, D., E. F. Zganjar, J. L. Wood, P. B. Semmes, and P. F. Mantica, 1998, Phys. Rev. C **58**, 771.

Rupnik, D., E. F. Zganjar, J. L. Wood, P. B. Semmes, and W. Nazarewicz, 1995, Phys. Rev. C **51**, R2867.

Rusev, G., *et al.*, 2005, Phys. Rev. Lett. **95**, 062501.

Sakurai, H., 2002, Eur. Phys. J. A **13**, 49.

Sakurai, H., 2005, Eur. Phys. J. A **25**, 403.

Sarazin, F., *et al.*, 2000, Phys. Rev. Lett. **84**, 5062.

Sarriguren, P., 2009, Phys. Rev. C **79**, 044315.

Sarriguren, P., E. Moya de Guerra, and A. Escuderos, 1999, Nucl. Phys. A **658**, 13.

Sarriguren, P., E. Moya de Guerra, A. Escuderos, and A. C. Carrizo, 1998, Nucl. Phys. A **635**, 55.

Sarriguren, P., R. Rodríguez-Guzmán, and L. M. Robledo, 2008, Phys. Rev. C **77**, 064322.

Satula, W., J. Dobaczewski, and W. Nazarewicz, 1998, Phys. Rev. Lett. **81**, 3599.

Sauvan, E., *et al.*, 2000, Phys. Lett. B **491**, 1.

Savajols, H., *et al.*, 2005, Eur. Phys. J. A **25**, 23.

Savelius, A., *et al.*, 1998, Nucl. Phys. A **637**, 491.

Scheit, H., *et al.*, 2004, Nucl. Phys. A **746**, 96.

Schiffer, J. P., *et al.*, 2008, Phys. Rev. Lett. **100**, 112501.

Schimmer, M., S. Albers, A. Dewald, A. Gelberg, R. Wirowski, and P. von Brentano, 1992, Nucl. Phys. A **539**, 527.

Schwarzenberg, J., J. L. Wood, and E. F. Zganjar, 1992, Phys. Rev. C **45**, R896.

Schwerdtfeger, W., *et al.*, 2009, Phys. Rev. Lett. **103**, 012501.

Sears, J. M., D. B. Fossan, S. E. Gundel, I. Thorslund, P. Vaska, and K. Starosta, 1997, Phys. Rev. C **55**, 1096.

Sears, J. M., *et al.*, 1998, Phys. Rev. C **58**, 1430.

Serot, B. D., 1992, Rep. Prog. Phys. **55**, 1855.

Serot, B. D., and J. D. Walecka, 1986, *Advances in Nuclear Physics* (Plenum Press, New York), Vol. 16, p. 1.

Shihab-Eldin, A. A., J. O. Rasmussen, M. A. Stoyer, D. G. Burke, and P. E. Garrett, 1995, Int. J. Mod. Phys. E **4**, 411.

Shimoura, S., *et al.*, 2007, Phys. Lett. B **654**, 87.

Signoracci, A., and B. A. Brown, 2007, Phys. Rev. Lett. **99**, 099201.

Siiskonen, T., P. O. Lipas, and J. Rikovska, 1999, Phys. Rev. C **60**, 034312.

Simkovic, F., A. Faessler, and P. Vogel, 2009, Phys. Rev. C **79**, 015502.

Simpson, E. C., J. A. Tostevin, D. Bazin, B. A. Brown, and A. Gade, 2009a, Phys. Rev. Lett. **102**, 132502.

Simpson, E. C., J. A. Tostevin, D. Bazin, and A. Gade, 2009b, Phys. Rev. C **79**, 064621.

Simpson, G. S., *et al.*, 2006, Phys. Rev. C **74**, 064308.

Singh, B., R. Zywina, and R. B. Firestone, 2002, Nucl. Data Sheets **97**, 241.

Skoda, S., J. L. Wood, J. Eberth, J. Busch, M. Liebchen, T. Mylaeus, N. Schmal, R. Sefzig, W. Teichert, and M. Wiosna, 1990, Z. Phys. A **336**, 391.

Skyrme, T. H. R., 1956, Philos. Mag. **1**, 1043.

Skyrme, T. H. R., 1959a, Nucl. Phys. **9**, 615.

Skyrme, T. H. R., 1959b, Nucl. Phys. **9**, 635.

Smirnova, N. A., P.-H. Heenen, and G. Neyens, 2003, Phys. Lett. B **569**, 151.

Soloviev, V. G., 1992, *Theory of Atomic Nuclei: Quasiparticles and Phonons* (IOP, Bristol).

Sorensen, B., 1974, Nucl. Phys. A **236**, 29.

Sorlin, O., and M.-G. Porquet, 2008, Prog. Part. Nucl. Phys. **61**, 602.

Sorlin, O., *et al.*, 1995, Nucl. Phys. A **583**, 763.

Sorlin, O., *et al.*, 1993, Phys. Rev. C **47**, 2941.

Speidel, K.-H., S. Schielke, J. Leske, J. Gerber, P. Maier-Komor, S. Robinson, Y. Sharon, and L. Zamick, 2006, Phys. Lett. B **632**, 207.

Speidel, K.-H., *et al.*, 2008, Phys. Lett. B **659**, 101.

Srebrny, J., *et al.*, 2006, Nucl. Phys. A **766**, 25.

Stephens, F. S., 1975, Rev. Mod. Phys. **47**, 43.

Storm, M. H., A. Watt, and R. R. Whitehead, 1983, J. Phys. G **9**, L165.

Stuchbery, A. E., *et al.*, 2006, Phys. Rev. C **74**, 054307.

Styczen, J., J. Chevalier, B. Haas, N. Schulz, P. Taras, and M. Toulemonde, 1976, Nucl. Phys. A **262**, 317.

Sugawara, M., *et al.*, 2003, Eur. Phys. J. A **16**, 409.

Sugawara-Tanabe, K., A. Arima, and N. Yoshida, 1999, J. Phys. G **25**, 917.

Svensson, C. E., *et al.*, 1998, Phys. Rev. Lett. **80**, 2558.

Svensson, C. E., *et al.*, 1997, Phys. Rev. Lett. **79**, 1233.

Svensson, C. E., *et al.*, 1999, Phys. Rev. Lett. **82**, 3400.

Svensson, L. E., 1989, Ph.D. thesis, University of Uppsala.

Svensson, L. E., C. Fahlander, L. Hasselgren, A. Bäcklin, L. Westerberg, D. Cline, T. Czosnyka, C. Y. Wu, R. M. Diamond, and H. Kluge, 1995, Nucl. Phys. A **584**, 547.

Takada, K., and S. Tazaki, 1986, Nucl. Phys. A **448**, 56.

Takeuchi, S., *et al.*, 2009, Phys. Rev. C **79**, 054319.

Talmi, I., 1993, *Simple Models of Complex Nuclei: The Shell Model and Interacting Boson Model* (Harwood Academic Publishers, Chur).

Tarasov, O. B., *et al.*, 2007, Phys. Rev. C **75**, 064613.

Tarasov, O. B., *et al.*, 2009, Phys. Rev. Lett. **102**, 142501.

Tarpanov, D., H. Liang, N. V. Giai, and C. Stoyanov, 2008, Phys. Rev. C **77**, 054316.

Terasaki, J., H. Flocard, P. H. Heenen, and P. Bonche, 1997, Nucl. Phys. A **621**, 706.

Terry, J. R., *et al.*, 2008, Phys. Rev. C **77**, 014316.

Thiamova, G., D. J. Rowe, and J. L. Wood, 2006, Nucl. Phys. A **780**, 112.

Thibault, C., R. Klapisch, C. Rigaud, A. M. Poskanzer, R. Prieels, L. Lessard, and W. Reisdorf, 1975, Phys. Rev. C **12**, 644.

Thouless, D. J., and J. G. Valatin, 1962, Nucl. Phys. **31**, 211.

Timis, C., *et al.*, 2005, J. Phys. G **31**, S1965.

Toh, Y., T. Czosnyka, M. Oshima, T. Hayakawa, H. Kusakari, M. Sugawara, Y. Hatsukawa, J. Katakura, N. Shinohara, and M. Matsuda, 2000, Eur. Phys. J. A **9**, 353.

Toh, Y., *et al.*, 2001, J. Phys. G **27**, 1475.

Tonev, D., A. Dewald, T. Klug, P. Petkov, J. Jolie, A. Fitzler, O. Möller, S. Heinze, P. von Brentano, and R. F. Casten, 2004, Phys. Rev. C **69**, 034334.

Tostevin, J. A., and B. A. Brown, 2006, Phys. Rev. C **74**, 064604.

Tostevin, J. A., G. Podolyák, B. A. Brown, and P. G. Hansen, 2004, Phys. Rev. C **70**, 064602.

Towner, I. S., and J. C. Hardy, 2008, Phys. Rev. C **77**, 025501.

Tripathi, V., *et al.*, 2008a, Phys. Rev. C **77**, 034310.

Tripathi, V., *et al.*, 2006, Phys. Rev. C **73**, 054303.

Tripathi, V., *et al.*, 2005, Phys. Rev. Lett. **94**, 162501.

Tripathi, V., *et al.*, 2007, Phys. Rev. C **76**, 021301.

Tripathi, V., *et al.*, 2008b, Phys. Rev. Lett. **101**, 142504.

Twin, P. J., *et al.*, 1986, Phys. Rev. Lett. **57**, 811.

Urban, W., *et al.*, 2001, Nucl. Phys. A **689**, 605.

Urban, W., *et al.*, 2003, Eur. Phys. J. A **16**, 11.

Urban, W., *et al.*, 2004, Eur. Phys. J. A **22**, 241.

Utsuno, Y., T. Otsuka, T. Glasmacher, T. Mizusaki, and M. Honma, 2004, Phys. Rev. C **70**, 044307.

Utsuno, Y., T. Otsuka, T. Mizusaki, and M. Honma, 1999, Phys. Rev. C **60**, 054315.

Utsuno, Y., T. Otsuka, T. Mizusaki, and M. Honma, 2001, Phys. Rev. C **64**, 011301.

Valor, A., P.-H. Heenen, and P. Bonche, 2000, Nucl. Phys. A **671**, 145.

Van den Berg, A. M., R. V. F. Janssens, G. T. Emery, A. Saha, and R. H. Siemssen, 1982, Nucl. Phys. A **379**, 239.

Van de Vel, K., *et al.*, 2002, Phys. Rev. C **65**, 064301.

Van Duppen, P., E. Coenen, K. Deneffe, M. Huyse, and J. L. Wood, 1985, Phys. Lett. B **154**, 354.

Van Duppen, P., and M. Huyse, 2000, Hyperfine Interact. **129**, 149.

Van Duppen, P., M. Huyse, and J. L. Wood, 1990, J. Phys. G **16**, 441.

Vanhorenbeeck, J., P. D. Marmol, E. Coenen, M. Huyse, P. V. Duppen, and J. Wauters, 1991, Nucl. Phys. A **531**, 63.

van Rij, W. I., and S. H. Kahana, 1972, Phys. Rev. Lett. **28**, 50.

Varnestig, B., 1987, Ph.D. thesis, University of Uppsala.

Vautherin, D., 1973, Phys. Rev. C **7**, 296.

Vautherin, D., and D. M. Brink, 1972, Phys. Rev. C **5**, 626.

Venhart, M., *et al.*, 2011, Phys. Lett. B **695**, 82.

Venkova, T., *et al.*, 2005, Eur. Phys. J. A **26**, 19.

Vergnes, M., 1980, in *Proceedings of the 6th European Physical Society Nuclear Division Conference on Structure of Medium-Heavy Nuclei*, Inst. Phys. Conf. Ser. No. 49 (IOP, Bristol, London), p. 25.

Vergnes, M. N., and G. Rotbard, 1988, Phys. Rev. C **37**, 418.

Vergnes, M. N., G. Rotbard, E. R. Flynn, D. L. Hanson, S. D. Orbesen, F. Guilbaut, D. Ardouin, and C. Lebrun, 1979, Phys. Rev. C **19**, 1276.

Vergnes, M. N., G. Rotbard, F. Guilbaut, D. Ardouin, C. Lebrun, E. R. Flynn, D. L. Hanson, and S. D. Orbesen, 1978, Phys. Lett. B **72**, 447.

Vergnes, M. N., G. Rotbard, R. Seltz, F. Guilbaut, D. Ardouin, R. Tamisier, and P. Avignon, 1976a, Phys. Rev. C **14**, 58.

Vergnes, M. N., G. Rotbard, R. Seltz, F. Guilbaut, D. Ardouin, R. Tamisier, and P. Avignon, 1976b, Phys. Rev. C **14**, 58.

von Oertzen, W., M. Freer, and Y. Kanada-En'yo, 2006, Phys. Rep. **432**, 43.

von Schwarzenberg, J., 1991, Ph.D. thesis, Georgia Institute of Technology.

von Schwarzenberg, J., J. L. Wood, and E. F. Zganjar, 1998, Phys. Rev. C **57**, R15.

Vyvey, K., D. Borremans, N. Coulier, R. Coussement, G. Georgiev, S. Teughels, G. Neyens, H. Hübel, and D. L. Balabanski, 2002a, Phys. Rev. C **65**, 024320.

Vyvey, K., *et al.*, 2002b, Phys. Rev. Lett. **88**, 102502.

Vyvey, K., G. D. Dracoulis, A. N. Wilson, P. M. Davidson, A. E. Stuchbery, G. J. Lane, A. P. Byrne, and T. Kibédi, 2004, Phys. Rev. C **69**, 064318.

Wadsworth, R., *et al.*, 1993, Nucl. Phys. A **559**, 461.

Wadsworth, R., *et al.*, 1996, Phys. Rev. C **53**, 2763.

Walecka, J. D., 1974, Ann. Phys. (N.Y.) **83**, 491.

Wang, S. Y., *et al.*, 2010, Phys. Rev. C **81**, 017301.

Wang, Z. M., *et al.*, 2010a, Phys. Rev. C **81**, 054305.

Wang, Z. M., *et al.*, 2010b, Phys. Rev. C **81**, 064301.

Warburton, E. K., J. A. Becker, and B. A. Brown, 1990, Phys. Rev. C **41**, 1147.

Wauters, J., N. Bijnens, P. Dendooven, M. Huyse, H. Y. Hwang, G. Reusen, J. von Schwarzenberg, P. Van Duppen, R. Kirchner, and E. Roeckl, 1994, Phys. Rev. Lett. **72**, 1329.

Wauters, J., N. Bijnens, H. Folger, M. Huyse, H. Y. Hwang, R. Kirchner, J. von Schwarzenberg, and P. Van Duppen, 1994, Phys. Rev. C **50**, 2768.

Weeks, K. J., T. Tamura, T. Udagawa, and F. J. W. Hahne, 1981, Phys. Rev. C **24**, 703.

Weissman, L., *et al.*, 2004, Phys. Rev. C **70**, 024304.

Werner, T. R., J. A. Sheikh, M. Misu, W. Nazarewicz, J. Rikovska, K. Heeger, A. S. Umar, and M. R. Strayer, 1996, Nucl. Phys. A **597**, 327.

Werner, T. R., J. A. Sheikh, W. Nazarewicz, M. R. Strayer, A. S. Umar, and M. Misu, 1994, Phys. Lett. B **333**, 303.

White, E. R., *et al.*, 2007, Phys. Rev. C **76**, 057303.

Wiedeking, M., *et al.*, 2008, Phys. Rev. C **78**, 037302.

Wilson, A. N., G. D. Dracoulis, A. P. Byrne, P. M. Davidson, G. J. Lane, R. M. Clark, P. Fallon, A. Görgen, A. O. Macchiavelli, and D. Ward, 2003, Phys. Rev. Lett. **90**, 142501.

Wimmer, K., *et al.*, 2010, Phys. Rev. Lett. **105**, 252501.

Winger, J. A., P. F. Mantica, and R. M. Ronningen, 2006, Phys. Rev. C **73**, 044318.

Winger, J. A., P. F. Mantica, R. M. Ronningen, and M. A. Caprio, 2001, Phys. Rev. C **64**, 064318.

Wirowski, R., M. Schimmer, L. Esser, S. Albers, K. O. Zell, and P. von Brentano, 1995, Nucl. Phys. A **586**, 427.

Wolinska-Cichocka, M., *et al.*, 2005, Eur. Phys. J. A **24**, 259.

Wood, J. L., 1984, Nucl. Phys. A **421**, 43.

Wood, J. L., R. W. Fink, E. F. Zganjar, and J. Meyer-ter Vehn, 1976, Phys. Rev. C **14**, 682.

Wood, J. L., K. Heyde, W. Nazarewicz, M. Huyse, and P. V. Duppen, 1992, Phys. Rep. **215**, 101.

Wood, J. L., E. F. Zganjar, C. D. Coster, and K. Heyde, 1999, Nucl. Phys. A **651**, 323.

Wu, C. S., and L. Wilets, 1969, Annu. Rev. Nucl. Sci. **19**, 527.

Wu, C. Y., *et al.*, 1996, Nucl. Phys. A **607**, 178.

Wu, C. Y., D. Cline, E. G. Vogt, W. J. Kernan, T. Czosnyka, K. G. Helmer, R. W. Ibbotson, A. E. Kavka, B. Kotlinski, and R. M. Diamond, 1991, Nucl. Phys. A **533**, 359.

Wu, C. Y., H. Hua, and D. Cline, 2003, Phys. Rev. C **68**, 034322.

Wu, C. Y., H. Hua, D. Cline, A. B. Hayes, R. Teng, R. M. Clark, P. Fallon, A. Goergen, A. O. Macchiavelli, and K. Vetter, 2004, Phys. Rev. C **70**, 064312.

Xu, C., and Z. Ren, 2007, Phys. Rev. C **75**, 044301.

Xu, F. R., R. Wyss, and P. M. Walker, 1999, Phys. Rev. C **60**, 051301.

Yamagami, M., and N. Van Giai, 2004, Phys. Rev. C **69**, 034301.

Yanagisawa, Y., *et al.*, 2003, Phys. Lett. B **566**, 84.

Yao, J. M., J. Meng, P. Ring, and D. P. Arteaga, 2009, Phys. Rev. C **79**, 044312.

Yao, J. M., J. Meng, P. Ring, and D. Vretenar, 2010, Phys. Rev. C **81**, 044311.

Yoneda, K., *et al.*, 2006, Phys. Rev. C **74**, 021303.

Yordanov, D. T., K. Blaum, M. De Rydt, M. Kowalska, R. Neugart, G. Neyens, and I. Hamamoto, 2010, Phys. Rev. Lett. **104**, 129201.

Yordanov, D. T., M. Kowalska, K. Blaum, M. D. Rydt, K. T. Flanagan, P. Lievens, R. Neugart, G. Neyens, and H. H. Stroke, 2007, Phys. Rev. Lett. **99**, 212501.

Yoshida, K., 2009, Phys. Rev. C **79**, 054303.

Yoshida, S., and N. Takigawa, 1997, Phys. Rev. C **55**, 1255.

Yu, C.-H., *et al.*, 1999, Phys. Rev. C **60**, 031305.

Zegers, R. G. T., *et al.*, 2010, Phys. Rev. Lett. **104**, 212504.

Zeldes, N., T. S. Dimitrescu, and H. S. Köhler, 1983, Nucl. Phys. A **399**, 11.

Zheng, D. C., D. Berdichevsky, and L. Zamick, 1988a, Phys. Rev. C **38**, 437.

Zheng, D. C., D. Berdichevsky, and L. Zamick, 1988b, Phys. Rev. Lett. **60**, 2262.

Zheng, D. C., L. Zamick, and D. Berdichevsky, 1990, Phys. Rev. C **42**, 1004.

Zielinska, M., 2004, Int. J. Mod. Phys. E **13**, 71.

Zielinska, M., *et al.*, 2002, Nucl. Phys. A **712**, 3.